APPLICATION OF ISOKINETIC SAMPLING TECHNIQUE FOR LOCAL SOLID DENSITIES IN UPWARD LIQUID-SOLID FLOWS THROUGH AN ANNULUS

A THESIS SUBMITTED TO THE GRADUATE SCHOOL OF NATURAL AND APPLIED SCIENCES
OF
THE MIDDLE EAST TECHNICAL UNIVERSITY

BY

GÜLDEN CAMÇI

IN PARTIAL FULLFILLMENT OF THE REQUIREMENTS FOR THE DEGREE
OF
MASTER OF SCIENCE
IN
THE DEPARTMENT OF CHEMICAL ENGINEERING

SEPTEMBER 2003

Approval of the Graduate School of Natural and Applied Sciences

_____

Prof. Dr. Canan Özgen
Director

I certify that this thesis satisfies all the requirements as a thesis for the degree of Master of Science.

_____

Prof. Dr. Timur Dogu
Head of Department

This is to certify that we have read this thesis and that in our opinion it is fully adequate, in scope and quality, as a thesis for the degree of Master of Science.

_____

Prof. Dr. Tülay A. Özbelge
Supervisor

Examining Committee Members

Prof. Dr.Aysel Atimtay (Chairperson) _____

Prof. Dr. Tülay A. Özbelge _____

Prof. Dr. H. Önder Özbelge _____

Prof. Dr. Hayrettin Yücel _____

Assoc. Prof. Dr. Yusuf Uludag _____

ABSTRACT

APPLICATION OF ISOKINETIC SAMPLING TECHNIQUE FOR LOCAL SOLID DENSITIES IN UPWARD LIQUID-SOLID FLOWS THROUGH AN ANNULUS

CAMÇI, Gülden

M. Sc., Department of Chemical Engineering
Supervisor: Prof. Dr. Tülay A. Özbelge

September, 2003, 150 pages

In this study, radial solid density distributions in upward flowing water-feldspar mixtures through a concentric annulus were investigated. Local solid density measurements were performed at a test cross-section in the fully developed flow region of a concentric annulus, which is a part of a closed-loop system consisting of a head tank, a variable speed slurry pump, an orificemeter, a heat exchanger, an annulus, a temperature probe, and a drain line. The solid particles with mean diameters of 72 and 138 μm at two different feed solid concentrations of 1 and 2 % v/v were used in the prepared slurries. The dependent variables being local solid density, local mixture velocity, and axial frictional pressure drop along the test-section, an experimental work was performed to obtain the radial solid density profiles and axial pressure gradients at different operating conditions.

To determine the local solid densities, a sampling probe was used. At the beginning, this probe was used as a pitot tube to measure the local velocities in the test cross-section. Making use of these data, local solid densities were measured with the same probe under isokinetic and nonisokinetic conditions to compare both.

For this purpose, an isokinetic sampling unit was designed and constructed to withdraw the samples under isokinetic flow conditions, at which the sampling velocity in the probe equated to the true flow velocity in the annulus very closely. The required constant back-pressure was supplied by pressurized N2 gas to equate these velocities to each other. The amounts of solids in the slurry samples collected at seven different radial locations in the test area under isokinetic and non-isokinetic conditions were determined by the gravimetric method.

Local solid densities showed more uniform trends at the feed solid concentration of 1% v/v than those at 2% v/v. Increasing the feed solid concentration and particle size changed the shape of these profiles. The obtained local solid densities were generally higher near the outer wall than those near the inner wall; this result was consistent with the literature. As a general trend, local solid densities showed a decreasing trend at around a dimensionless radial distance of λ=0.4, where the slurry velocity profile had its maximum value. It was observed that the two-phase axial frictional pressure gradients along the test section in the fully developed flow region increased with increasing feed solid concentration and the particle size at a constant slurry flow rate.

Isokinetic sampling results showed that the local solid densities increased consistently with the increasing slurry velocity at all radial distances in the annular gap, while this trend was not observed clearly in the non-isokinetic measurements. Also the variations of the local solid densities along the radial distance were more obvious in the isokinetic results while these variations were obscured under nonisokinetic conditions by the experimental error at a higher level.

Keywords: Local solid density; Isokinetic sampling; Two-phase axial frictional pressure drop; Radial solid concentration distribution; Annular flow.

ÖZ

ESMERKEZLI IKI BORU ARASINDAKI YUKARI YÖNLÜ SIVI-KATI AKISLARINDA LOKAL KATI DERISIMLERI IÇIN IZOKINETIK ÖRNEKLEME TEKNIGININ UYGULANMASI

CAMÇI, Gülden

Yüksek Lisans Tezi, Kimya Mühendisligi Bölümü
Tez Yöneticisi: Prof. Dr. Tülay A. Özbelge

Eylül 2003, 150 sayfa

Bu çalismada esmerkezli iki boru arasinda (annulus) yukari yönlü akan su-feldspat karisimlarinin bölgesel kati yogunlugu dagilimlari incelenmistir. Bölgesel kati yogunlugu ölçümleri annulus'un tam gelismis akis alanindaki kesitinde ölçülmüstür ve annulus'un dahil oldugu kapali-devre sistemde bir besleme tanki, bir hizi ayarlanabilen çamur pompasi, bir orifismetre, bir isi degistirici, bir sicaklik sondasi ve bir bosaltma hatti yer almaktadir. Çamur karisimlari 72 ve 138 mikron olmak üzere iki degisik büyüklükte kati parçacik kullanilarak ve hacimsel olarak %1 ve 2 olmak üzere iki degisik kati besleme konsantrasyonunda hazirlanmistir. Degisik çalisma kosullarinda radyal yöndeki kati yogunlugu profilleri ve test bölgesindeki eksenel sürtünmeli basinç kayiplarini elde etmek için gerçeklestirilen deneylerde, bagimli degiskenler: bölgesel kati yogunlugu, bölgesel karisim hizi ve test bölgesindeki eksenel sürtünmeli basinç kaybi olmustur.

Bölgesel kati yogunlukari bir örnekleme sondasi kullanilarak ölçülmüstür. Bu sonda baslangiçta bölgesel hizlari bulmak için bir pitot tüp olarak kullanilmistir. Bu veriler kullanilarak, bölgesel kati

yogunluklari ayni örnekleme sondasiyla izokinetik ve karsilastirma yapmak amaciyla izokinetik olmayan sartlarda da gerçeklestirilmistir.

Bu amaçla, numuneleri izokinetik örnekleme sartlari altinda alabilmek için bir izokinetik örnekleme ünitesi tasarlanmis ve kurulmustur. Bu durumda sondadaki örnekleme hiziyla gerçek akis hizini çok yakin olarak esitlemek mümkün olmaktadir. Hizlari esitlemek için gerekli olan sabit dengeleyici basinç, Azot gazi ile saglanmistir. Test alanindaki yedi degisik radyal noktada alinan izokinetik ve izokinetik olmayan sartlardaki numunelerin içindeki kati miktarlari gravimetrik yöntemle tayin edilmistir.

Hacimsel olarak % 1 kati besleme konsantrasyonunda elde edilen bölgesel kati yogunluklari, % 2 kati besleme konsantrasyonuna göre daha tekdüze bir davranis göstermistir. Artan kati parçacik konsantrasyonu ve parçacik büyüklügü, bölgesel kati konsantrasyonu grafiklerinin seklini degistirmistir. Bölgesel kati yogunluklari genellikle literatürdeki çalismalara benzer olarak annulus'un dis duvari civarinda iç duvar yakinindakilere göre daha fazla bulunmustur. Kati yogunluklari λ=0.4 olan boyutsuz bir radyal uzaklikta, hiz profillerinin maksimum oldugu noktada, genel olarak azalan bir trend göstermistir. Test bölümü boyunca tam gelismis akis bölgesinde iki-faz eksenel sürtünmeli basinç degisimlerinin sabit bir karisim hizinda, artan kati besleme konsantrasyonu ve parçacik büyüklügüyle arttigi gözlemlenmistir.

Izokinetik örnekleme sonuçlari, bölgesel kati yogunluklarinin artan karisim hiziyla her radyal uzaklikta arttigini göstermektedir. Bu davranis, izokinetik olmayan sartlarda yapilan ölçümlerde net olarak gözlenememistir. Ayrica, bölgesel kati yogunluklarindaki radyal uzaklik boyunca gerçeklesen degisimler izokinetik örnekleme sartlarinda daha açik olarak izlenebilmistir. Izokinetik olarak yapilmayan ölçümlerde bu degisimler daha yüksek deneysel hatanin etkisiyle açikça gözlenememistir.

Anahtar Sözcükler: Bölgesel kati yogunlugu; Izokinetik örnekleme; Iki-fazli eksenel sürtünmeli basinç kaybi; Radyal kati konsantrasyon profili; Annular (es-merkezli iki-boru arasinda) akis.

To my parents

ACKNOWLEDGEMENTS

I wish to express my deep gratitude to my supervisor Prof. Dr. Tülay A. Özbelge for her valuable supervision, excellence in scientific guidance, and willingness to motivate me throughout the course of my research.

I offer sincere thanks to Prof. Dr. H. Önder Özbelge and Baris Ünal for their invaluable suggestions, comments, help, encouragement, and support during my study.

TÜBITAK (The Scientific and Technical Research Council of Turkey) is gratefully appreciated for funding the project through MISAG-226 and for the scholarship. Thanks are also due to Middle East Technical University (M.E.T.U.) for partial support on this project.

I thank FERRO International Trade Inc., Sevgi Akin, and Ferit Akin for their support to this thesis.

I extend my appreciation to Çanakkale Seramik for supplying the solid material.

The staff and technicians of the Chemical Engineering Department especially Mehmet Erili, Ertugrul Özdemir, Adil Demir, Süleyman Nazif Kushan, Nevzat Bekçi, and Isa Çaglar are greatly acknowledged for their help in the construction of the experimental set-up.

I thank Coal Research Lab staff of the Chemical Engineering Department for supplying the manometer fluids.

Kamil Alptekin, the draftsman of the Chemical Engineering department, is acknowledged for drawing the schematics of the experimental set-up.

Particular thanks are extended to Bahattin Coskun from M.E.T.U. Civil Engineering Department, for his help in arrangement of angle of the inclined manometer by using the level equipment.

I thank my colleague Alper Uzun for his help about some computer applications.

I wish to express my special appreciation to my friend Günes Ünal for his help in the calibration part of this study, construction of the isokinetic sampling unit, drawing the schematics of this unit, also for his friendship and for bringing delicious foods during the writing stage of this thesis.

Peculiar thanks must go to my friends in the Chemical Engineering Department; Gaye Yücel Çakal, Göknur Tütüncü, Ela Eroglu, Belma Soydas, Funda Erol, and Ebru Acar, for their patience, hospitality, and support throughout the course of this study and for not to feel myself alone.

My deepest gratitude is to my parents Gülser and Salih Camçi for their very special care, great support, understanding, patience, and for their faith in me, during all my education and especially for their lifetime effort on me.

Last but not the least, I offer sincere thanks to my sister Gülcan Camçi for her continuous encouragement, patience, and support during all stages of my life.

TABLE OF CONTENTS

APPENDICES

LIST OF TABLES

TABLE

LIST OF FIGURES

FIGURE

LIST OF SYMBOLS

A_{ann} : Area of the annulus, m^2

A_p : Area of the sampling probe, m^2

C_0 : Orificemeter coefficient

D_e : Equivalent diameter of the annulus, m

DRD : Dimensionless radial distance

d_p : Mean particle size, μm

f : Friction factor

f_c : Friction factor from correlation

f_e : Experimental friction factor from pressure drop data

f_m : Friction factor for liquid-solid mixture

f_w : Friction factor for water

FSC : Initial feed solid concentration, % v/v

FSD : Initial feed solid density, kg/m^3

g : Gravitational accelation, m^2/s

h : Interval length for Simpson's rule, m

ΔH : Manometer reading, m

ΔH_{CCl4} : Manometer reading for carbontetrachloride, m

ΔH_{Hg} : Manometer reading for mercury, m

ΔH_{im} : Manometer reading for inclined manometer, m

ID_p : Inner diameter of the sampling probe, m

ID_1 : Inner diameter of the outer pipe, m

ID_2 : Inner diameter of the inner pipe, m

K : Pitot tube coefficient

L : Length of the test section, m

LSD : Local solid density, kg/m^3

$\dot{m}$: Mass flow rate of water, kg/s

m_w : mass of water, kg

N : Number of points for Simpson's rule (pp. 116-117)

OD_p : Outer diameter of the sampling probe, m

OD_1 : Outer diameter of the outer pipe, m

OD_2 : Outer diameter of the inner pipe, m

ΔP : Pressure drop, Pa

ΔP_c : Axial pressure drop from correlation, Pa

ΔP_{csh} : Axial pressure drop from correlation including static head, Pa

ΔP_e : Experimental axial pressure drop, Pa

ΔP_{esh} : Experimental axial pressure drop including static head, Pa

ΔP_{im} : Pressure drop obtained from inclined manometer, Pa

ΔP_{tp} : Two-phase axial pressure drop, Pa

ΔP_w : Pressure drop for water, Pa

Q : Volumetric flow rate of water, m^3/s

r : Radial distance from the center of the pipes, m

R : Inner radius of the outer pipe, m

Re : Reynolds number

Re_m : Reynolds number for liquid-solid mixture

Re_w : Reynolds number for water

s : Standard deviation for pitot tube coefficient

s_D : Standard deviation for local solid density data

s_v : Standard deviation for local velocity data

t : time, s

T : Temperature, ^0C

TF : (Benzene+CCl_4) mixture as manometer fluid

U_{ann} : Average mixture velocity in the annulus, m/s

U_0 : Velocity through orifice, m/s

U_S : Average velocity from Simpson's rule applied to local velocity data

V_L : Local velocity, m/s

W_p : Weight of the solid particles, g

W_t : Tare weight, g

W_{t+s} : (Tare weight+feldspar), g

W_w : Weight of water, g

W_{t+w+s}: (Tare weight+water+feldspar), g

Latin Symbols

α : inclination angle, ^{0}

κ : Aspect ratio of the annulus

ϕ_a : correction factor for laminar flow

$\bar{\phi}_s$: Average volume fraction of solids, % (v/v)

λ : Dimensionless radial distance $(R-R_1)/(R_2-R_1)$

ρ : Density, kg/m^3

ρ_{tf} : Density of the two-fluid mixture, kg/m^3

ρ_p : Density of solid particles, kg/m^3

ρ_w : Density of water, kg/m^3

$?_{CCl_4}$: Density of carbontetrachloride, kg/m^3

$\overline{?}_m$: Average transport density of the liquid-solid mixture, kg/m^3

$\overline{?}_s$: Area average transport density of solid phase, kg/m^3

μ : Viscosity, Pa.s

μ_w : Viscosity of water, Pa.s

$\overline{\mu}_m$: Average transport viscosity of the mixture, Pa.s

CHAPTER 1

INTRODUCTION

Multiphase fluid systems contain more than one phase, at least one of them being a fluid. The disperse phase may consist of solid particles, gas bubbles, or liquid droplets when the continuous phase is a liquid. The dynamics of multiphase systems comprises of mass, energy, charge, and momentum transports in these systems. Multiphase systems might have gas-solid particles, gas-liquid droplets, liquid-gas bubbles, liquid-liquid droplets, and liquid-solid particles. The last system has applications in fluidized beds, flotation, and sedimentation [1].

There are two methods of approach to the dynamics of multiphase systems: (i). considering the dynamics of a single particle and then extending it to a multiphase system in an analogous fashion, like in molecular (kinetic) theory of gases. (ii). investigating the continuum mechanics of single-phase fluids, then using a similar way to explain what happens in the presence of particles. Kinetic theory of gases is based on the molecular interactions, which can be considered analogous to interactions among particles. Generally, the shapes of the particles in multiphase systems are not spherical. To make irregular shapes as ideal, particles are assumed to be as spherical. Small liquid droplets attempt to be spherical because of the surface tension phenomenon. If field effect or gravity comes into picture, droplets tend to have shapes that cause minimum potential or smallest resistance to flow [1].

The factors that affect the solid-liquid flows can be stated as follows: particle-particle interaction, the virtual mass affect, particle inertia, crossing-trajectories effect, drag, turbulence, and the Magnus effect. If the volumetric concentration of solids is less than 0.3%, the particle-particle interactions are considered to be negligible for spherical particles [2]. When having neutrally buoyant particles, velocity of solid phase and velocity of fluid are accepted as equal in the laminar flow regime even if the concentration of solids is large ([3],[4]). Particle interactions can be neglected in dilute slurries [5].

Particle behavior in gas-solid flows depends on [6]:

1. Drag force (due to slip velocity)
2. Lift force (because of the rotation of particles and gas velocity gradient)
3. Gravity force (important for horizontal flow)
4. Particle-particle and particle-wall interactions
5. Electrostatic forces

Transportation of solid-fluid mixtures finds many use in industry; such as food processing and sterilization operations [7-9]. The design of sterilization equipment is difficult because of the complexity in predicting the velocity and heat transfer rates. These parameters affect the quality of the product [10]. Suspension flows have largely been used in the transportation of solid raw materials, products, solid wastes and sludges [11], mining and beneficiation plants [12]. Also circulating fluidized beds, hydraulic transportation of minerals and ores, mining and beneficiation plants, mineral and chemical process industries, chemical and fossil energy applications are some of the other examples of slurry flows [13]. If the flows of such kind of mixtures are not understood well enough, it causes some inefficiencies in the use of the equipment or some problems in the operations depending upon the improper design of them. This subject is not clear enough yet. Most of the present deficiencies are raised from the lack of experimental data [14].

Different flow patterns can be observed in liquid-solid flows as in the other flow systems. Geometry of the system, operating conditions and physical properties of the fluids, altogether affect the flow pattern [15]. Internal flow pattern plays a role in the performance of a system. By knowing the local concentrations, this phenomenon could be understood. Also pressure drop, corrosion, erosion, and power requirements depend on the concentration of solids in slurry systems [13]. Estimation of the pressure drop in slurry pipeline design is not easy because of the complexity of the process. Shape and size distributions of solid particles are significant factors in predicting the pressure drop through a pipeline, which is very important in the design of hydrotransport systems [11]. On the other hand, restricted amount of experimental data makes difficult to get valid estimations for large-scale plants [16].

Pressure drop increases when the solid particles are present in the fluid, since the velocity between the solid particles (interstitial velocity) is higher than the superficial velocity. Another reason yielding higher pressure drops in the presence of solid particles is because of the higher turbulence in solid-liquid flow than that in single-phase flow, and due to the increase in the form drag [17].

The application of upward liquid-solid flows in hydraulic transport in industry require the operating velocity being high enough to keep the continuous flow of solids. Nonetheless, high velocity causes excess energy losses or sometimes pipe wear [18]. In the hydraulic transportation of settling solids in horizontal pipes, the transport velocities smaller than the suspending velocity are used at most of the time, to be more economical [19]. Slurry flow in pipes is different from the homogeneous liquid flow in several aspects: for the latter case, the nature of the flow depends on the physical properties of the fluid, while for the former case two different types of flow affect the system:

i) Homogeneous slurries: These slurries have uniform solid particle distribution in liquid medium. Size of the particles is very small (fine) and solid concentration is high.

ii) Heterogeneous slurries: Distribution of the solid particles is not uniform. There are concentration gradients through the vertical axis of a horizontal pipe, even at high flow rates, since the solid and fluid phases keep their identities so that particle-fluid interactions may be significant. Particle sizes are larger and solid concentration is lower than the homogeneous slurries [11].

To be able to predict the pressure gradients for slurries flowing in horizontal pipes more correctly, slurries can be divided into two main groups: settling and non-settling. In non-settling slurries, the mixture is assumed to behave as a homogeneous fluid and the settling tendency of solid particles could be neglected. However, settling slurries are considered as two-phase mixtures and settling velocity of solids cannot be ignored. Four flow patterns can be defined for slurries: stationary bed, sliding bed, heterogeneous suspension, and pseudo-homogeneous suspension [20]. Flow velocity well above the terminal velocity of particles prevents the settling of solids in vertical pipelines, while turbulence prevents the settling of solids in horizontal pipelines [11].

Experimental studies related with upward liquid-solid flows have been performed for years. Nevertheless, experimental work about annular geometry is not encountered prevalently. Although, it has large application areas in industry, the complexity in analyzing the system prevents to get enough data. Double pipe heat exchangers, nuclear reactor coolers, extruders, slurry transport reactors, and fluidized beds are some of the examples from industry [21].

Knowledge of radial solid phase concentration distribution is necessary in modeling the transport processes in dispersed flow systems [22]. Local solid concentrations in such systems can be determined by several methods such as with vertical counter flow meters, straight pipe concentration meters, γ-Ray beam absorption, ultrasonic methods, photographic methods, conductivity methods, and isokinetic sampling. Isokinetic sampling is chosen since it is the best

for the set-up that will be studied due to economical and practical reasons. This system is not expensive, and its construction is easy. Isokinetic sampling condition is satisfied when the undisturbed flow velocity and the withdrawal velocity within the sampling probe are equal to each other. Mixture is flowing in a large flow area before coming to the sampling tube. Velocity of the mixture changes due to the presence of the sampling tube, which restricts the flow area. In this situation velocity increases because of the decrease in the diameter. To equalize the velocities flowing in the pipe and within the sampling tube, isokinetic sampling is used.

Prediction of radial solid density distributions is crucial especially in food industry. Design of the process equipment depends on those predictions. Power, operating cost, and heat transfer rates are affected by density distributions. These altogether affect the quality of the product. For example, in the design of a sterilizer, conservative assumptions made due to the lack of data will cause a product that is commercially sterile, but well overcooked, less desirable and healthy for the consumer [9]. The measurement of radial local solid densities was performed previously [21] in the same set-up under non-isokinetic sampling conditions. These results did not give consistent trends. Therefore, the aim of this study is to design and construct an isokinetic sampling unit for the accurate measurement of local solid densities in upward liquid-solid flows through same the concentric annulus of the closed-loop system used in the previous study [21], thus to obtain reliable and reproducible experimental data necessary for the modeling and design of these systems. The results between non-isokinetic and isokinetic sampling will be compared to explain the reasons of getting different trends in solid density profiles.

CHAPTER 2

LITERATURE SURVEY

Hydraulic transportation of solid waste, coal and minerals is more economical and ecological over the conventional transportation techniques. Many experimental studies were performed related with slurry flows and some correlations were obtained in terms of measurable quantities. However, many of the correlations are limited due to the short range of examined variables. Analytical studies are restricted since the flow nature of such mixtures is rather complex [23]. Suspension flow finds use in the transportation of solid raw materials, products, solid wastes, and sludges. It is necessary to simplify the conditions to use correlations. For instance, although slurries consist of mixed sized of particles, mean value of the diameters is taken. Also particle shape is a factor to find the particle size distribution and it is assumed to have spherical shape for all particles [11].

Some examples for gas-solid type of transportation are solid-propellant rockets, nuclear-propulsion equipment, H-iron processes, and pneumatic conveying [24]. Some other industrial examples of gas-solid flows can be given as follows: moving bed catalytic reactors, combustion of metallized propellant in rocket nozzles, pneumatic conveying devices, nuclear reactor cooling, and gas-solid separator

systems. Design and control of such systems need the knowledge of local concentration and local velocity of gas and solid phases since slip velocity is needed [25].

Flow characteristics of solid-liquid slurries were searched in horizontal pipelines [23]. To find pressure drop and shear stress at the pipe wall, mixing length theory was used. Modeling was performed considering the two-phase fluid as a variable density fluid. Velocity profiles were found by solving the proper Navier-Stokes equations. Thus, various flow parameters were determined. A similar approach was used in modeling the upward flow of dilute slurries through a concentric annulus [26].

Experiments were performed to be able to understand the effect of solid particles on fluid turbulence for fully developed slurry flows [27]. Upward flow of solid-water suspensions was studied in a pipe. A vertical 3-in ID pyrex pipe was used and solid concentration range changed from 0.5 to 2.5 % v/v. Solid particles were glass and copper spheres. Samples were taken at different positions along the diameter at different distances from the injector. The potassium chloride content (diffusing content) of the samples was analyzed by measuring the electrical conductivity of the samples. It was reported that, if average slip velocity between the solid and the fluid was small, then solids had not a significant effect on the diffusion rate of KCl in low solid concentration cases. Also diffusion rate was investigated in the turbulent flow region. Rate of diffusion to the fluid was affected by the concentration of solids and the ratio of the slip velocity to the fluid velocity. Also with the increasing Reynolds number, solids had smaller effect on the fluid turbulence. When having low solid concentrations, velocity fluctuations were small in the radial direction and motion was linear. Liquid samples were taken by a stainless steel tube. It was driven by a micrometer screw.

2.1. Concentration and Voidage Distributions

In order to predict mass transfer, pressure drop, and reaction between the liquid and particles, it is necessary to know the local and average particle concentration and velocities [28].

Transportation of solid-liquid mixtures with hydraulic pipeline systems is a useful method in the industry only if proper instrumentation is used to measure the solid concentration and flow rate of such suspensions, which are not easy because of having much variables involving the process. Some examples are iron ore pipelines [29], shipping of bulk solids [30], and movement of in-plant fines.

Interstitial voidage profiles were measured in both static and flowing beds of nearly buoyant granular materials in aqueous solutions by γ-ray tomography technique [7]. Experimental apparatus was a clear acrylic hopper and a detachable vertical stand-pipe. The flow regime transitions were observed during vertical transport of the granular solid-liquid mixtures. A ball-valve control led the outflow of the stand-pipe. Steady state conditions were taken into account. Wall friction and interparticle effects were neglected. Three different plastic particles were used as testing material in the flow experiments. Material A was hard and particle shape was nearly spherical. Material E and material F were soft. Density of the particles was between 1030 and 1094 kg/m^3. Particles of E and F were nearly cylindrical and nearly spherical, respectively. Equivalent diameters of A, E and F were 3.76, 4.46, and 4.11 mm, respectively. Also, with equivalent diameter of 9.56 mm and density of 1130 kg/m^3, the soaked peas were tried in the experiments. Dynamic (flowing) voidage profiles were obtained using the steady-state discharge from a hopper through a vertical stand-pipe of coarse granular solid-liquid mixtures, using the tomographic data. It was concluded that, the flow regime transitions depended strongly upon the solid material properties. Radial and horizontal line profiles of interstitial voidage were obtained at different heights within the conical hopper and vertical stand-pipe sections.

A capacitive method was used to determine the instantaneous spatial solid content of a mixture [31]. A measuring sensor having

two capacitors was installed in the pipeline system. To be able to measure quick changes in time and shorten the measuring space, the author used such a method. When the dielectric constant changed, the capacity of a parallel plate capacitor would change. The small change in the dielectric constant of water was depending on the temperature and it was accepted as negligible. Horizontal flow was studied. The capacity of both capacitors was accepted as equal. The horizontal pipe had 39.8 mm internal diameter and was made of plexiglass. At the end of the experiments it was reported tat the amount and the distribution of solid body content caused changes in capacity. Also some relations were developed related with the capacity and spatial solid body content for hydrotransportation of mixtures.

Calibrated conductivity probes can be used to measure the electrical conductivity of liquids [32]. The operation frequency of these devices is generally equal or above 1kHz. Foods having high moisture or highly concentrated fluids show a strong dependence on electrical conductivity. It is a function of frequency in such a case. This property is important in the food sterilization processes. To optimize the design of them the frequency that would be used in the process should be determined carefully. Because, it is important for the amount of power supply and thus the economic aspect of the design.

Phase distribution and turbulent structure of solid/fluid upflows were investigated in a vertical pipe [8]. They measured the volume fraction by using a Laser-Doppler Anemometer (LDA). Specific gravity and mean diameter of the ceramic and expanded polystyrene particles used in the experiments were 2.45, 2.32 mm and 0.032, 1.79 mm, respectively. Mean diameter of 2 mm of spherical particles was experimented. Ceramic particles whose specific gravity were higher than water and expanded polystyrene particles whose specific gravity were lower than water were used as solid materials. Size distribution of the large spherical particles was measured. Both the radial and axial velocities were evaluated. Because of having negative buoyancy, particles lagged in the liquid phase near the center of the pipe. The particle velocity was higher near the wall. If the liquid flow rate was

increased, then the relative velocity between the particles and the liquid becomes lower at the center of the pipe. That was true for ceramic particles and the reverse was valid for polystyrene particles. Unlike polystyrene particles, ceramics had larger inertia. At low flow rates the volume fraction profiles indicated that, unlike polystyrene particles, ceramic particles have a uniform distribution. However, increased flow rate caused coring. Local volume fraction, local velocity, turbulence intensity, Reynolds stresses were measured by LDA. A single-beam γ-ray Densiometer was used for correction. Liquid flow rate was measured by a calibrated magnetic flowmeter.

A high speed cine photography technique was used to measure the concentration and velocity of solid particles. Different flow rates of carrier fluid were tried [33]. A hydraulic conveying test rig was used in the experiments. It had a pumping system, a pipe, and a separator. The pump was able to minimize the contamination of the solution. Pump and valves were plated with a nickel phosphorus alloy to minimize the effect of abrasion. The pipeline was made of glass with 40 mm internal diameter. The study was performed after steady state conditions were attained. Dynamic equilibrium situation was evaluated considering the mixing and gravitational settling of the particles. Horizontal pipe flow was taken into account. Concentration profiles were obtained in tree-dimensional form. Liquid was a mixture of arocolor and propanol, and solid phase consisted of borosilicate glass particles. Some particles were marked and put in the suspension to be able to follow them. Test section of the pipe was also made of borosilicate glass. Then the motion of the marked particles started to be observed. It was recorded by a high-speed cine camera. Frame speed range was between 500 to 3000 frames per second. A digital data plotter evaluated these recordings. The analysis was made at the circular cross-section of the pipe. The relative concentration was obtained by counting the marked particles at a definite length. The particle velocity was reached by counting the marked particles at a definite length and time. 580 μm of mean particle size was used in the study. Axial velocity and axial fluxes were determined. The average vertical concentration profiles were compared for gamma attenuation

method and high-speed cine camera technique. It was reported that the agreement was well.

Solids concentration was measured with an economic and basic method in slurry lines [13]. The instrument was based on the resistance of slurry. Dependent variables were fluid properties, velocity, temperature, particle size, and pipe-wall material. The aim of that study was to measure the concentration of solids over a small volume with a conductivity probe to obtain an effective calibration procedure and to compare the conductivity method with γ-Ray absorption and isokinetic sampling methods. 5 cm ID of aluminium pipeline, a variable-speed motor pump, a heat exchanger, a magnetic flowmeter, a stand tank, and a rotatable joint were present in the experimental set-up. An L-shaped conductivity probe made from stainless steel was used. Spherical and irregular particles were the testing material. They consisted of glass beads, polystyrene, fine sand, medium sand, and coarse sand particles. Ranges of the mean diameter and density were 0.19-5.5 mm and 1.06-3.0 g/cm^3, respectively. Measurements were made at different points along the pipe. The liquid was tap water. At 25^0 C, tap water had a resistivity of 2720 Ω. Different probe positions were tried. If the probe approached the pipe wall, then the voltage increased. 15 runs were performed. It was observed that velocity was not an important factor. Water resistivity and sensor voltage decreased while temperature was enhanced. The results were compared with the results obtained by isokinetic sampling and γ-Ray Absorption techniques. The results were close and consistent with each other. Concentration of solids was measured at different points of the pipe by conductivity probe, isokinetic sampling, and γ-Ray absorption (Chord-average concentrations were found by γ-Ray absorption, while sampling probe gave local concentration in situ values). Bulk velocities were measured by a magnetic flow meter.

Concentration of solids, density, size of the solid particles, viscosity and density of the liquid affect the settling characteristics of the slurries. If the density of the fine particles is very close to the density of the carrier liquid in a slurry, these are called non-settling

slurries which follow the pseudo-homogeneous flow. If the density and size of the particles are large, they are called settling slurries. Some examples for such solids are sand, gravel, and coal. The behavior of a flow-sedimentation of a slowly settling suspension flow was modeled in a circular pipe [34]. To do this, scaled down experimental data was used at constant pressure. According to the authors, first sedimentation occurred at the lower section of the pipe, then flow was decreased. Later plug flow region covered the whole cross-section. It was reported that laminar flow of slowly-settling slurries could be reached with small pipe diameters. By the flow sedimentation model, characteristics of the slowly-settling slurries were investigated. Pseudo-steady state conditions were accepted when making derivations. An oven drying method was used to obtain solid concentration of samples. To model such kind of flow, generally fully empirical correlations were used.

The study for upward solid-liquid flow in a vertical pipe was presented here [16]. The aim of this study was to get the concentration profile, velocity profile, and pressure drop in vertical pipes for upward solid-liquid flows. Equation of motion for two-fluid model was used. Equation of continuity and motion were used to derive the two-fluid model in the turbulent flow regime. Steady state two-dimensional flow was considered. In this study, the effects of solids phase were searched to find the non-uniformity in the concentration profiles. This non-uniformity affects the velocity profile and changes the pressure loss, especially at high mean velocities. Pressure drop can be estimated by energy balances. Mechanical properties of solid and mean velocity of flow affect the concentration profile of solids. Experiments were performed in a vertical square duct of 40 mm inner side. Its construction material was a transparent resin. Polycarbonate pellets with specific weight of 1.14 and silbeads (silica gel spheres) having specific weight of 1.88 were the solid materials tested in the fluid phase of water. The particles had spherical shape and 3mm in diameter and they were semi-transparent. The effects of density of solids on the flowing mixture were clarified. The experiments showed that concentration was not uniform in the radial direction at a cross-section of the pipe. Also it was changed

uniformly with density and flow rate of solids. At the end of the experiments it was realized that, there was a great difference in the concentration profiles of the tried solid materials because of their different specific weights. This was caused by the magnitude of the forces applied on the particles. It was dependent on the relative motion of fluid and solid velocity gradients. Fluid velocity was measured with the help of a pitot tube of 1.0 mm in diameter. Concentrations were measured by the absorption of light beam. Since the particles were semi-transparent, the effect of overlapping of the particles was neglected [16].

Liquid-solid mixtures have been largely used in food processing industries [9]. They generally have neutrally buoyant particles in non-Newtonian fluids. When a continuous sterilization plant is attempted to perform, a conservative assumption has to be made because of having not enough data. This assumption is, product flow occurs in the laminar Newtonian flow regime. Aseptic food processing was studied here [35]. Particle and liquid velocity profiles and solid concentration profiles were obtained, horizontally in the laminar flow regime. Viscosities of Newtonian fluids were between 0.009 and 0.237 kg/ms. Spherical particles of $0.16 < \kappa$ (radius of particle/radius of pipe) < 0.10 and $1.002 < s$ (relative density: particle density/liquid density) < 1.014 were tried. Liquid velocities were always greater than those of the solid particles. Particle concentration and velocity of liquid were measured by 'hot wire' method. Velocity of particles was determined by a pulsed ultrasonic Doppler velocimeter.

Hydrodynamics of water feldspar ($K_2O.Al_2O_3.6SiO_2$) was investigated [36]. Experiments were performed in a horizontal copper pipe having 41.5 mm internal diameter. 0.081, 0.161, and 0.227 mean diameters of feldspar particles were used. The volume fraction range of solids was between 0.05-0.03. Density of the particles was 1698 kg/m3. Reynolds number changed from 14,000 to 115,000. By changing the operating conditions, consistency distributions of solids over a cross-section were reported in the turbulent flow region. A specially designed sampling probe was used to measure solid consistencies through the various points of the pipe, axially. Inside

and outside diameters of the probe were 2 and 4 mm, respectively. Taylor's series screens were used to get a uniform size distribution of the solid particles. Solid consistency measurement was made by gravimetric methods. From the recorded data, isoconsistency lines of solids were drawn. With decreasing solid consistency and particle size, Reynolds number was increased. Therefore, a more uniform solid distribution was observed across the cross-sectional area of the pipe. Three different orientations of the sampling probe were tried. They realized that flow patterns of solid-liquid suspensions were dependent upon the particle size and the flow Reynolds number in a horizontal pipe along the vertical diameter. Minimum and maximum consistencies were near the upper wall and at the lower wall, respectively. They found that the nature of the flow was strongly dependent upon the inlet consistency of solids, the particle size, and the flow Reynolds number, in horizontal slurry flows.

The upflow characteristics of feldspar-water mixtures were investigated in an annulus [21]. This kind of transportation is preferable because of their low maintenance and operating costs. The experimental set-up consisted of a vertical annulus, a by-pass line, two pressure transducers, a head tank, a heat exchanger, a U-tube manometer, a sampling probe, an orificemeter, a rotameter, a temperature probe, a centrifugal slurry pump and a drain line. Horizontal and vertical lines were made of galvanized iron. Inner and outer diameters of the annulus were 12.5 and 2.5 cm, respectively. Therefore aspect ratio was equal to 0.2. Steady state conditions were taken during the experiments. Both the laminar and the turbulent flows were tried. Hydraulic diameter was 10 cm. Frictional pressure drop was measured with a U-tube manometer that had CCl_4 in it. 2^0–10^0 of inclination of manometer plane with the horizontal was used, in the measurement of very small pressure drops. When two-phase flow experiments were making, inclination angle was increased to 90^0, since pressure drops became greater. Radial local solid concentrations (RLSCs) were measured in a flow area perpendicular to flow by a specially designed sampling probe at a cross-section of the annulus. Inner and outer diameters of the sampling probe were 0.2 and 0.32 cm, respectively. An orificemeter that was calibrated for water was

used to measure the flow rates. To prepare the testing feed solution, a stainless steel head tank was utilized. Mean particle diameters of 0.0064, 0.0115, 0.0138, 0.0165, and 0.0230 cm of feldspar particles were used. Density of feldspar was 2.4 g/cm3. Solid concentration range of 0.3-2.3 (% v/v) feed slurries were tried. Mixture velocity was changed from 0.8 to 19.3 cm/s in the annulus. 273 runs were conducted totally. At the end, RLSCs and axial two-phase pressure drops were determined. The experimental data related with single-phase water flows were compared with the literature. Local solid concentrations (LSCs) were found to be higher near the outer wall and lower near the inner wall of the annulus. For the same mixture velocity, two-phase pressure drops increased with increased feed solid concentration (FSC) at each particle size. Also for the constant mixture velocity and FSC, two-phase pressure drop increased with the particle size. They claimed that, local solid concentrations did not change too much in the radial direction at very small particle size and very low FSC cases, but increased toward the outer wall for larger particles at higher FSCs. Axial pressure drops were measured by pressure transducers. With a rotameter, the calibration of orificemeter was checked for water flow only. By a gravimetric method, LSCs were measured.

Sand-water mixtures were used to get on-stream velocity, particle size, and concentration [37]. Upward flow of mixture was in a 2.5 cm ID of perspex vertical pipe. Concentration and velocity ranges were 1.0x10-4–1.0 % w/w and 0.5-3.0 m/s, respectively. It was realized that, the particle size and concentration had significant effects on the results. In the experiments, two 5mW He-Ne laser beams were used. Solids in the mixture were continuously agitated. Laser light scattered by the solids was taken by a photodetector and the resultant electric signals were autocorrelated. Then the relationship between the size, concentration, and velocity of flowing solids was obtained. The difficulties in the on-stream measurement of particle concentration and size were reported as:

1. Physical characteristics of slurries are not understood clearly,
2. Definition of the measurement parameters is not enough,
3. The nature of the on-line measurements is not easy,

4. The operating conditions of the equipment are demanding.

Instantaneous local solid concentrations were measured by a conductivity probe, when there is mixing in the electrolytic solution [38]. They searched the effects of volume fraction and solid size on the concentration signals. Concentration signals gave information about the mixing time and mixing mechanism of the solution. Turbulent flow regime was studied. At the center of the pipe, there was copper at the top and platinum wire at the bottom. By sharpening the wire tip, the desired spatial resolution could have been arranged. The tip of the sensing electrode was 190 μm in diameter. For calibration, the concentration range of 0 to 0.03 M NaCl solutions were used. Errors might have been caused from the change in temperature or electronics. The resistivity was about 104 Ω. CaCO3 particles with the density of 2700 kg/m3 were used as the solid material. The effect of particles on this measurement was found to be dynamic. Fluctuations in the conductivity signal were arised from the presence of solid particles. If solid volume fraction was lower than 5%, the effect of the solids on the instantaneous electrolyte solution was diminished. The spatial resolution and frequency response of the local concentration signal was used in this method. Therefore unmixed mass eddies could have been found. The studied conductivity probe had one large and a small electrode. The small one was the sensing electrode. The spatial resolution of the probe was provided by the sensing electrode. Frequency response range was 400-700 Hz and 10^{-4} cm^3, respectively. The concentration measurement of an electrolytic solution required the calibration of the conductivity probe. To do this voltage versus concentration of the electrolyte graph was plotted. By changing surface of the electrode, calibration curve would also change. The sensing electrode metal was the most important parameter that affected the time dependency of the calibration curve (drifting). Other factors were temperature, metal ions, frequency of the AC source, and spatial resolution of the sensing electrode [39].

Local solid concentrations were determined by a conductivity probe and sample withdrawal [40]. The uniformity of the samples depended on the particle inertia, structure of the flow, and particle

bouncing. Sampling errors caused from the sampling position, design of the sampling probe, bulk solid concentration and particle size were all studied. Particle size, bulk solid concentration, mixer rotational speed were the dependent variables for solid concentration profiles. Errors were significant when the size of the particles were larger than 1000 μm. The tested solids were sand particles. Concentration of sand particles was measured in a mixing tank. This tank was made of plexiglass with a diameter of 0.292 m, three different tip angles of sampling tubes were used. By a variable speed peristaltic pump, samples were taken. Sampling velocity range was between 0.3 and 3 m/s and sand particles were non-conducting solids. Calibration of the conductivity probe was needed. Sampling probe was inserted in the liquid medium and then a potential was applied to the two electrodes. So some current could have flowed. By increasing the amount of solids in the solution, resistance of the surrounding medium was increased. Concentration of solids could have been reached by measuring the voltage between these two electrodes. Solid concentration was changed from 0.05 to 0.35 % v/v. Polystyrene particles were the testing solid material having density of 1050 kg/m^3. Mean size of the sand particles were 82, 255, 410, 500, and 1000 μm. At the end of the experiments it was found that, sampling errors were raised from the sampling velocity and axial positions in the studied tank. The use of small diameter sampling tube enhanced the sampling errors.

A double cross-beam Laser method was developed to determine local particle concentrations for gas-solid suspensions in the turbulent flow regime along a horizontal rectangular duct [41]. Experimental study was carried out at von Karman Institute (VKI). Air was the gas phase. Solid particles were glass beads having 500 μm mean diameter. An LDV device was used to measure the mean solid velocity. Both single beam and cross beam methods were used to get the solid concentration distributions. Concentration and mean velocity of the particles were measured simultaneously at the same points between the upper and lower walls of the rectangular channel. Solid loading ratios of 1.25, 2.25, and 3.40 were tried.

A multiphase flow model was developed for settling, non-colloidal, and dense solid-liquid mixtures in horizontal pipes [42]. By this way concentration and velocity distributions were estimated. Some numerical simulations were performed. Results obtained from the derivations and experimental results were compared and consistent with each other. To derive the velocity distribution equation, the local volume-averaged time-smoothed mass and momentum conservation equations were used. Convective diffusion equations were used to obtain the concentration distribution equations. Also eddy diffusivity was added to the derivation. Two different pipe diameters were tested that changed from 4 to 49.5 cm. Solid particle size range was between 38.3 and 13,000 μm.

It was reported that if fine particles were not used as the solid material or if the suspension was a dense one or if the sampling velocity was high, some serious errors might have been produced during the particle size and concentration measurements [43]. An L-shaped sampling probe was used in the wall sampling to get the concentration and size distribution of solid particles. In this method, a small aperture is drilled in the wall of the pipe. Operation is simple here.

Concentration distribution of solid particles were obtained in a vertical pipe studying both downward and upward flows [44]. Concentration profiles of upward flow were opposite to those of downward flow, if small Reynolds numbers were studied. Radial concentration distribution of solid particles was obtained in the fully developed flow region through the vertical pipe. A hopper was used to fed the solid particles to the system. Internal diameter of 52 mm of a pipe was the test section. By taking photographs, concentration distribution of solid particles was obtained. To hinder any lens effect, a transparent polyacrylate plates were detached to the test section. The light source was a xenon flash tube for the photographic system. The photograph that was obtained from this system was divided into eleven equal sections and the number of particles was counted in each of these sections. Therefore solid concentration distributions were obtained. Different mean diameters of different solid particles such as

glass bead, urea resin A, B, C, D, and polystyrene were used in the experiments. In the vertical upward flow studies liquid velocity strongly affected the solid concentration profiles when glass beads or urea resins were used. Concentration of solids was high near the pipe wall, when low liquid velocities were studied. Concentration of solids decreased near the wall of the pipe as the liquid velocity was increased. The concentration of solids was found to be low near the pipe wall but increased toward the axis of the pipe when polystyrene particles were used as the solid particles, which had slightly higher density from water. These results were consistent with another study [45]. Concentration distributions were explained by the following forces:

i) Particle-eddy diffusivity is a significant factor when two-phase flows are considered. The value of eddy diffusivity increases with increasing liquid velocity. By this way Re_t (stream Reynolds number) rises. So the effect of particle-eddy diffusivity enhances. Therefore concentration profiles become smooth.

ii) Velocity gradient of liquid creates a force that acts on the particles suspended near the pipe wall. One example is Saffman's force. If particles are small, Saffman's force is valid.

iii) Anisotropy can cause turbulence in a pipe. This force is accepted as proportional to the square of the velocity. Also this force acts on particles through the axis of the pipe.

LDA was used to get the concentration and velocity profiles of concentrated suspensions in a rectangular channel [46]. Optical turbidity problems were prevented by closely matching the refractive indices of solid and liquid phases. There were some small mismatches of the refractive indices and some impurities in the solid particles. These caused the residual turbidity which created a Doppler signal when a particle passing in the scattering volume. The local volume fractions were reached by counting the Doppler signals in a definite period of time. Concentration profile showed a maximum near the center of the channel while velocity profiles were blunted. Experimental results and theoretical predictions were compared. Mean particle diameter of 89, 50, and 30 μm of monodispersed polystyrene

(divinylbenzene cross-linkage) were used in the experiments. Refractive indices were measured by a refractometer. Refractive index of the liquid phase was functions of temperature, and laser wavelength. The magnitude of the blunting of velocity profile increased with increasing particle concentration. The amount of particles was high in the center part of the channel. Local particle concentration was not uniform along the gap of the duct. Slip velocity between the particles and the fluid increased with increasing particle concentration.

2.2. Velocity

Solid-liquid food mixtures behaving as non-Newtonian fluids were discussed in this study [10]. A model of stratified flow through a tube was developed. Rheological features of the fluid and solids loading affect the velocity profile of any phase. In stratified flow, local particle concentrations and velocities were different and formed different regions. A homogeneous flow model was adapted to a heterogeneous one. Particle diameter was 0.01 m and both density of the fluid and solids was 1000 kg/m^3. Manipulated variables were slip velocity, solids fraction, and inter-fluid heat transfer coefficient. Flow was assumed to be one-dimensional.

Operating velocity of a mixture should surpass the terminal settling velocity of the largest particles by a factor of 4-5 in the vertical coarse-particle pipe system designs [18]. If this is achieved, then pressure drop of the system can be found as if the single-fluid case. This research was made to get stable and safe operating conditions for the vertical transportation of mineral-water mixtures. Increasing interest on hydraulic transportation of minerals and ores directed the author to perform this study. Size, density and concentration of the particles are the key parameters for such systems. Experimental studies about the effects of turbulence on the settling conditions of particles were performed [18]. Mineral-water mixtures were used to get rid of the effect of turbulence, vertical crushed granite particles of 10-15% by volume were transported in a vertical pipe in upward direction. True transportation case was

considered. Experimental set-up consisted of a sampling tank, a hoisting pipeline, a pump, a motor, a mixing tank, a return pipe, and a timed-sampler. A 10 m length vertical pipe having an inner diameter of 0.094 m was used in the experiments. Flow was controlled by a pump during the experiment. The range of the size of the particles was between 1mm to 30 mm. Also pipe diameters of between 0.1-0.3 m were considered in this study. Irregular shape of crusted granite particles decreased the terminal settling velocity. For example, if cube shaped particles were used, terminal-settling velocity was decreased by 50%. Conservation of mass rules were utilized and steady state conditions were taken into account.

Upward flow of ceramic spheres in a vertical 20 m length pipe with 0.2 m of diameter was studied [47]. The ceramic spheres were 13 mm in diameter. He reported that slip velocity was approximately equal to the terminal settling velocity of solids, at low water velocities. Nevertheless, relative motion was decreased at higher velocities. In his experiments, solid density was 2300 kg/m^3 and solids had a concentration of 3.8% v/v. Average mixture velocity was about equal to the water velocity at low solid concentrations. Results of the experimental work showed that the terminal settling velocity indicated the relative motion of single particles. Water velocities were three times greater than the settling velocity. As velocity increased, slip was decreased. With the help of a radioactive tracer technique, velocity of spheres was determined.

Industrial plants that transport coal and ores verified that operating velocity should be higher than twice the terminal settling velocity of particles [48]. Most of such plants operate at the condition of negligible relative velocity between the constituents. The uniform velocity of the particle due to the effect of gravity is called the terminal settling velocity. This is valid for a single smooth sphere that is non-rotating. The standard drag curve explains the relation between the drag coefficient and the particle Reynolds number. Particle shape, particle roughness, rotation, and boundary surfaces affect the motion of particles in still fluids. For example, irregular shape decreases the terminal settling velocity. It is important to know that the definition of

the terminal settling velocity is based on the assumption of neglecting the effects of turbulence. However, turbulence exists little or much, in reality.

Vertical upward transportation of solid-liquid mixtures was investigated in a pilot plant [48]. Velocity, concentration, and energy consumption were the significant design parameters. These were searched for lead ore, different iron ores, complex ore, and perlite mineral. Particle sizes were large. Maximum particles were 8 mm in diameter. Solid density range was 2300-4200 kg/m^3. Concentration range was between 25%-40% v/v and velocities were observed between1.3-1.9 m/s for the mixtures of lead ore, iron ore, and perlite. He found the lowest possible flow velocity for a steady state stable operation, was about 4-6 times of the terminal settling velocity of the largest particles. Then the mixture behaved as if a homogeneous mixture. He said that total pressure drop could be reached assuming the solid-water mixture as a homogeneous Newtonian fluid.

Liquid-particle velocity profiles were obtained in a water suspension flowing in the upward direction [1]. It was observed that, the particles that were denser than the fluid was near the center of the pipe. Nonetheless, particles were flowing faster than the fluid near the pipe wall. With increasing flow rate, slip velocity between the particles and the fluid was decreased at the center of the pipe. However, it was also observed that, the particles that were less dense than the fluid flowed quicker than the liquid at all particle sizes. Volume fraction profiles of the denser particles proved that there was a uniform distribution if the flow rate was low. Nevertheless, if the flow rate was increased then coring occurred. There were almost no particles in the region of $0.8 < [(r/R)=\kappa] < 1.0$. Less denser particle volume fractions showed that there was a maximum close to the pipe wall, if the flow rate was low. However, with the increasing flow rate, profile was flattened. Particle velocity profiles were determined by a laser-Doppler anemometer.

Experiments on the upward flow of solid-liquid food mixtures were conducted in vertical pipes to obtain the particle velocity profiles

[9]. Delivered solid concentration range was between 0-10% by (weight/volume). Fresh carrot cubes with edge size range of 6-10 mm were the solid particles in the experiments. They were stored at 5^0C. A vertical tube of 44 mm in diameter was used. The carrier fluid was carboxymethylcellulose (CMC) solution. Carrier viscosity range was 0.3-0.8% CMC solutions. Density range of solid particles was 1016-1030 kg/m^3. Experiments were performed at the steady state. At the end, carrier viscosity, particle size, and particle concentration effects on the velocity profiles of particles were obtained. With increasing particle concentration, particles moved closer to the wall, number of particles were decreased at the center and velocity profile of the particles became flat near the center of the pipe. Also velocities close to the center line were diminished. As concentration increased, the shape of the velocity profiles became more dependent on the size of the particles.

Gas-solid mixtures are used largely in chemical and mechanical engineering areas. Some examples are nuclear reactor cooling, fluidized beds, dust collection, and pneumatic conveying. Hydrodynamic characteristics of dilute gas-solid suspensions were investigated theoretically [49]. Upward flow of suspensions was studied in a vertical pipe. By using a computer program at each solids loading ratio (SLR), the voidage, the external force caused by particle-wall and particle-particle interactions, and the relative velocity between the two phases were calculated. Experimental data and theoretical results were consistent with each other. In the theoretical analysis, all of the flow parameters were accepted as uniform along the radial direction. The macroscopic momentum balances were performed for both gas and solid phases through the axial direction. Iterations were made to determine the drag velocity. Solid and gas density, pipe diameter, and particle size were the parameters that govern the flow behavior.

Plug flow characteristics of pulp suspension were searched in a vertical circular duct [50]. Downward flow was considered. Local velocity and velocity gradient at the wall of the pipe were determined utilizing an electrochemical method. Pressure transducers measured

the pressure drop. The pulp suspensions were accepted as Newtonian liquid evaluating the relations between velocity gradient and shear stress, flow rate and pressure drop, experimentally. However, these pulp suspensions were different from Newtonian liquids considering the experimental relation between flow rate and velocity gradient at the wall of the pipe and measured velocity profile. Also a relationship explaining the radial distribution of viscosity was obtained. Measured and calculated velocity profiles were consistent with each other. This difference was caused by the different viscosity values of the pulp suspension at a radial position. The pulp suspension was a combination of potassium ferricyanide and potassium ferrocyanide electrolytes, ion exchanged water, and beaten hardwood bleached craft pulp.

An L-shaped sampling probe was used to get the velocities of both phases [51]. Cross-correlation method was utilized. Flow rate of slurry can be measured by ultrasonic Doppler meters, venturi flow meters, or magnetic flux flow meters. These devices give mean velocity values. On the other hand, local velocities are required for the theoretical analysis to find the velocity distribution. In the cross-correlation method the transit time between the sensor pairs displaced axially by a known distance is measured. 0.47 mm mean dimeter of sand-water, 1.7 mm of acrylic-water, and 4.4 mm PVC-water slurries were used in the experiments. Due to some kind of a boundary layer effect, probe failure was observed if the flow was laminar. Horizontal flow was studied.

Velocity profile of the fluid in a pipe can be found by drawing the graph of the local time-averaged axial velocity at one point from the pipe axis or wall graph. To have fully develop flow, the shape of the above plot should not be dependent on the axial distance from the entrance of the pipe [52].

A separated-phase flow model was used in an annular channel by means of vertical downward flow for liquid-gas mixtures [53]. Velocity distribution and temperature distributions in the liquid film layer and liquid film thickness were predicted. The studied heat flux

and mass flux ranges were between 6000 and 12000 W/m^2 and 500-1100 kg/m^2s, respectively. Thickness of the liquid film was about a couple of micrometers. Heat transfer coefficient ranged between 2800-7800 W/m^2K for liquid nitrogen. It was boiling in the annular channel. Also heat transfer coefficient and pressure drop along the annular channel were obtained. The calculated heat transfer coefficients were 29% lower than the measured values. Heat transfer coefficient and pressure drop increased while the gap of the annular channel was decreasing and the mass flux was increasing.

Videotaping particles were used in suspended form in sodium carboxymethylcellulose (CMC) solutions in a transparent holding pipe [55]. This apparatus used in the experiments was similar to the commercial aseptic food processing units. Log-normal models could have explained the velocity distribution of food particles. Particle-fluid interactions were important at the studied concentrations in that work. Solid phase was polystyrene particles having 0.95 cm of mean diameter and 1044.5 kg/m^3 density. Motion of the particles was recorded on videotape and analyzed. Three different carrier viscosities (0.2, 0.5, and 0.8 % CMC concentration), three pump speeds (100, 120, and 140 rpm), and four different particle concentrations (0.2036, 0.4072, 0.6108, and 0.8145% v/v) were tried. At the end, it was seen that the most important factor affecting the velocity distributions was the viscosity. If viscosity was low, fastest particle was present at the center-line. Also there were no particles moving faster than twice of the mean velocity.

Some differential equations were used to reach the velocity and concentration distributions of slurries [12]. These had quasi-uniform characteristics. To interpret the interaction between the solid particles and the pipe wall, a *'supported load'* concept was used. It was seen that the size of the solid particles affected the mixing effects, turbulent shear stresses, and particle interactions. Mean diameters of 0.165, 0.48, 0.52, and 13 mm of sand particles were tested. Water was the flowing liquid in 50 and 500 mm diameter pipes. Tried concentration values were less than 40 % v/v. Numerical and

experimental results were compared in terms of concentration, velocity, and head loss, and the agreement was well.

A coal-liquid slurry was used to test the acoustic cross-correlation method [54]. Velocity profiles were reached by this way. Different conditions (i.e., location, rotation, or frequency) were studied to verify the method and results were satisfactory.

2.3. Pressure Drop

In the work, laboratory rheological data was scaled up with the help of the given equations [56]. They were valid for both the laminar and the turbulent flow cases. This method was applicable for also concentrated suspensions. Concentrated solutions were mostly pseudo-homogeneous. In other words they were essentially homogeneous. They were non-Newtonian fluids and their properties were measured by various viscometers in laboratories. These mixtures had relatively small particles (below 100 μm in diameter). Their yield stresses wee measurable. Some of the examples were clay, limestone, iron ore, bauxite, or coal. To predict friction loss, some rheological models of homogeneous flow were used for Bingham plastics and Power-law fluids. They had high shear. The obtained method was compared with the literature data, in different pipe sizes and flow rates. Friction loss estimation was made for Power-law and Bingham plastics using their specific model formulae.

Pressure drop and critical velocity were calculated for slurries [11]. Also, their computer program was able to obtain the pressure drop values for single-phase gas and liquid pipelines. Correlations were appraised with a BASIC computer program. They defined the ‘critical velocity’ as the fluid velocity, below which accumulation of solids starts (for horizontal flow). Normal flow velocity prevented the settling of the solids (in vertical pipelines). Turbulence prevented the settling of solids (in horizontal pipelines). Concentration of solids could affect the critical velocity and pressure drop in slurry flows. In that paper, pressure drop correlations were evaluated at four different

flow regions: flow with a stationary bed, saltation flow, heterogeneous flow and homogeneous flows.

Pressure gradients were estimated for turbulent flow of slurries in pipes, horizontally and without deposition [20]. Heterogeneous suspensions were taken into account. Also to get critical velocity, an equation was derived. To be able to obtain the pressure gradients for slurries flowing in horizontal pipes more correctly, slurries were divided into two main groups: 'settling' and 'non-settling'. In non-settling slurries, the mixture was assumed to behave a homogeneous fluid and the settling tendency of the solid particles could be neglected. However, settling slurries were considered as two-phase mixtures and settling velocity of solids could not be ignored. In this paper, particles were assumed to be in a narrow size range and there was a single settling velocity. The critical velocity was defined as the transition velocity between the heterogeneous suspension and the sliding bed regions. Pressure gradients were predicted based on the mechanism of energy loss.

A model was derived for flow patterns and pressure drop for horizontal slurry flow in pipes [57]. There was two-layer. At the bottom of the pipe there was a stationary or moving bed. However at the top, heterogeneous mixture was present. They assumed that there was no slip between the solid and liquid phases in the model. To investigate the effect of no slip assumption, this work was performed.

It was assumed that there was no relative motion between the solid and liquid particles, axially [58]. This was valid for the upper part of the mixture. There was turbulent mixing. On the other hand, for the lower part, this assumption was unrealistic. Since, wall friction affected the solid particles in this case. The liquid moved faster than the solid particles, actually. Therefore a relative velocity was present between them. This fact added an additional unknown phrase in the Ergun equation. At the end, the studied model was modified. According to this modification, it was reported that the no-slip acceptance was a valid approximation. The old model decreased the computation time. The results obtained from both of these two models

were compared and it was seen that the difference was small.

Ion exchange, catalytic cracking, adsorption, hydrometallurgical operations, sedimentation, bioreactors, classification and crystallization are some of the examples for industrial usage of solid-liquid fluidized beds (SLFBs). To know the value of pressure drop is significant, since the performance of the equipment depends on the pressure drop. Heat and mass transfer rates could be estimated by the help of pressure drop. Also energy dissipation rate is determined by knowing the pressure drop value [17].

Pressure drop was measured in a solid-liquid fluidized bed (SLFB) having 78 mm ID [17]. The bed voidage was changed from 0.4 to 0.9. Mean particle sizes were between 0.55 and 3.1 mm. Experimental results and model predictions were in a good agreement. The SLFB operated turbulently when Reynolds number was greater than 1000. By making energy balance, hydrodynamic aspects could be analyzed in this flow region. Net force of buoyancy and gravity balanced the friction force between the liquid and solid particles in fluidized beds.

A mathematical model related with the pressure forces was developed for dispersed fluid-fluid and solid-fluid systems [59]. Results were compared with currently used engineering treatment and found to be consistent if the volume average pressure and pressure near the solid particles or liquid droplets were not so similar. Engineering treatment worked accurately, if there were large differences in velocity between the phases. Also the mathematical model was developed to consist more viscous forces. Volume average pressure and pressure drag were the two components of the pressure in the continuous phase. Therefore one of them acted on each particulate matter like buoyancy force and it had slow variation. The latter one added to mass forces and it had rapid variation.

A circular pipe of 40.9 mm diameter was used to get pressure gradients [60]. Water and ethylene glycol solutions were the liquid phase. Mean diameters of 1.8 and 4.6 mm of spherical glass particles

were the solid material. Solid concentration range was between 9% to 38% v/v. Pressure gradients were evaluated in terms of particle friction factor.

2.4. Friction

Hydraulic transport devices can be designed properly when the measurement about solids could be performed accurately. Volumetric solid concentration, pressure loss, pipe wear, and cross-sectional mean velocity are important for solid-liquid suspension flows. To be able to obtain energy cost, it is necessary to know the pressure loss due to friction. The problems that would be encountered can be stated as follows: density distribution, grain size, terminal settling velocity, hardness, shape, attrition character of particles, roughness, and surface hardness of the pipe used. The measurements related with these parameters were performed [61]. To get a design procedure with reliable data, some experiments were conducted using solid-liquid mixtures in full-scale equipment. The major aim was to determine the pipe diameter and pressure loss for the transported material. Steady flow conditions were provided. A jet pump was used for the slurry transportation. The experimental rig was able to measure concentration and volumetric flow rate of the solution, pipe wear, pressure loss, and deposit velocity. The experimental set-up was a close-loop system, i.e., discharge end of the pipeline was connected to the slurry tank. Jet pump was provided to avoid attrition of pump.

Turbulences and instabilities could be brought about by a sudden change in the steady state flow [47]. Friction force was measured directly, on the pipe wall. He found that as the number of articles touching the pipe wall increase then the energy loss was also increased owing to the mechanical friction.

Results were obtained from correlations for pressure drop and hold-up with some experimental data, considering horizontal flow [62]. Also a new analysis was developed to get frictional pressure drop. At the end it was found that, Lockhart-Martinelli correlation was not

consistent with the selected experimental data about pressure drop. Correlations were not realistic.

A correlation was developed to find the mixture friction factors for upward flowing gas-solid systems [63]. Air was the gas phase. This new correlation was an extended form of the previously reported one for solid phase friction factor [64]. It was not necessary to have any pressure drop data to be used in both of these correlations. Therefore, it could safely be used in the systems where pressure drop measurements were difficult. Gas phase volume fraction, mixture friction factors, drag, solid density, solid phase friction factors, velocity of solid phase, and density of solid phase colud be obtained by the devised procedure.

Correlations were developed to obtain frictional pressure drop [65]. Upward flow through a packed bed of a gas-liquid mixture was studied in bubble flow, spray flow and pulse flow regions. Flow rates of gas and liquid affected the two-phase pressure drop differently in the different flow regions when developing the correlations. From literature more than 600 experimental data were taken and used in this study.

2.5. Annular Flow

Newtonian fluid flow was studied in concentric and eccentric annuli in the fully developed flow regime to obtain the mean velocity, and the corresponding Reynolds stresses Reynolds numbers ranged between 8900 and 26,600 [66]. Also a weakly electric shear-thinning fluid was studied at Reynolds numbers of 1150, 6200, and 9600. Eccentricity values were 0, 0.5, and 1.0 and the diameter ratio was 0.5. Friction factors were higher in concentric annulus than those in a smooth round pipe. The fluctuation levels were less in non-Newtonian flow than those in Newtonian flow.

Air was used as the working fluid in three different radii ratios of the vertical concentric annulus [67]. Fully developed flow case was studied. Shear stress distributions were obtained. Hot-wire

anemometry was used to find the location of zero-shear position. The results showed that the maximum velocity and zero-shear surfaces were not consistent with each other. Radii ratios of 0.088, 0.176, and 0.396 were tried. Shear stress equations were derived by a force balance at the zero-shear position. Also friction factors were determined.

Experiments were performed for upward annular flow of air-water mixtures, in a circular pipe of 31.8 mm in internal diameter and 10.8 m in length [68]. During the experiments, wall shear stress, film flow rate, film thickness, pressure gradient, disturbance wave velocity, and frequency were measured at different liquid and gas flow rates.

The importance of residence time of fastest moving particles in aseptic food processing system was investigated [69]. It is important that the slowest particle should not be overcooked when fastest particle is sterilized. Number of data about vertical flow of food systems is not sufficient. Vertical upward flow of neutrally buoyant alginate particles was examined in carboxymethylcellulose (CMC) solutions. 48 mm ID of a circular pipe was utilized. Mean diameter of the solid particles was 5 and 10 mm. Solid fraction range was 16-55%. Mean mixture velocities changed between 77 and 230 mm/s. 29-422 mPa.s mean apparent viscosity of carrier fluids were experimented. Tube Reynolds number was between 8.7 and 381. Visual traces and Hall effect sensors were used to measure the particle passage times. At the end, four different particle passage time distributions were detected. Minimum passage times were mostly affected by the concentration of solids. An annular particle region existed when particle Reynolds number was less than 0.08. This annular region created the maximum passage time.

The annular-core behavior of two immiscible liquids were studied in a horizontal pipe [15]. All possible flow situations were analized. Pressure drop and in-situ hold-up values were compared with the experimental data, and the results were in good agreement. Core-annular flow behavior was studied to be able to save power and to

reduce pressure loss in viscous oil transportation. Most reduction in pressure drop can be obtained by using a highly viscous fluid at the central core and less viscous liquid forming a uniform annulus near the inner side of the pipe wall. Simple expressions were derived to find the pressure drop.

Experiments were carried out in smooth concentric annuli having radii ratios of 2.88, 5.62, and 9.37 in fully developed unidirectional turbulent flow regime [70]. Reynolds number was changed from 6,000 to 90,000. Fluid was air. Velocity profiles were obtained. It was reported that the friction factor did not depend on the radii ratios. Also static pressure drops were found.

An analytical method was used to estimate the pressure drop in laminar flow at the entrance of the annular ducts [71]. Velocity distributions were obtained. Flow development in parallel plates was similar to that in annular ducts for ducts having radii ratios less than unity.

The parameters of heat transfer increment for water-feldspar mixtures were determined [72]. Fully developed upward flow was in a vertical annulus. At the end of the experiments it was found that flow Reynolds number and Prandtl number strongly affected the increase in the heat transfer rate. Also feed solid concentration, equivalent diameter to particle diameter ratio, and the aspect ratio of the annulus were the other factors. Flow properties of liquid-solid and liquid-gas mixtures were not investigated much in the annulus because of the complex geometry of such systems.

2.7. Isokinetic Sampling

Horizontal slurry flow was studied taking samples isokinetically [73]. The liquid mixture consisted of water-sand. It had 18% v/v solids. During the experiments, first isokinetic conditions were provided, then, isokinetic velocity and local concentrations were measured. Finally, particle size distribution analysis was made. A magnetic flow meter measured the velocity in the sampling probe. At

the end, it was reported that, the predicted velocity profiles and measured velocity profiles were close to each other. Also there was no need to use a different velocity tube, when the local concentration was in excess of 50% v/v. In these ranges, sampling probe accurately worked. This sampling probe was an L-shaped tube. Isokinetic sampling condition was satisfied when the undisturbed local velocity was equal to the velocity at the sampling tube. The sampling probe, also checked the stagnation pressure in it. Therefore, it could have measured the free stream velocity. This meant that there was no need for another tube to measure the local velocity. Isokinetic sampling method could also be used for two-phase liquid-gas flows [74].

It was reported that when electrified sampling probe and particles come into picture, isokinetic sampling technique did not give accurate results [75]. When large probes were used, electrostatic effects were less significant. Horizontal flow case was considered in ducts. They used inertia parameter also. Static electrification was large when smaller probes were used. Analysis of dust-laden gases was usually made isokinetically. However concentration was different from the concentration obtained by isokinetic sampling. If the diameter of the sampling probe was less than 0.5 cm, then errors became significant. Also numerical calculations were performed.

Concentration distribution of spherical particles were obtained in horizontal flow [22]. They derived a general equation for the prediction of vertical concentration distribution for slurries. This was valid for a wide range of particle size even if the concentration was high. If the velocity was small at steady state conditions, then particle segregation could be observed. The particles used in the experiments were 2.5 to 5.0 mm in diameter. The flow loop used in the experiments was about 22 m. Test sections were made of smooth acrylic plastic. A rotary pump was use and there was not any particle attrition. The volume of the stainless steel mixing vessel was 0.12 m^3. It provided a uniform distribution of particles. Flow rate was measured by a turbine type of flow meter. Providing the necessary isokinetic situation, samples were withdrawn. An L-shaped stainless steel tube took the sample. Outer diameter of the tube was 6.35 mm. A precision

dial indicator controlled the vertical position of the probe. The withdrawn sample was put in a 300 cm^3 plastic bottle. This bottle was put in a plexiglass vessel. The flow rate of sample was controlled by a graduated cylinder. A three-way ball valve determined the direction of flow. Using a regulator constant back-up pressure was adjusted. After equating the local velocity in the pipe and velocity of withdrawal, only five to seven samples were taken because of the difficulty in adjusting the sampling rate. Standard sieves were used for the analysis of the particle size. Small anion exchange resins beads were the testing plastic spherical particles. A transformer oil (diala) kerosene, and a 33% volume kerosene+67% diala mixtures were used. The data recorded during experiments fitted the literature well.

Local solid concentrations and local phase velocities of an air-solid particle system was measured in a horizontal pipe, isokinetically [25]. The pitot tube was used also as a sampling probe. This pitot tube was suspended with needle bearings to the pipe. Pressure, drag, and momentum were the forces acting on this probe. The operation principle of the isokinetic sampling probe was explained and some experimental data was obtained.

An image system was studied [76]. There was a droplet collection system, an image processing box, and an isokinetic sampling probe in the experimental set-up. Droplets were counted by the image processing software. This software also helped the size measurement of the droplets. Also droplet back-up, droplet deposition in the sampling probe, and coalescence were investigated during the experiments. Sampling probe was put parallel to the fluid flow stream. When the static pressures inside and outside of the probe were equal, then isokinetic condition was accepted to be reached. To prevent droplet deposition at high droplet sizes, a larger sampling tube was preferred. In every measurement, isokinetic condition was reached.

True local velocity could be measured by ‘isokinetic sampling’ method [77]. If solid concentration was low, then pitot tubes could make measurements accurately. At high concentrations, velocity

measurements could be made if the particle size in the aerosol was quite large.

In isokinetic sampling method, it was necessary to match the sampling velocity and the velocity of original undisturbed local flow, which was the velocity before the probe insertion (no-slip between the phases). By this way, direction and original rate of flow did not change.

Isokinetic Sampling: If true suspension velocity was equal to the sampling velocity it was called isokinetic sampling. When isokinetic flow condition was achieved, pressure gradient became higher inside the probe. Sampling accuracy could change according to the particle concentration, turbulence, probe size, and adhesion of particles [78].

2.6. Methods

Two-phase flow sampling methods were presented [79]. The detailed flow structure could not have been obtained since the derived theoretical models were not sufficient. Data about the two-phase flow structure was needed: to predict the critical heat flux in nuclear reactor coolers, to estimate the pressure drop and void fraction values, to see erosion problems in wet-steam turbines, to find sonic velocities in two-phase mixtures, to find the reaction rate and mass transfer in two-phase chemical reactor.

Sampling was performed in two ways by inserting a sampling probe directly into the flow, or property of the fluid was determined from outside of the flow [78]. One-phase flow instruments do not give reliable results when used in two-phase systems. For instance, pitot static tubes give local velocity of the fluid in one-phase systems. However, velocity and impact pressure relationship is complex when the flow is two-phase. Now, the flow is unknown and relative velocities are unknown. Also turbine type or deflection type of flowmeters or hot-wire anemometers are difficult to investigate in two-phase mixtures. Data reduction can be applied to homogeneous flow or constant slip ratio systems, but the validity of this method is

not proved. Data acquisition method can be used when it is necessary to equate two pressures but accuracy is not proven yet [79].

2.7.2. Concentration Measurement Methods

CONCENTRATION of SOLIDS: Concentration of solids is measured in terms of mass, not volume, due to the cheap operational installations. Mass concentration is defined as the ratio of total mass of solids in the slurry sample to the total mass occupied by the sample [80].

Sampling methods and attenuation of radiation or light methods are used to obtain the concentration of solids in a suspension. Particle flux or time average concentration is found by sampling methods. On the other hand, average concentration can be obtained at different positions by the radiation methods. Velocity distribution and concentration profiles are affected by the shape of the pipe [33].

In-situ concentration: is defined as the transport concentration where there are solid particles flowing in a pipe. Liquid and solid particles flow with different velocities in the pipe. As a result it is assumed to exist a slip velocity between liquid and solid particles ([51], [80]).

Delivered concentration: is defined as the concentration at the exit of the pipe where the velocities of the liquid and the solid phases are the same [80].

In-situ concentration is greater than the delivered concentration, if solid velocity is less than fluid velocity. Horizontal heterogeneous pipe flow and counter-gravity flow of large particle mixture are some of the examples for this type of flow [80].

The methods that are used to measure the concentration of solids rely on the concept of being able to obtain a specific property that is different for both of two phases. This property of the mixture depends on the concentration of the solids. If this property is known, then solid concentration could be reached by the help of a calibration curve. This property may be density, electrical conductivity, or

dielectric constant. If solids concentration is so low that is not enough to reach a critical value, then the result of this measurement would not be accurate. Solids concentration measurement techniques in terms of volume can be categorized into three groups [61]:

The methods *in the first group* give the average concentration over a large volume such as in a long pipe. Some examples are vertical counter meters, inclined and straight pipe concentration meters.

Counter flow-meter: to be able to get the delivered concentration of slurry, volumetric concentrations of upflow and downflow are assumed to be equal to each other. It can measure the concentration with 1% error. When the mean velocity of the slurry is greater than the settling velocity of the particle, then accuracy would be well [33].

Inclined pipe concentration meter: It is used to find the local solid concentration in heterogeneous suspensions. This device has two-equal length of pipe sections. One is horizontal and the other has a small inclination of about 5^0. Pressure loss due to friction is about the same in these two segments [61].

Straight pipe concentration meter: It is a simple device to measure the concentration accurately. It works well upto the pressure of 20 bar. To get local solid concentration weighing method is used. To be able to make measurement with this equipment, the density of solids should not be close to the density of water. Otherwise accuracy of the measurement would be decreased [61].

In the second group, average concentration is measured along a line. Collimated γ-ray beam absorption [81], ultrasonic methods [82], autocorrelation of the scattered laser light [37], and conductivity method are some of the examples for this group [61].

Nucleonic meters: these are of two types:

1. *Gamma-ray density meter:* a gamma-ray source and a pressurized ionization chamber are attached at opposite sides of a pipe. The absorbed radiation is determined by the thickness of the pipe wall and the density of the slurry. Pressurized ionization chamber obtains electric current from the radiation. Accuracy of this device is ± 1% [33].

2. *Neutron moderation meter*: This device is clamped to a pipe. It is made up of a radioisotope source of fast neutrons, a detector for slow neutrons, and a reflector made of graphite. The hydrogen in the water collides with the fast neutrons and makes them to slow down. Then the probe can detect the slowing ones. Therefore, the volumetric concentration of water might be obtained. Accuracy is ± 1% [33].

Electrical conductivity-meter: the cross-sectional area shared by the solids and the liquid is determined by the change in conductivity. Two cells measure the conductivity difference of the slurry and the liquid. Then, volumetric concentration of the solids would be measured. This instrument can measure with ± 2% accuracy [33].

Tomographic methods are largely used in medical applications. Also, it is a reliable technique for many industrial purposes. This is called as process tomography. Some examples for tomographic methods are as follows: electrical methods, X-ray, γ-ray, and positron emission tomography (PET) systems, magnetic resonance imaging (MRI), ultrasonic techniques, optical, and infrared tomography. Some factors affecting to choose a method are: the spatial and temporal resolution of imaging, cost and physical dimensions of the equipment, physical properties of the components would be used in the measurements, human resources for operation and personnel potential hazards. Electrical tomography is a fast method, and its operation is simple. Therefore, it is a popular technique used in process design and control. However, the major disadvantage is low spatial resolution (i.e. 3-10% of a pipe diameter) of these devices. Cross-sectional profiles and velocity distribution of solids were obtained from tomographic data [83]. Electrical capacitance tomography (ECT) and electrical resistance tomography (ERT) were used in the experiments.

The distribution of electrical conductivity in a substance can be reconstructed with an ERT. Current injection method is used between one pair of neighbourhood electrodes. Then, the differential potential of the remaining ones is measured. This is made many times until a full electric field rotation is reached. The typical frequency range is between 20-50 kHz in an ERT device. Similar partial differential equations are used for both ECT and ERT systems, adopting the theoretical parameters into experimental results in a forward problem actually. This can be seen when calculating the capacitance inside the sensor. By arranging the boundary conditions this problem can be solved. Also to obtain parameters from experimental results is an inverse problem.

In the third group, average concentration is evaluated over a small volume. This category includes isokinetic sampling, and photographic methods [33].

g-ray absorption or tomography: are non-intrusive methods. 3-Dimensional spatial resolution of solids concentration [84] can be obtained by these methods, however, time resolution results do not give satisfactory results. These are expensive methods. Some critical safety precautions are compulsory. Instrumentation is large and cumbersome [85].

Solids concentration was measured with an economic and basic method in slurry lines [13]. Working principle of the instrument was based on the slurry resistance. There are some studies about the simultaneous measurement of particle size, concentration, and velocity: [86], [87], [88], [89], [90].

Concentration and velocity of solid-liquid mixtures flowing in horizontal and vertical pipes in the upward direction were measured [28]. Ion exchange resins and glass beads were used as the solid materials. Mean diameter of these particles was between 321 and 1840 μm, and density range was between 1190 and 2500 kg/m3. 1.92, 3.00, and 5.42 m of tube diameters were used. Using local particle concentration and velocity, average particle velocity was calculated.

Concentration and velocity distributions were found by a conventional photographic technique for vertical upward and horizontal flows. Two new developed laser methods were used for vertical upward flow. One method was for local concentration and the other was for local velocity values. At the end, it was seen that laser methods were more suitable than photographic method to get local particle concentration and local velocities.

Three different techniques were compared to find solid concentration of slurries [91]. These methods were sample removal, gamma ray absorption, and slurry resistivity. Gamma ray absorption could give accurate results when the mean solid concentration was high and density difference of the phases were very different. Sample removal was generally used when the sampler was tapered or thin-walled; slurry resistivity was used to find the concentration of solids by Maxwell's equation. Experiments were carried out in a horizontal pipe. Sand and polystyrene particles were the solid phases. Water was the liquid phase. In the sample removal method, an L-shaped tube was used. Also local particle velocities were found by the same tube. In the conductivity meter, concentration and velocity were measured by the same probe. The methods gave similar results when concentration was low. If concentration was intermediate, conductivity probe gave higher results around the bottom of the pipe. When concentration was high, conductivity probe gave higher concentration results than those by the gamma ray method. At the end, it was concluded that, the most reliable method to measure concentration of solids in mixtures was the isokinetic sampling.

It was suggested that to find local solid concentration for electrolytic turbulent flow using a conductivity probe was a proper technique [39]. The drifting behavior in NaCl solutions of conductivity probes was affected from the ion concentrations in water, resolutions of space, and temperature, mainly. Evaluating these characteristics, errors in concentration measurements were tried to be minimized. In this study, a low concentration of NaCl solution was the electrolyte. A Pt/Rh-wire in the ratio of 9/1 was used to construct the sensing electrode. Drifting behavior was tried to be decreased along

measurements. Also the response of the probe against the rapid concentration changes, were observed. There were two electrodes in the conductivity probe. The large electrode had about 5 cm2 surface area and the sensing electrode had about 0.001 mm^2 surface area. The electrodes were connected to an AC power supply by a resistance. To prevent electrolysis, AC was used. A sensing electrode having small surface area was always preferable. The Platinum/Rhodium wire was put on in a glass tube having 5 mm inside diameter. One end of the tube was sharply shaped. The tip diameters of 100 microns and 300 microns of two probes were used in this study. The diameter of the tip determined the space resolution. Electrolyte concentration was measured around the metal tip of the sensing electrode. Space resolution meant the volume of the sphere on the tip. Calibration curve of the conductivity probe was plotted as voltage versus concentration graph. Known concentrations of NaCl solutions were used to obtain the voltages. With increasing concentration, voltage was decreased. Time dependency of the calibration curve was called as 'drifting'. The factors affecting drifting were the frequency of the AC power supply, space resolution of the probe, cleaning method of sensing electrode, change of temperature in the solution, and metal ions in the tap water. At the end of the experiments, it was concluded that softened water should be preferred as the solvent. Small probe tips had large drifts. If the frequency of AC supply was decreased, drift was increased. The most proper one was 30 kHz. Increasing temperature increased the drift.

2.7.3. Velocity Measurement Methods

Flow measurement can be divided into three main groups:

i) Velocity-Flow measurement: Velocity-flow measurement devices give results that are proportional to the average fluid velocity. Multiplying it by the metering area, volumetric flow rate could be obtained. To find the average velocity of the fluid, the following metering principles could be applied: target, variable area, fluid turbine, fluidic, ultrasonic, and vortex shedding.

ii) Volumetric-Flow measurement: They are so called positive displacement flow meters. Volumetric flow rate is obtained by entrapping a known volume of a fluid. Some volumetric flow meters are nutating disc, oval gear, rotary, helical gear, and oscillating piston.

iii) *Inferential-Flow Measurement:* This type of measurement uses an empirical correlation related with the volumetric flow rate and the differential pressure along the meter. Some of the examples for differential pressure flow meters can be given as; pitot tube wedge, orifice plate, venturi, and nozzle.

Point velocity can be measured by pitot tubes [92]. Impact port part of the pitot tube is hitted by the fluid and its velocity becomes zero. Also velocity (kinetic energy) is converted to pressure head (potential energy) at that time. Both the velocity head and static pressure are present at the impact port. Velocity head is the pressure difference between the static pressure and impact pressure at the same point.

Pitot tubes can be used for both liquids and gases. It has simple operation and its performance is good. Design literature and references are available since pitot tubes have been used for many years. Since the tube diameter is very small, therefore this method can be accepted as less intrusive than the other sensing methods. For this reason, accuracy is affected less by this method. The operating temperature is dependent on the material of the pitot tube. The blockage of the pressure transmitting parts is the failure that is encountered mostly. By removing the blocked parts and cleaning them, this problem could be overcome. Overranged flow conditions can not give damage to the pitot tube. These are the major advantages. On the other hand, there are also some drawbacks: the square root of the differential pressure is a limit for velocity. As the flow rate (also pressure) decreases, accuracy decreases. Fluid density is an important factor since it affects the output so it should be measured carefully. Pitot tubes are not suitable for dense suspensions since particles might cause clogging in the pressure transmitting

parts. The results that are obtained from the pitot tube measurements are not linear [92].

An annular tube with static pressure ports is present on a pitot-static tube. Velocity head is the difference in the pressure between the two ports [92]. There are two pressure tapping holes to sense the static and total (stagnation) pressure on a pitot-static tube. Static pressure is determined by the static tapping holes, but the total pressure drop is sensed at the probe tip. First the differential pressure signal is detected and then the two concentric tubes transmit the pressure signals. Lastly, the pressure signals arrive the differential pressure sensors, which is placed at the end of the pitot probe.

POINT SOLIDS MASS FLOWMETERS:

Impact Meters: Mass flux of solids can be found by inserting an obstacle in the flow. The exerted force on this obstacle is measured. Impact meters were studied here [93], [94]. If large particles are present, force of impact can be counted. The effect of large particles was studied [1]. Some examples for impact flow meters are: strain gauges, sensitive total flow meters, micrometer-positioned electrical contact, and optical microscopes [78].

Optical particle counting: Particles are counted by a light beam through a very small volume, in this method. For high concentration mixtures, it is not a suitable method, since there may be more than one particle crossing a light beam. A mass flowmeter was developed [95].

Acoustics: Flow instruments should endure vibration, erosion, corrosion, and should be able to operate at high temperature and pressure. Also the operation of them should be easy, have inexpensive cost, and be well built. Attenuation, velocity, and scattering are to be the measured values in acoustic methods for solid-liquid mixtures. Range of frequency, signal processing, and geometry of the transducer are the significant experimental variables in the

measurement optimization. Processing operating frequency increases the resolution in particle size measurements. Attenuation and frequency squared are inversely proportional to each other [95].

Hot-wire anemometer: In this method, a particle hit the hot-wire anemometer. Then the signal from the anemometer is used [96].

Electrostatic flow meters: It was suggested that mass flux of solids and current from the probe was proportional [1].

Counter flow meters: It is an U-shaped pipe. It measures the pressure through a definite length of a pipe in two sections. This equipment uses the equation of continuity for both two phases. According to the theory, head loss is equal to the static head plus friction loss caused by the flow. This method gives 15% error (provided flow rate is 0.016 m^3/s) in experimental results. Construction of this equipment is easy and fittings are standard. To be able to use the pressure transducers, flow should be at steady state, so the locations should be arranged carefully. This instrument measures both the concentration and velocity of the slurry [81].

Magnetic flow meter: The working principle of this equipment is based on the electromagnetism law of Faraday. This is true when the magnetic field over the detector-head tube becomes uniform. If the slurry has magnetic particles, then magnetic flow meter is not used. Because, magnetic field become stronger in such a situation, then induced voltage will change. The detector-head liners of magnetic flow meters are generally made of polyurethane, soft natural rubber or PTFE. Electrodes of such devices are made of Hastelloy, stainless steel, Platinum/Iridium alloy, or hardened K-Monel. The error percentage of such devices is ± 2%. Magnetic flow meter measures the velocity of a slurry [81].

Cross-correlation technique meter: This equipment determines the slurry velocity by measuring the transit time of a disturbance between two definite points. Solid concentration might be measured by an electrical conductivity transducer or an ultrasonic transducer. The

time mentioned above is measured with the help of a cross-correlator. To do this, the multiplication of the output of the downstream transducer and output of the time-delayed situation of the upstream transducer is taken. Then the result is integrated over a definite time. Accuracy is ± 2% of full-scale range [81].

LDV method uses the differences between the signal amplitudes and visibilities [14]. For instance, small particles produce LDV signals with smaller amplitude and higher visibility than the larger particles. Also it is accepted that, the intensity is the highest at the center and lowest at the edges of the measuring volume. However, intensity distributions are not equal; that means, an LDV signal from a large particle at the edge of a control volume might have smaller amplitude than a signal from a small particle in the center of the same control volume. This property makes the measurement not exact. LDV method is useful when having small concentration of solid particles (i.e. when mixture is sufficiently transparent). For opaque solutions with higher solid concentrations, there would be some problems. For example, scattered light might be restricted to reach the detector, since the laser light can diffuse in all directions over randomly distributed particles. To overcome this difficulty, a refractive index matching method may be used.

SOLIDS VELOCITY:

Radioactive tracer methods: Average suspension velocity might be determined by giving a pulse of air in the flow stream [97]. A radio-pill was used to observe the movement of a static bed [78].

Mass and volumetric flow rates of each the phases was measured in ducts [98]. Solid-fluid two-phase flow was studied. A Coriolis type mass flow meter and an inductive volumetric flow meter were utilized to get total flow rates. Individual ones were calculated by the known densities of the components. Water-sand particles were the studied mixture. 0.125 mm mean diameters of quartz particles were added to water to get the solid-liquid mixture. Solid particles

were present in suspended fashion in water due to the continuous stirring.

Coriolis flow meter: A U-tube measures the flow in the Coriolis flow meter. A driver and counterbalance provide the oscillatory angular motion in the tube. Oppositely flowing fluid in the opposite legs of the U-tube exposed oscillatory Coriolis forces and they are transmitted in the U-tube. A twisting motion is created by the resulting torque along the x-axis. . When the flow and density distributions are symmetric about xy-plane, total mass flow rate of the flowing mixture can be determined by the help of this oscillatory twisting motion. The practical application of this kind of flow meters is not easy. Since, the cost of this equipment is high and installation is difficult. The results obtained from Coriolis flow meter are successful in homogenous steady flow systems [1].

Optical and tracer techniques: Scattering and absorption caused the attenuation of light in solid-fluid systems. Scattering depends on the size of the solid particles, while attenuation is mainly affected by the optical frequency [1].

Phase Doppler Anemometry (PDA): This method was first used by [99]. The working principle of PDA is based on the Doppler difference technique. This is also used in conventional LDA. The phase shift of the scattered light from reflection and refraction coming from the intersection of laser beams are used to get the size of the particle. If two or more photodetectors are added to the receiving optical system, size, and velocity of the spherical particles can be reached simultaneously. Mass flux or concentration of particles can be found by using PDA. PDA is a single particle counting equipment.

Flow rate of a fluid between two coils was measured by nuclear magnetic resonance (NMR) [100]. One of the coil recorded the volume of the fluid. The other was a receiving coil and it fixed the passage time of the recorded volume. It was reported that this time was proportional to the flow rate of the tested fluid. There was a need to the linear conversion of the duration of pulse to a digital form. A

sample-and-hold instrument recorded pulses and chose the maximum one. Linearity was obtained with 0.25 % error.

2.7.4.Pressure Drop Measurement Methods

PRESSURE DROP IN STRAIGHT PIPES: By finding the pressure gradient in a conveyor, flow rate of solid particles has to be known. If particle size is large then the relation between the flow rates of each individual phase becomes linear [78].

PRESSURE DROP IN BENDS: To create a great pressure loss measurements are made around a pipe bend. Solids loading and pressure drop relation is linear also here. Pipe bend was used as if a flow meter [78]. If the length of the pipe is too short or frictional drop through a pipe is not enough, pressure drop along a bend is measured. Pressure drop changes within the change in the amount of solids [77].

Electrical noise method: This method does not create any pressure loss ([101], [102]). It is easy to change its location in a system and it is a reliable equipment. By two capacitor-transducer through the pipeline working at different positions, noise signals are correlated [78].

Momentum flow meters: The flow in the orifice plates is not smooth. The fluid is contracted when passing through the orifice. It is a common instrument to measure the pressure in industry. Construction of it is easy [103].

Venturimeters and orifice plates: Good pressure recovery could be obtained by using venturimeters. On the other hand, orifice plates could achieve poor pressure recovery [103].

Advantages of orifice plates: They have been used for many years. Installation is easy. They are well defined and design procedures are available. Also their uncertainty can be calculated [103].

Disadvantages of orifice plates: Pressure drop is high. Sensitivity to the installation effects is high. Construction should be carried out carefully. Useable range is small, results are non-linear. Pulsation errors can arise [103]. Pressure is measured by means of a height in manometers. However, contamination of tubes may occur. Also Bourdon gauge or transducer can be used for pressure measurement purposes. Measurement of pressure loss might be made by water-manometers, Bourdon-type instruments, or pressure transducers [61].

Disadvantage of U-tube manometer: It is difficult to read the pressure value when there is a significant amount of fluctuation in pressure, since both heights cannot be read simultaneously in such a case. To use a movable scale may eliminate this negative effect, or single-leg manometers may be used in processes where fluctuations occur [104]. When pressure is less than the value of 4 in (10.16 cm), U-tube or single-leg manometers do not give accurate readings. The inclined tube manometer is a well type manometer. It is used when pressure or vacuum values are small. To make accurate readings are possible by using inclined tube manometer [105]. Pressures around 0.0002 in can be measured by micromanometers (e.g. Prandtl-type micromanometer).

Diaphragm type pressure transducer (pressure differential): The design of this device was made by the authors of this paper [61]. There was a diaphragm, a connecting chamber above the diaphragm, and the transport pipe above the connecting chamber in the system. The connecting chamber was filled with a protecting fluid. The deformation of circular diaphragm determined the equation of stress arised from the given differential pressure acting on the diaphragm. The diaphragm converted the strain gauges into electrical signals. The connecting chamber was connected to the actual pressure measurement device. This equipment prevented the direct contact of the coming mixture and the strain gauges. Therefore, strain gauges were not affected from the particles. This device could be used also in processes where there is no need to prevent the undesired chemical and health damage effects. Pressure of pure fluids would be obtained

with this equipment. The connecting chamber is not used in such cases.

CHAPTER 3

EXPERIMENTAL PART

Hydrodynamic characteristics of upward solid-liquid flows were investigated in a vertical concentric annulus. Local dispersed solid densities, local mixture velocities at a cross-section of the annulus, and axial pressure drops in the fully developed flow region were measured at two different feed solid concentrations, for two different particle sizes, and at various flow Reynolds numbers.

3.1. Experimental Set-Up

The experimental set-up is shown in Figure 3.1. It is situated on the first and second floor of the laboratory. It consists of a vertical annulus, by-pass line, stainless steel head tank, heat exchanger, U-tube manometers, sampling probe, orificemeter, temperature probe, centrifugal slurry pump, drain line and a specially designed isokinetic sampling unit.

The overall length of the vertical concentric annulus is 5 m. It has a 2 m long test section. To provide fully developed flow conditions, an entrance length of 2.25 m was used. Inner and outer pipes of the annulus are made of steel. Inner diameter of the outer pipe, and outer diameter of the inner pipe are 123 mm (D_2) and 43.2 mm (D_1) respectively. Hydraulic diameter (D_2-D_1) is 79.8 mm.

A variable speed centrifugal slurry pump (Standard Pompa-PC-40/160-VX E.M.P. (2/1450)) is used to pump the slurry from the head tank to the annulus in a closed-loop system. The flow velocity in the system could be adjusted to very small values by means of a frequency

converter connected to the slurry pump. There are two flared mixing chambers at the entrance and exit parts of the annulus. Homogeneous flow is provided by the help of the baffles in the chambers.

Axial frictional pressure drops were measured by a U-tube manometer. Specific gravity of the manometer fluid (CCl_4) is 1.59. Radial local solid densities at a cross-section of the annulus were measured by the sampling probe previously designed [36]. The schematic diagram of the sampling probe is shown in Figure 3.2. Consistency measurements were carried out at seven points along the diameter of the test area under nonisokinetic and isokinetic conditions, for each particle size, feed solid concentration, and mixture velocity. The sampling probe is also used as a pitot tube to determine the local slurry velocities. This probe was placed into the annular gap horizontally, the tip of which being in the vertical plane facing the flow and aligned with the stream-lines. The inner and outer diameters of the sampling probe are 3.4 and 4.9 mm, respectively. A screw mechanism connected to the sampling probe was used to traverse the probe in the radial direction at the test cross-section. A needle moving along a scale shows the position of the probe tip as it traverses radially. This position was read from the scale. The sampling probe is at a distance of 1.45 m below the top end of the annulus.

A by-pass line parallel to the annulus was used when necessary to ensure the homogeneous dispersion of solids in all system. The length of the by-pass line is about 9 m and it is made of galvanized iron. A calibrated orificemeter ($D_0/D_p = \beta = 0.65$) was used to measure the volumetric flow rate of the solid-liquid mixture. Orifice-hole diameter is 20.65 mm. The orificemeter is placed below the annulus and it is 1.1 m above the bottom end of the experimental set-up. The calibration curve of the orifice is given in Appendix A.

A Hg-manometer was used to measure the flow rates higher than 40 L/min, and a CCl_4-manometer (more sensitive) was used for more accurate measurements of the lower flow rates. The manometer differentials were first recorded as m-Hg and then they were converted to m-CCl_4 by a sample calculation given in Appendix B.

A temperature probe (Cole-Parmer 1997-1998 Catalogue Number: 93821-00) was used to measure the temperature of the slurry. It was placed at the top end of the annulus. A digital meter (Cole-Parmer 1997-1998 Catalogue Number: 08129-70) connected to the temperature probe displayed the temperatures.

A heat exchanger was placed on the exit line from the head tank. The aim is to keep the slurry temperature constant during the experiments; since there is mixing and friction in the system, the slurry temperature increases during experiments. Cooling water was used between the inner and outer pipes of the double-pipe heat exchanger for cooling. Slurry flows in the inner pipe of the exchanger.

The head tank with a cylindrical upper part and a conical bottom part, made of stainless steel to prevent corrosion problems, was used to prepare feed slurry. To get good mixing, an industrial mixer (Cole-Parmer 2001-2002 Catalogue Number: U-50323-20) was placed in the head tank. A vertical line made of galvanized iron connected the centrifugal slurry pump to the head tank. A drain line was used to wash out the slurry from the system. It was connected vertically on the head-tank exit-line with a T-connection having ball valves on each line. To find the attrition behaviour of the solid particles, samples were taken from the drain line at the end of some runs, and particle size distribution of the used particles was determined.

Water-feldspar ($K_2O.Al_2O_3.6SiO_2$) mixture was used as the slurry in the experiments. Solid particles with mean particle diameters of 138 and 72 μm were utilized to prepare the feed slurries. Feldspar particles are chosen as the solid material because, feldspar is inert to water. ASTM standard sieves were used to get uniform size of solid particles. The average opening between the consecutive sieves is used to determine the mean diameter of solids.

Isokinetic sampling unit was designed to equalize the pressures and velocities in the undisturbed flow region to those within the sampling probe. The local slurry velocity and concentration can be

obtained quite accurately by this way [22]. Schematics and the photograph of the isokinetic unit are shown in Figure 3.3 and Figure 3.4, respectively. Isokinetic sampling unit consisted of a N_2 gas cylinder (1), a pressure regulator (2), a sample receiving flask (3), a sampling box (4), a graduated volume-meter (5), a digital pressure gauge (7), an inclined manometer (8), and some necessary fittings. Pressurized Nitrogen gas was used to supply a constant back-up pressure in the isokinetic system as needed. The pressure regulator in the isokinetic unit (Cole-Parmer 2001-2002 Catalogue Number U-03270-13) (2) is a two-stage one, which regulates the working pressure accurately. The pressure gauge (7) displays the pressure value up to the two digits after the decimal point, and also shows the change in the system-pressure when it is regulated with the pressure regulator (2).

The sampling box (4) has a diameter of 80 mm. It is made of glass. The flanges above the glass box are made of aluminium, which are fixed on the glass box by a special glue called metal epoxy. A sampling flask (3) is placed into the box (4). Each sample was collected in the sampling flask (3) after equalizing the velocity within the probe to that in the flow area, where the sample was withdrawn. The graduated volumetric flask (5) having graduation lines on it indicating the calibrated known volumes, was used to adjust the volumetric flow rate of the slurry through the probe to yield the desired withdrawal (sampling) velocity by trial-error as explained in the section of experimental procedure.

3.2. Experimental Parameters

In this experimental work, the independent variables are mean particle diameter (72 and 138 μm), feed solid concentration (1.0 and 2.0% v/v), and average mixture velocity (0.0120-0.2267 m/s); axial frictional pressure gradient ($\Delta P_{tp}/L$) in the test section, velocity profile and radial solid density profiles at a cross-section of the annulus are the dependent variables.

In isokinetic sampling, the velocity of the upward flowing mixture in the annulus, and the sampling velocity through the probe are equalized by the help of an isokinetic sampling set-up. Pressure or vacuum is applied in the isokinetic-sampling unit as required in order to equalize these velocities mentioned above [22]. In the present set-up, vacuum was not needed due to the high head of water existing above the test area; applying the same method in a horizontal pipe flow, vacuum also was needed at low slurry velocities to withdraw the samples [22].

3.3. Experimental Procedure

Water-feldspar ($K_2O.Al_2O_3.6SiO_2$ (ρ=2.4 g/cm^3)) mixtures were used as the liquid-solid mixture. Feed slurries with average solid concentrations of 1% or 2% v/v were prepared in the head tank. Mixture velocity was changed from 0.0120 to 0.2267 m/s corresponding to the mixture Reynolds number range of 934-20116. The prepared water-feldspar mixtures at different feed solid concentrations flow upward through a concentric annulus; in the fully developed region of the flow, local mixture velocities and local solid-phase densities at a cross-section perpendicular to flow, and the axial pressure gradients were determined experimentally.

At the beginning of the experiments, batches of solid particles were prepared at the desired sizes. ASTM standard sieves were used for this purpose. Mean particle sizes were obtained by taking the average of mean diameters of the consecutive sieves. The slurry at the desired consistency was prepared in the head tank (on the second floor of the laboratory) by adding the necessary amount of solid particles to the approximately known volume of the whole closed-loop system filled with water. The mixer in the head tank was started to get a homogeneous feed slurry. Later, pump (at the first floor) was started.

Calibration of the orificemeter was performed using water. The flow rate was adjusted according to the calibration curve given in Appendix A. The calibration was not repeated with the dilute slurry for

the two-phase flow experiments, due to the negligible error. A Hg-manometer and a CCl_4-manometer were used in the calibration.

To keep the slurry temperature constant, a heat exchanger was placed on the exit line from the head tank. Cooling water was started. Slurry temperature was monitored using the temperature probe at the top section of the annulus.

Volumetric and Erlenmeyer flasks and their corresponding corks were weighed individually, and they were numbered. In every run, at each point of measurement, a slurry sample was collected in a flask which was closed with its corresponding cork, and was weighed. Since its tare weight is known, then the mass of the slurry is calculated. After removing the cork, the Erlenmeyer flask was placed in an oven to be dried overnight at about 105 ^{0}C. As soon as it was taken out of the oven, it was closed with its cork again to avoid capture of moisture, and then put in a desiccator for cooling. Afterwards, it was weighed once more with a sensitive balance, its accuracy being ± 0.0001 gram. By this way, amount of solids was determined. Thus the local solid density was calculated. This procedure was repeated with each flask containing a slurry sample from a different radial location. The transport average mixture density was also measured by taking samples from the sampling line placed 130 cm above the probe. Also, slurry samples were taken from the head tank to determine feed solid density.

There are two manometer taps at 2.25 and 4.25 m distances from the bottom end of the annulus. A U-tube CCl_4-manometer is connected to these taps to measure the axial pressure gradients in the test section at different operating conditions. For small pressure drop measurements (single-phase flow experiments), U-tube manometer was used with an inclination angle of 2.126^0 to be more accurate. This inclination was increased to 90^0 when the two-phase flow experiments were performed, thus the frictional pressure gradients were measured for slurry.

In the first part of the experimental work, the local slurry velocities in the annular flow area were measured using the sampling probe as a pitot tube. For this purpose, an inclined manometer, having a manometer fluid of CCl_4+benzene mixture (ρ_{tf} = 1218.5 kg/m^3) and an inclination angle of α=0.94^0, was connected to the probe in a proper fashion. At a certain point in the annular area, where the probe tip was situated, the pressure differential between the stagnation and static pressure (P_a-P_b) of the pitot tube was measured quite accurately by opening only the valves F and C, while all the other valves of the isokinetic sampling unit were closed. Each point velocity was calculated approximately by taking the pitot tube coefficient K as unity at first, later to be corrected as it is explained below. The local velocity measurements were carried out at ten different radial distances by traversing the probe radially using the screw mechanism. As a result, a plot of local velocity versus radial distance was drawn. The average velocity was obtained by using Simpson's rule [107] as explained in Appendix B; then, this calculated average velocity was compared with the flow average velocity according to the calibration curve of the orificemeter, and their ratio was obtained. This ratio (1/K) yielded the approximate pitot tube coefficient, K, with a standard deviation of 1.6823±0.0714, as calculated and shown in Appendix B. As it is seen in the results, K value is greater than unity indicating that the average velocities determined from the pitot tube measurements are lower than those obtained from the orificemeter measurements; therefore, the approximate local slurry velocities, calculated from the data of inclined manometer differentials by assuming K as unity, were corrected by multiplying them with the true value of K to find the local velocities as accurate as possible. After the completion of this job, the inclined manometer was disconnected by closing the valves F and C, as shown in Figure 3.3.

In the second part of the experimental work, the local solid density measurements were performed using the isokinetic sampling unit. For this, a back-up pressure required to obtain an uninterrupted continuous flow of slurry into the sampling flask for each flow velocity was determined by trial and error at each radial location, this back-up

pressure should remain constant during the sampling period. According to this procedure, at first a certain backup pressure was applied with N_2 gas to the isokinetic unit by opening the valve (B). Under this condition, volume of the slurry collected in the graduated volumetric flask (5) during the sampling period was measured, and the volumetric flow rate was determined by dividing this volume by the time recorded with a stopwatch. To get the sampling velocity of slurry, volumetric flow rate is divided by the cross-sectional area of the sampling probe. The velocity obtained from here was compared with the true local velocity of flow, and this procedure was repeated until a very small difference between these velocities could be achieved by trial and error. If the sampling velocity was still higher than the flow velocity, the constant back-up pressure was increased, and the procedure for equating the sampling and flow velocities to each other was repeated until the correct value of the constant back-up pressure needed to provide a continuous flow of slurry sample into the flask with a sampling velocity equal to the true flow velocity corresponding to that radial location was obtained. Supplying a constant back-up pressure to the system is important, since the amount of slurry sample taken is dependent upon this constant back-up pressure. During the experiments, it was observed that the back-up pressure increased as the sample was collected from the sampling box (4), since the volume of sampling box (4) was smaller than the volume of flask (5). After giving the same back-up pressure to the isokinetic unit, volumes of the slurry samples obtained from the sampling box and graduated volumetric flask were found as different from each other. As a result, it would be better to take samples from the graduated volumetric flask (5), after equalizing the velocities at the undisturbed flow area and those within the sampling probe. Thus, the slurry sample was collected in graduated flask (5) under nearly isokinetic condition keeping the required back-up pressure almost constant. This procedure was repeated at each of the seven points along the radial coordinate in the annular gap. Four samples were collected at each radial location in an experimental run, to determine the standard deviation in the local density measurements.

The experimental data will be useful to obtain practical correlations for the design and modeling studies of these systems in further studies. Ranges of the experimental parameters studied are given in Table 3.1.

Table 3.1. Ranges of the experimental parameters

Mean particle size ($d_{p,}$ μm)	72-138
Feed solid concentration (FSC) (% v/v)	1.0-2.0
Velocity of the mixture in the annulus ($U_{ann,}$ m/s)	0.0120-0.2267
Slurry Reynolds number (Re_m)	934-20116

CHAPTER 4

RESULTS AND DISCUSSION

Liquid-solid upflow through a concentric annulus was studied and radial local solid densities were determined experimentally by isokinetic sampling technique in a vertical annulus. In literature, data related to such systems are limited because of the complexities about the nature of multiphase flows. Here, water-feldspar mixtures were used at different feed solid densities and different mixture velocities. Also single-phase (water) experiments were carried out to determine the accuracies of the experimental set-up and isokinetic sampling unit. Radial local solid densities were measured at both isokinetic and non-isokinetic conditions.

Single-phase and two-phase axial pressure drops along the test section were measured with a U-tube manometer. In single-phase experiments (using only water) U-tube manometer had an inclination angle of 2.126^0. The following well-known equations were used to calculate the friction factors and pressure drops:

Laminar flow

$$f_w = \frac{16}{Re_w}\phi_a \quad \text{.....Equation (4.1)}$$

where ϕ_a is the correction factor to eliminate the error arised from using hydraulic diameter in the laminar flow regime; its value is

$\phi_a = 1.48$ for $\kappa = 0.345$ [106].

$$?P_w = \frac{32 \mu_w L U_{ann}}{D_e^2} \quad \text{..... Equation (4.2)}$$

Turbulent flow

$$f_w = \frac{0.0791}{Re_w^{0.25}} \quad \text{..... Equation (4.3)}$$

$$?P_w = \frac{2 f_w L U_{ann}^2 ? w}{D_e} \quad \text{....Equation (4.4)}$$

Table 4.1. Friction factors for single-phase flow

$U_{ann}x10^3$, m/s	f_c (from correlation)$x10^3$	f_p (from pressure drop data)$x10^3$	% error in friction factors
26.2	11.5	9.4	19
30.8	11.1	9.1	18
38.7	10.5	8.6	18
43.9	10.1	7.8	23
51.6	9.7	8.1	17
58.5	9.4	7.5	20
64.8	9.2	7.7	16
70.7	9.0	7.8	14
85.5	8.5	7.7	10
110.0	8.0	8.2	2
120.0	7.8	6.9	12
* 138.2	7.5	6.8	10
156.1	7.3	6.2	15
173.7	7.1	6.4	9
183.1	7.0	6.4	8
192.2	6.9	6.4	7
202.1	6.8	63	7
209.5	6.7	6.4	5
229.6	6.6	6.1	7

* Sample calculation is given for this run in Appendix B

By this calculation, % errors between theoretical and experimental friction factors were observed to decrease from 19 to 7. When Reynolds number was low, axial pressure drops were also very small, therefore errors related to reading these small pressure drops were higher than those of high Reynolds numbers.

Table 4.2. Pressure drops for single-phase flow

$U_{ann}x10^3$, m/s	ΔP_c, Pa	ΔP_e, Pa	ΔP_{csh}, Pa	ΔP_{esh}, Pa
26.2	0. 4	0.3	19589.4	19589.4
30.8	0.5	0.4	19589.6	19589.5
38.7	0.8	0.7	19589.8	19589. 7
43.9	1.0	0.8	19590.0	19589.8
51.6	1.3	1.1	19590.3	19590.1
58.5	1.6	1.3	19590.7	19590.3
64.8	1.9	1.6	19591.0	19590.7
70.7	2.2	1.9	19591.3	19591.0
85.5	3.1	2.8	19592.2	19591.9
110.0	4.8	5.0	19593.9	19594.0
120.0	5.6	5.0	19594.7	19594.0
**138.2	7.2	6.5	19596.2	19595.5
156.1	8.9	7.5	19597.9	19596.6
173.7	10.7	9.7	19599.7	19598.7
183.1	11.7	10.8	19600.8	19599.8
192.2	12.7	11.8	19601.8	19600.9
202.1	13.9	12.9	19602.9	19602.0
209.5	14.7	14.0	19603.8	19603.0
229.6	17.3	16.1	19606.3	19605.2

** Sample calculation is given for this run in Appendix B

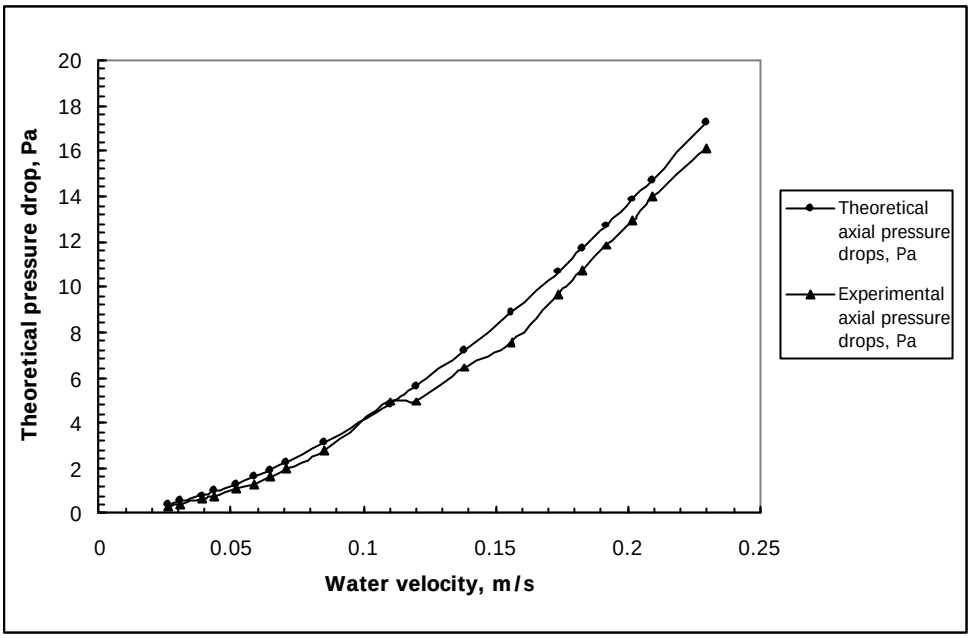

Figure 4.1.a. Theoretical and experimental pressure drops for single-phase flow

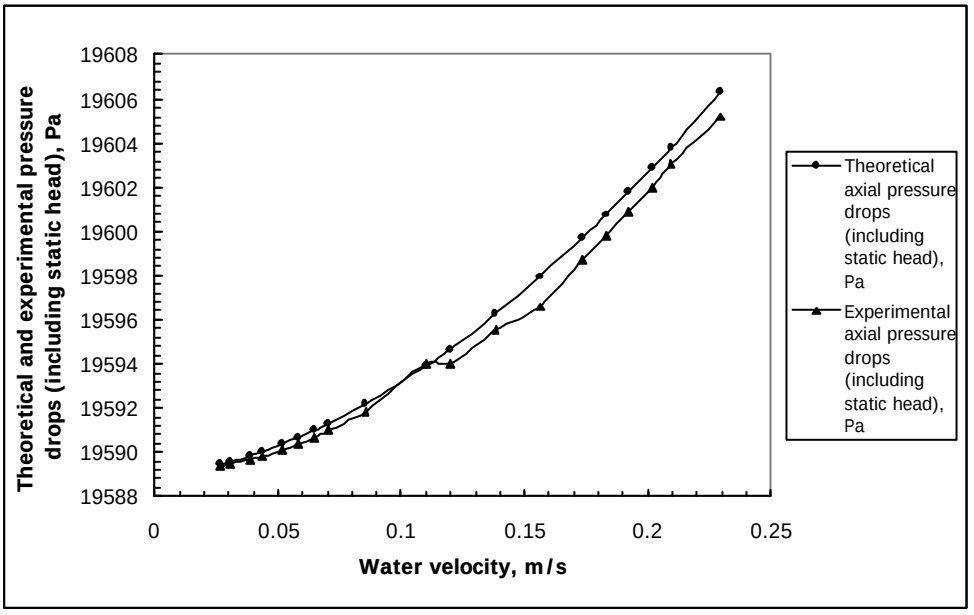

Figure 4.1.b. Theoretical and experimental pressure drops (including static head) for single-phase flow

In the two-phase flow experiments, inclination angle was increased to 90^0 because of having larger pressure drops. Axial frictional pressure drop versus mixture velocity graphs were plotted with and without static head values. Two-phase frictional pressure drops were calculated by the following formula:

$$?P_{tp} = g(?_{CCl_4} - \overline{?}_m)?H_{tp} \quad \text{..... Equation (4.5)}$$

Here, ΔP_{tp} indicates two-phase axial frictional pressure drop, $\overline{\rho}_m$ is the average density of the mixture, and ΔH_{tp} is the manometer reading.

Point velocities were measured by using the sampling probe as a pitot tube. It was connected to an inclined manometer, its inclination angle being 0.94^0. After finding all the point velocities by the well-known pitot tube equation (Eqn. 4.6) [106];

$$V_L = K\sqrt{\frac{2?P_{im}}{?_w}} \quad \text{..... Equation (4.6)}$$

These values were plotted against the radial distance assuming K=1, to be corrected later. Simpson's rule [107] was used to obtain the average velocities from these graphs. Also the average velocity in the annulus was known from the calibration data of the orificemeter. Point velocities were multiplied by a constant, called pitot tube coefficient, to get the definite average velocity. By this way, true point velocities were obtained and local velocity vs. radial distance plot is shown in Figure 4.2.

Radial local solid densities were measured by isokinetic sampling technique at seven different points along the diameter of the annulus in the fully developed flow region. Results are given in Figures 4.3.a to 4.5.b.

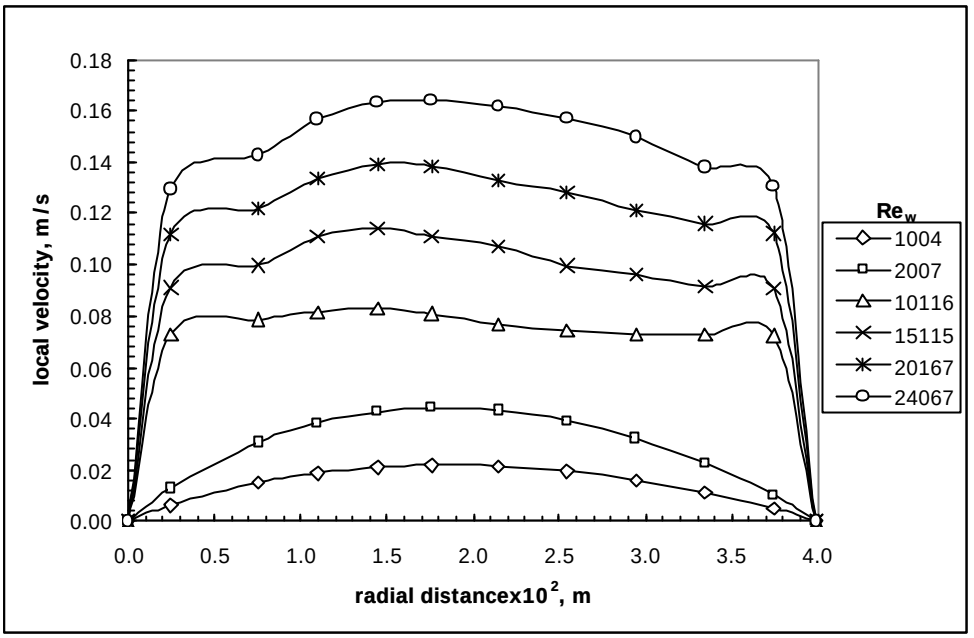

Figure 4.2. Local velocity vs. radial distance for different Reynolds numbers

In the experimental set-up, glass bulbs were connected to the manometers to prevent the solid accumulation along the manometer arms. Some solids were accumulated in these bulbs and they were discharged from time to time by opening the plastic hoses at the bottom of the glass bulbs. Therefore no clogging occurred in the connections to the manometers.

Local velocities could not be determined very exactly because of the following reasons. If manometer differences are less than 4 inches of liquid, manometers are not suitable devices for pressure measurement. However in this study there was no choice other than using a manometer [103].

To be able to make more precise pressure measurements, manometer liquid was changed. New manometer liquid should be immiscible with water. Carbontetrachloride and benzene mixture was found to be suitable for this purpose. The density of this mixture was determined with a pycnometer. The procedure is given in Appendix B.

Using a manometer fluid (CCl4+benzene mixture) with a density (1218.5 kg/m3) lower than that of CCl4 alone increased the precision of the pressure measurements. This mixture was used in the inclined manometer. After measuring pressure differentials at 10 different radial positions, the local velocities were calculated from Equation (4.6). Later, local velocity versus radial position plots were drawn at four different Reynolds numbers. These results were presented in Figure 4.2. Pitot tube coefficient was calculated as 1.6823 with a standard deviation of 0.0714.

The digital pressure gauge (7) displayed the system pressure during the experiments, was used to show two digits after the decimal point. Nevertheless a more sensitive pressure gauge displaying more digits after the decimal point (three, or preferably four digits) is needed to obtain more accurate local solid density measurements. Also velocity adjustment would be easier by this way.

Radial solid density profiles were plotted for different particle sizes, feed solid concentrations and mixture Reynolds numbers. They are shown in Figures 4.3.a to 4.6.a and 4.9.a to 4.12.a. The local solid densities were drawn against dimensionless radial distance when mixture Reynolds number was fixed. Same values were plotted against mixture Reynolds number when dimensionless radial distance was kept constant in Figures 4.3.b to 4.6.b and 4.9.b to 4.12.b.

When the particle size was 72 μm and feed solid concentration was 1% v/v (at nonisokinetic condition), the local solid densities did not show much change across the test cross-section at a constant mixture Reynolds number. In this situation, interactions between solid and liquid phases were thought to be small. When radial position was fixed, local solid densities increased with the mixture Reynolds number up to the Re_m=13535 then decreased at Re_m=17534 and increased again at Re_m=20000. This behavior can be observed in Figures 4.3.a and 4.3.b.

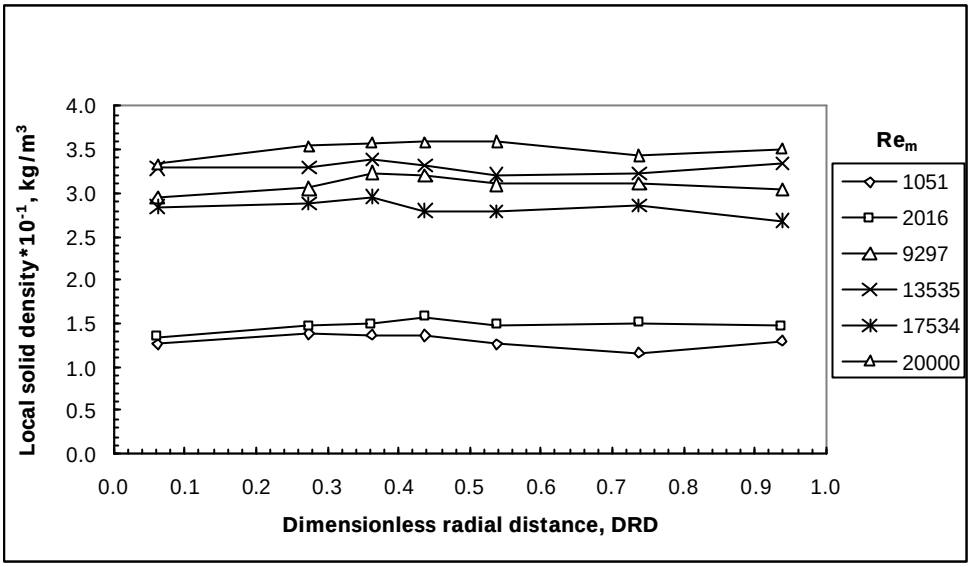

Figure 4.3.a. Local solid density (ρ_s*10^{-1}) vs. dimensionless radial distance when mixture velocity is fixed, for d_p=72 μm and C_f= 1% (v/v) at nonisokinetic conditions

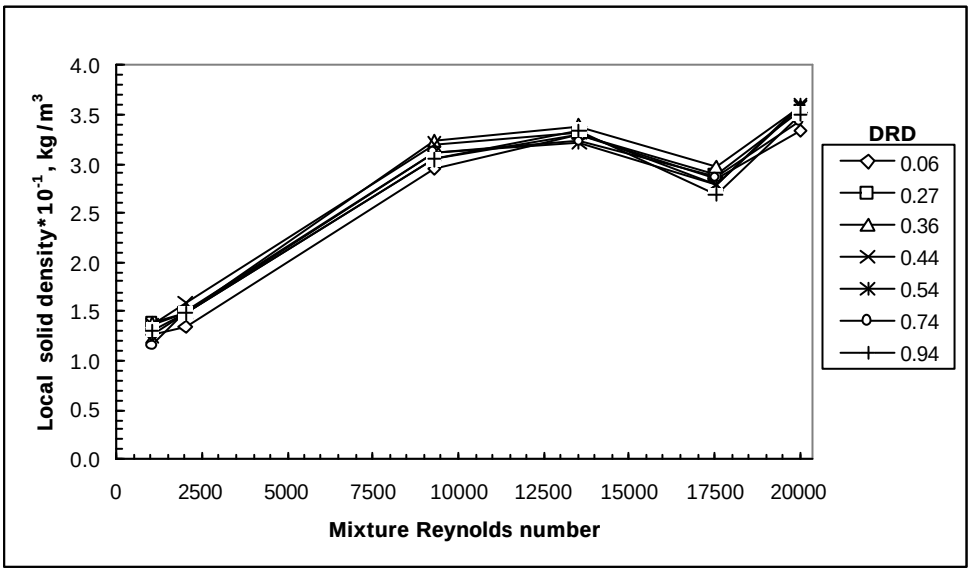

Figure 4.3.b. Local solid density (ρ_s*10^{-1}) vs. mixture Reynolds number when dimensionless radial distance is fixed, for d_p=72 μm and C_f= 1% (v/v) at nonisokinetic conditions

When the particle size was 72 μm and feed solid concentration was 1% v/v (at isokinetic condition), local solid densities increased with increasing mixture Reynolds number if radial position was fixed. This could be attributed to the increasing solid carrying capacity of the liquid phase as the slurry velocity was increased. It seems that local solid densities show a decreasing trend at around dimensionless radial distance of λ=0.4, where the velocity profile has its maximum value. At this radial location, water moves faster than the solid particles, therefore solid density decreases at that point. The particles lag behind the liquid phase at the highest velocity and relative velocity between the liquid and solid phases is highest at that point [8]. The inverse is true at the walls of the annulus. Solid particles move faster than the liquid thus, solid density is higher near the annulus walls than those in the center (Figures 4.4.a and 4.4.b). The similar behavior was previously reported [8].

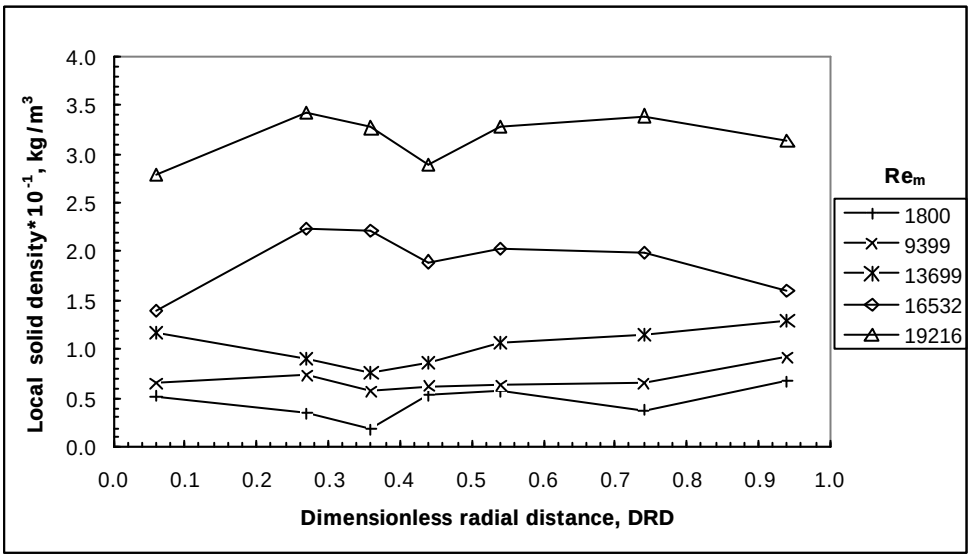

Figure 4.4.a. Local solid density ($\rho_s * 10^{-1}$) vs. dimensionless radial distance when mixture velocity is fixed, for d_p=72 μm and C_f= 1% (v/v) at isokinetic conditions

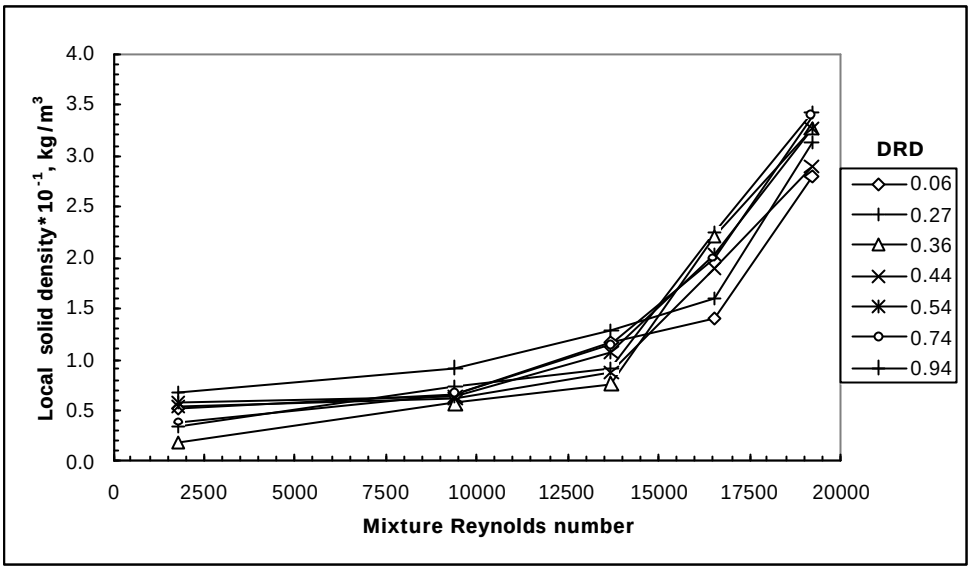

Figure 4.4.b. Local solid density ($\rho_s * 10^{-1}$) vs. mixture Reynolds number when dimensionless radial distance is fixed, for d_p=72 μm and C_f= 1% (v/v) at isokinetic conditions

In Figures 4.5.a and 4.5.b, when particle size was 72 μm and feed solid concentration was 2% v/v (at nonisokinetic condition), local solid densities increased up to the mixture Reynolds number of 12616 and decreased at 15999, then started to increase again. This was the same behavior observed at 1% v/v feed solid concentration previously. The local solid densities showed a decrease as a general trend around a dimensionless radial distance of λ=0.4.

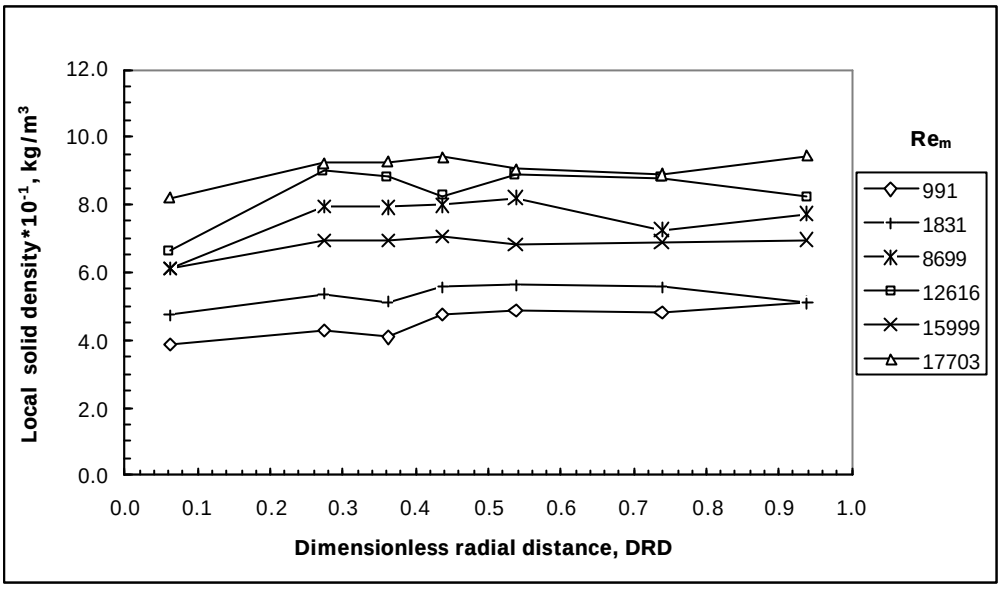

Figure 4.5.a. Local solid density (ρ_s*10^{-1}) vs. dimensionless radial distance when mixture velocity is fixed, for d_p=72 μm and C_f= 2% (v/v) at nonisokinetic conditions

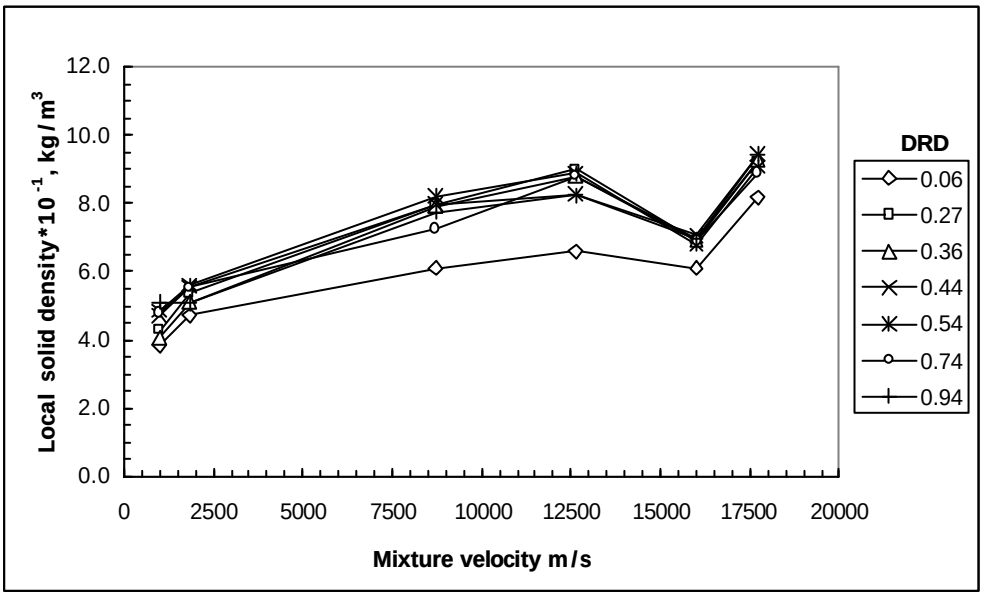

Figure 4.5.b. Local solid density (ρ_s*10^{-1}) vs. mixture Reynolds number when dimensionless radial distance is fixed, for d_p=72 μm and C_f= 2% (v/v) at nonisokinetic conditions

When the particle size was 72 μm and feed solid concentration was 2% v/v (at isokinetic condition), local solid densities increased with increasing mixture Reynolds number if radial position was fixed as a general trend. The local solid densities decreased at around the dimensionless radial distance of λ=0.4 as observed in Figures 4.6.a and 4.6.b.

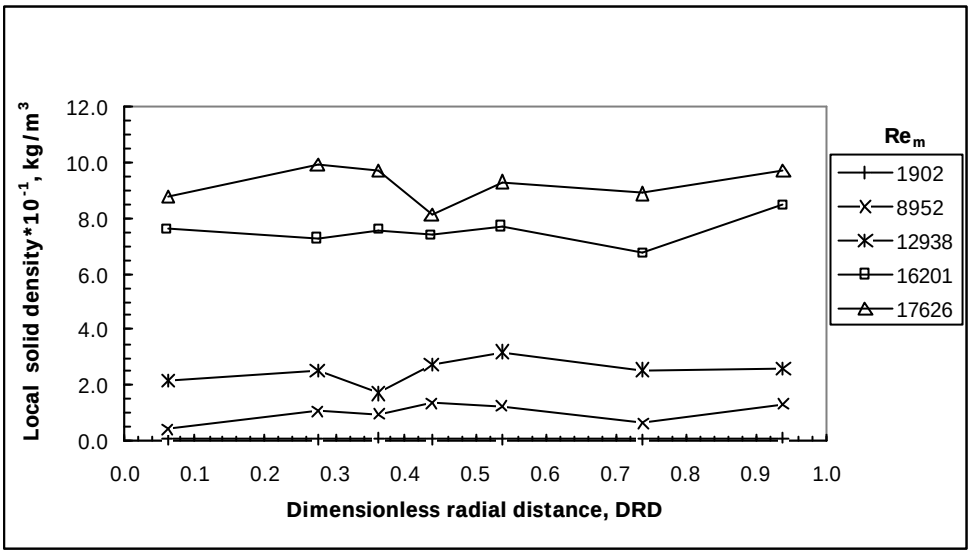

Figure 4.6.a. Local solid density (ρ_s*10^{-1}) vs. dimensionless radial distance when mixture velocity is fixed, for d_p=72 μm and C_f= 2% (v/v) at isokinetic conditions

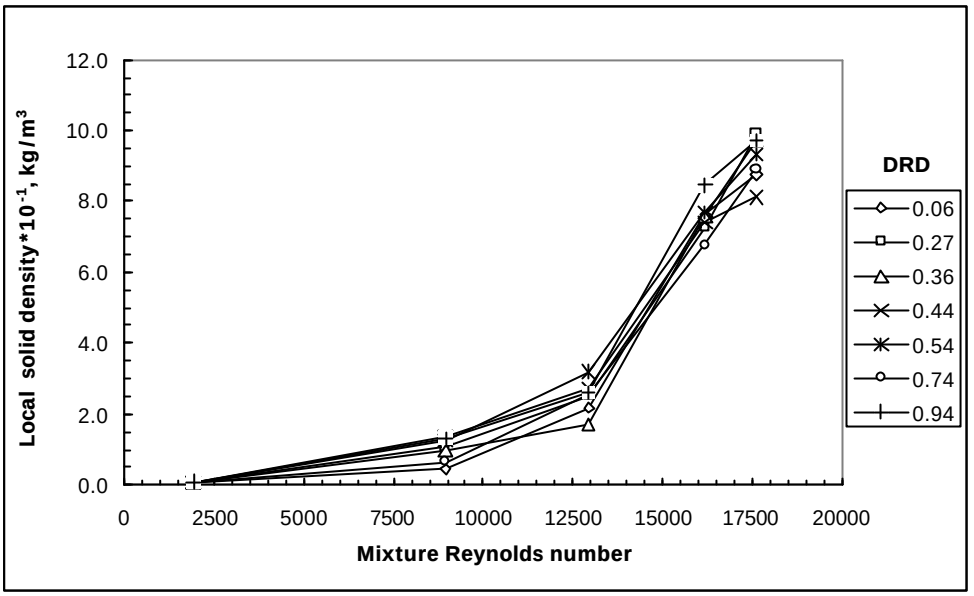

Figure 4.6.b. Local solid density (ρs*10-1) vs. mixture Reynolds number when dimensionless radial distance is fixed, for dp=72 μm and Cf= 2% (v/v) at isokinetic condition

Two-phase axial frictional pressure gradients and two-phase axial frictional pressure gradients including static head graphs were drawn against the mixture velocity, and they are shown in Figures 4.7.a to 4.7.b. They indicated almost the same trends. Two-phase axial frictional pressure gradients increased with the increasing feed solid concentration and particle size at a constant value of mixture velocity.

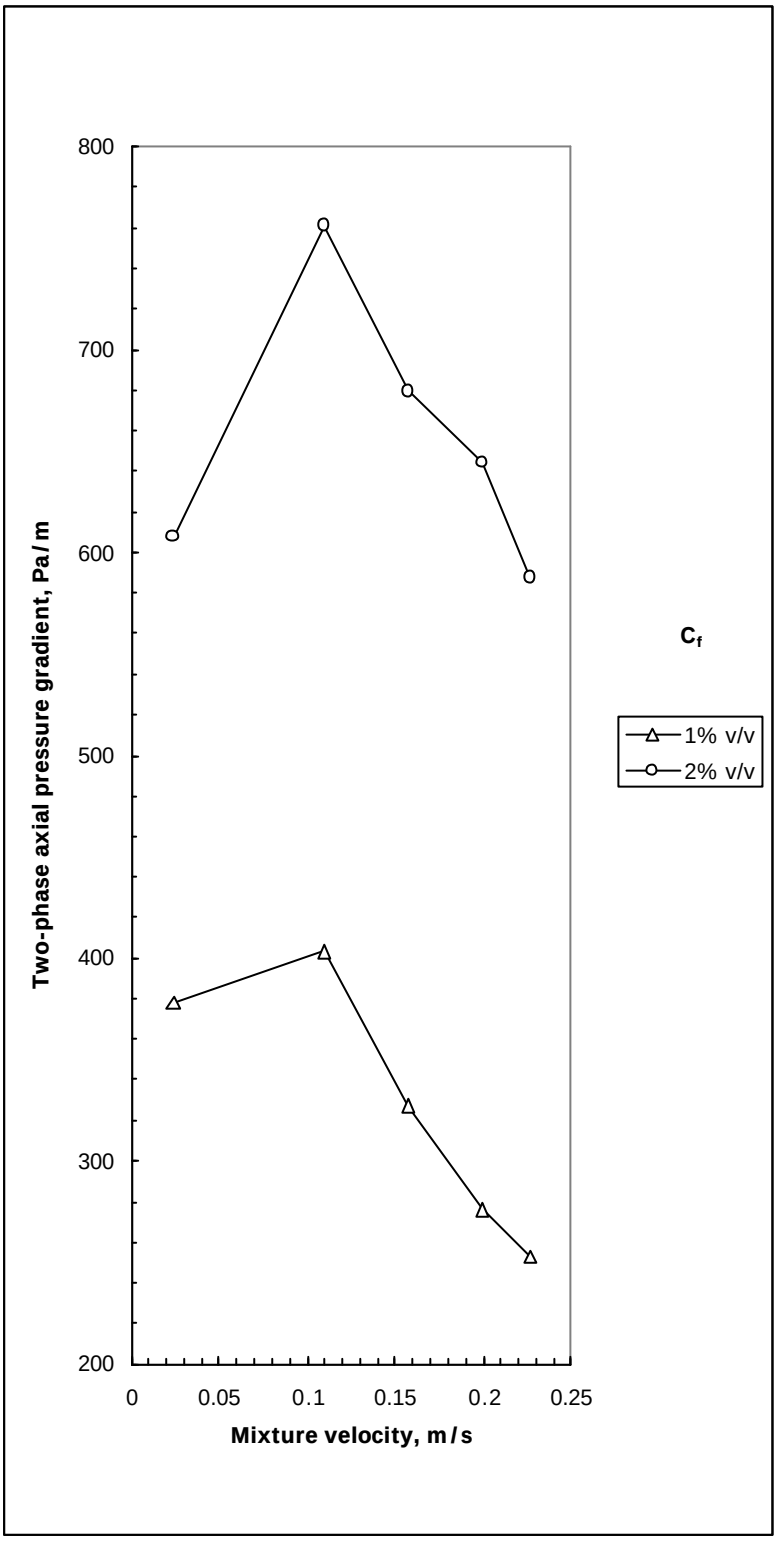

Figure 4.7.a. Two-phase axial pressure gradient vs. mixture velocity for different feed solid concentrations of particle size d_p=72 μm at isokinetic condition

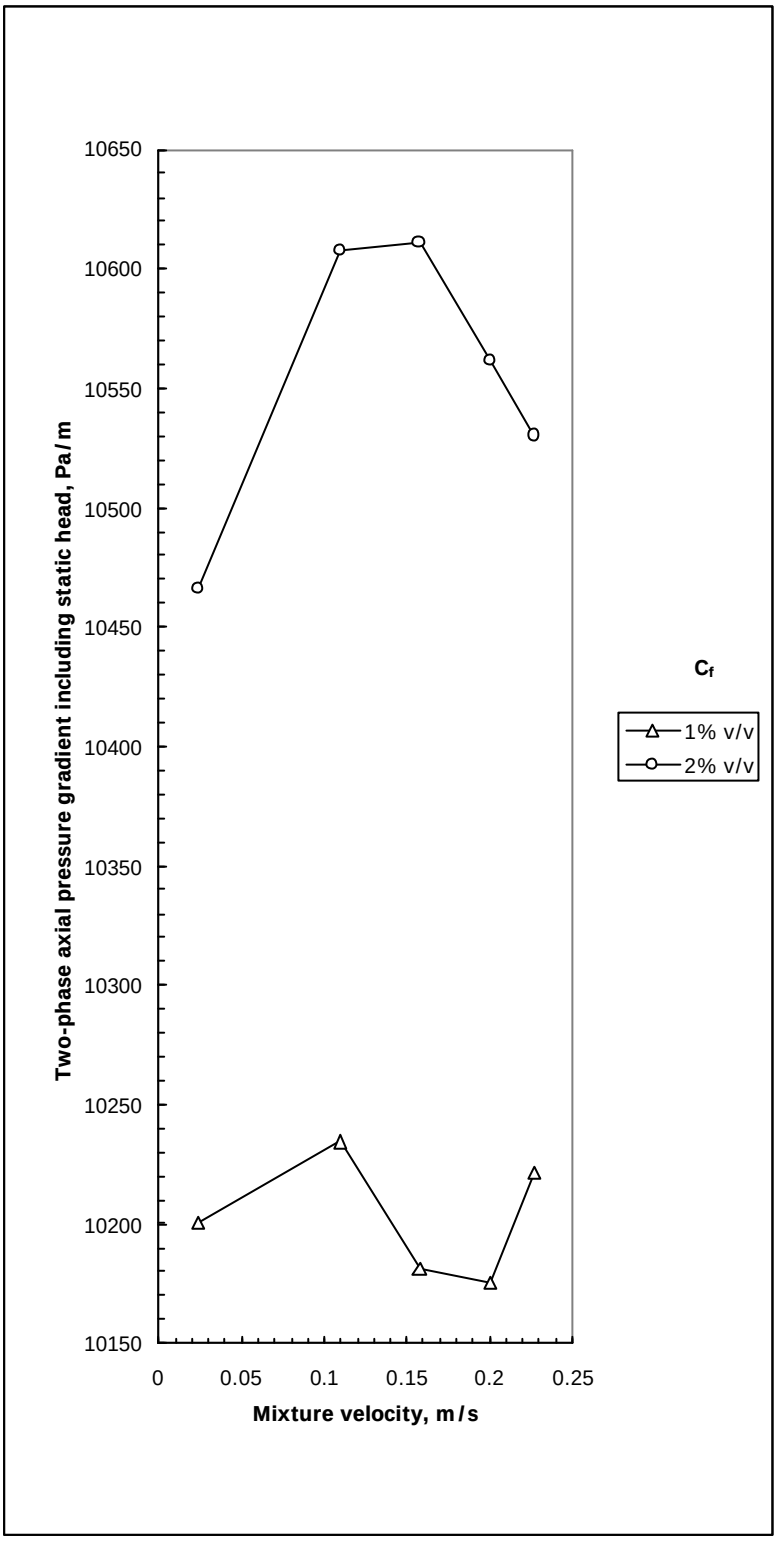

Figure 4.7.b. Two-phase axial pressure gradient (including static head) vs. mixture velocity for different feed solid concentrations of particle size $d_p = 72$ μm at isokinetic condition

Two-phase experimental friction factor versus mixture velocity graphs for 72 μm particles is presented in Figure 4.8. It is observed that there is a decreasing trend in two-phase experimental friction factors as the mixture velocity increases for both feed solid concentrations of 1% and 2% v/v, as expected.

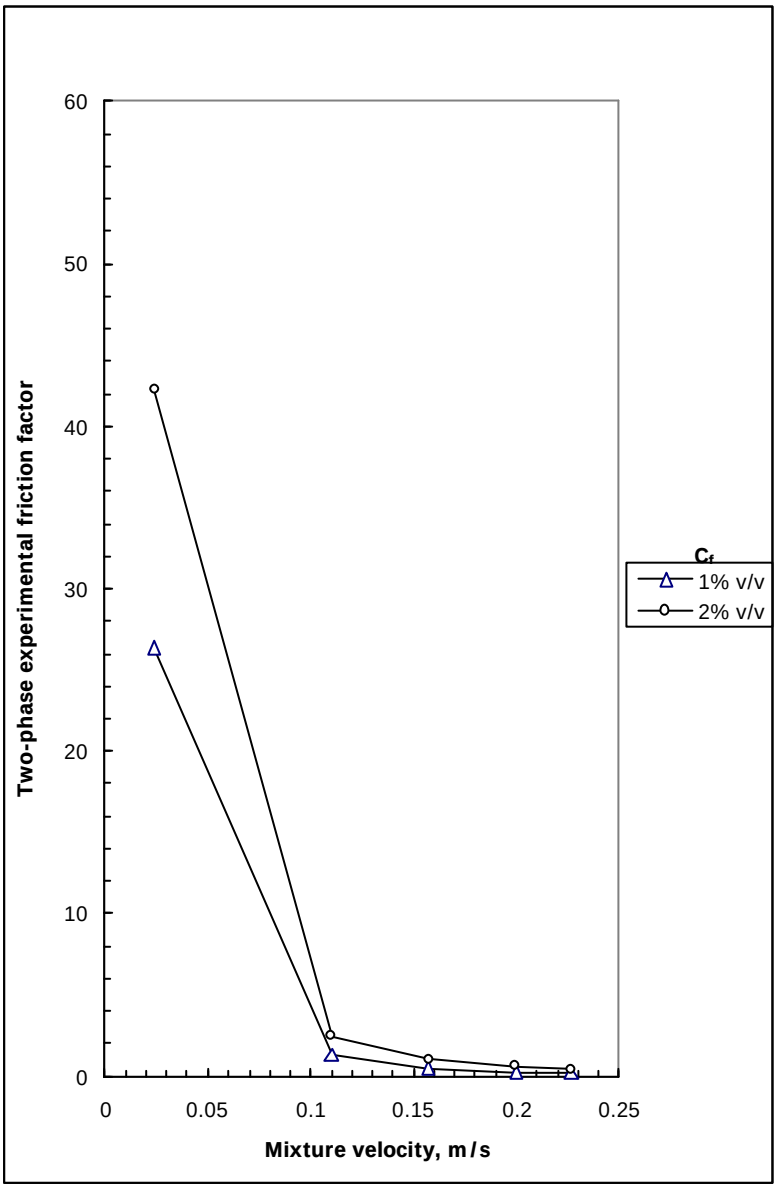

Figure 4.8. Two-phase experimental friction factor vs. mixture velocity when feed solid concentration is fixed, for d_p=72 μm at isokinetic condition

When the particle size was 138 μm and feed solid concentration was 1% v/v (at nonisokinetic condition), local solid densities were almost constant with respect to the radial distance (Figure 4.9.a). The local solid densities increased with the mixture Reynolds number at all the radial distances, as observed in Figure 4.9.b.

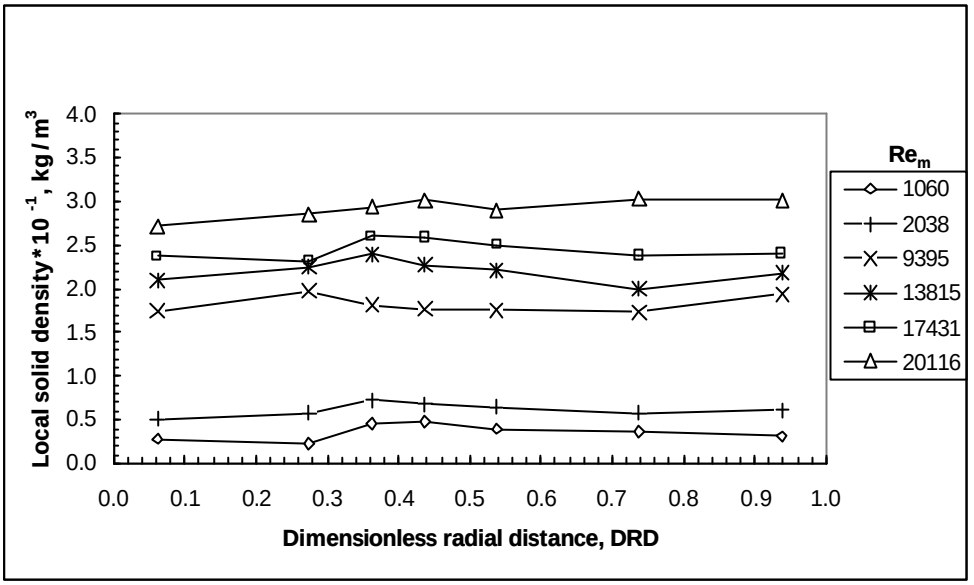

Figure 4.9.a. Local solid density ($\rho_s * 10^{-1}$) vs. dimensionless radial distance when mixture velocity is fixed, for d_p=138 μm and C_f= 1% (v/v) at nonisokinetic conditions

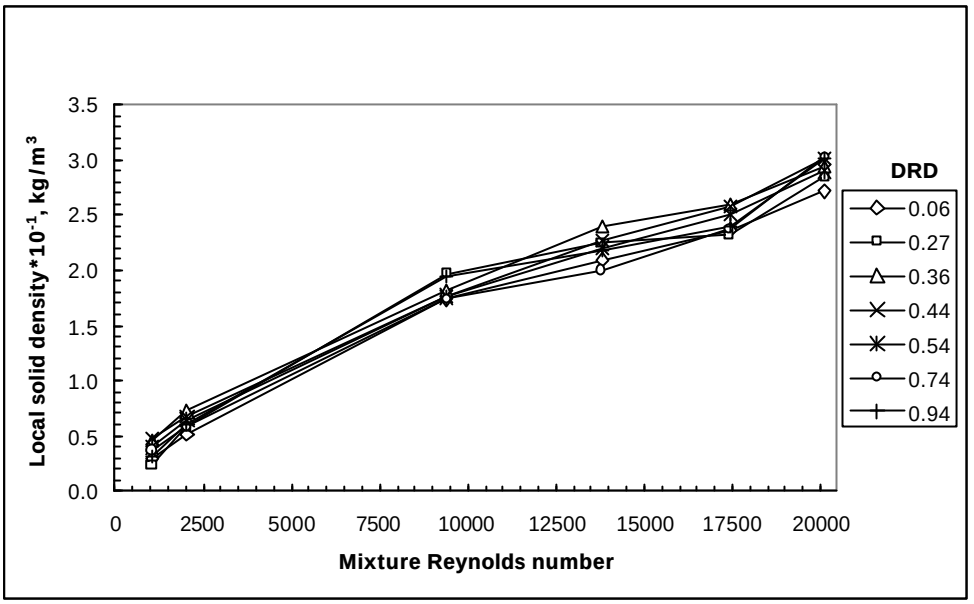

Figure 4.9.b. Local solid density ($\rho_s * 10^{-1}$) vs. mixture Reynolds number when dimensionless radial distance is fixed, for d_p=138 μm and C_f= 1% (v/v) at nonisokinetic conditions

When the particle size was 138 μm and feed solid concentration was 1% v/v (at isokinetic condition), local solid densities showed fluctuations as observed in Figures 4.10.a and 4.10.b. The local solid densities indicated a maximum at around λ=0.4 for the mixture Reynolds number of around 19000.

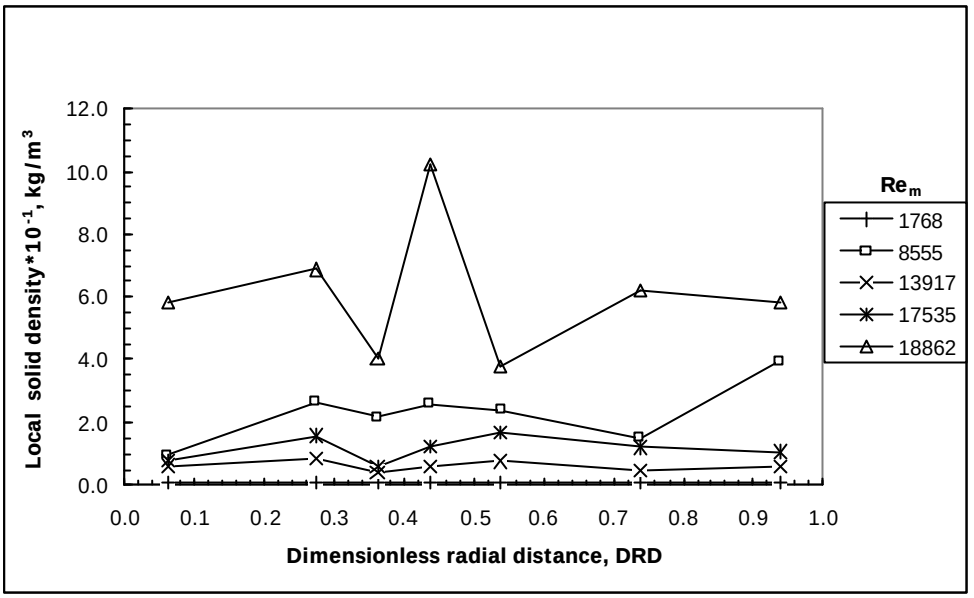

Figure 4.10.a. Local solid density (ρ_s*10^{-1}) vs. dimensionless radial distance when mixture velocity is fixed, for d_p=138 μm and C_f= 1% (v/v) at isokinetic conditions

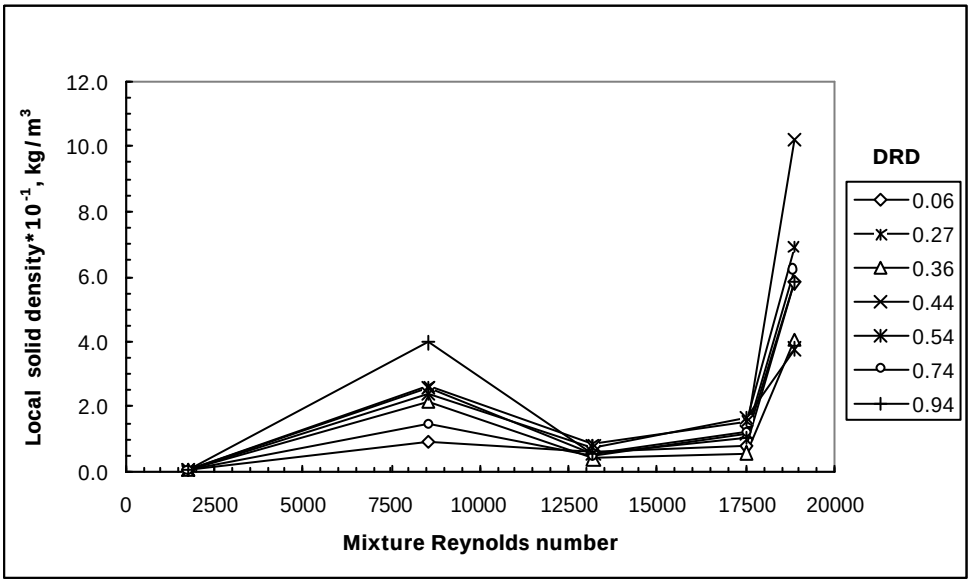

Figure 4.10.b. Local solid density (ρ_s*10^{-1}) vs. mixture Reynolds number when dimensionless radial distance is fixed, for d_p=138 μm and C_f= 1% (v/v) at isokinetic conditions

In Figures 4.11.a and 4.11.b, when the particle size was 138 μm and feed solid concentration was 2% v/v (at nonisokinetic condition), the local solid densities increased up to the mixture Reynolds number of 14502 and then decreased at 16364. Local solid densities decreased as a general trend at around the dimensionless radial distance of $\lambda = 0.4$.

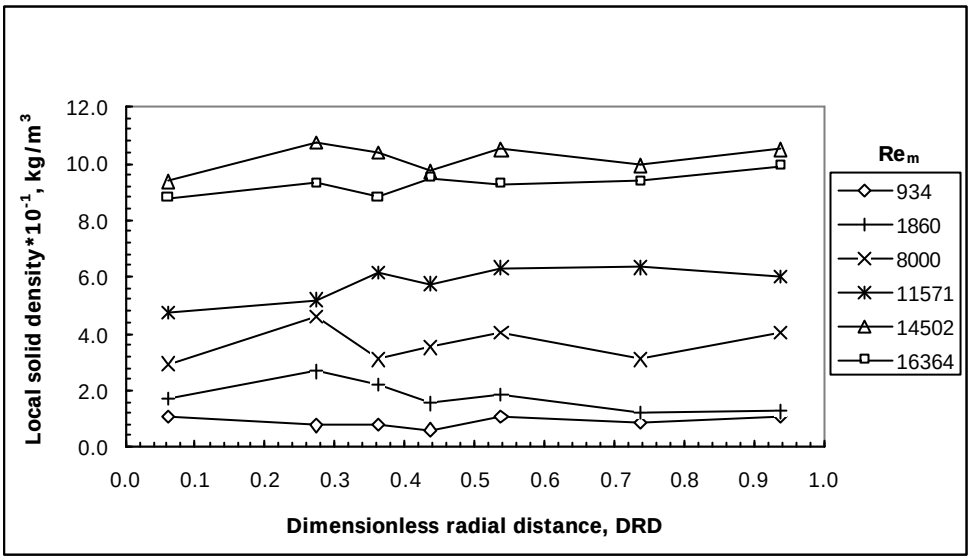

Figure 4.11.a. Local solid density ($\rho_s * 10^{-1}$) vs. dimensionless radial distance when mixture velocity is fixed, for $d_p = 138$ μm and $C_f = 2\%$ (v/v) at nonisokinetic conditions

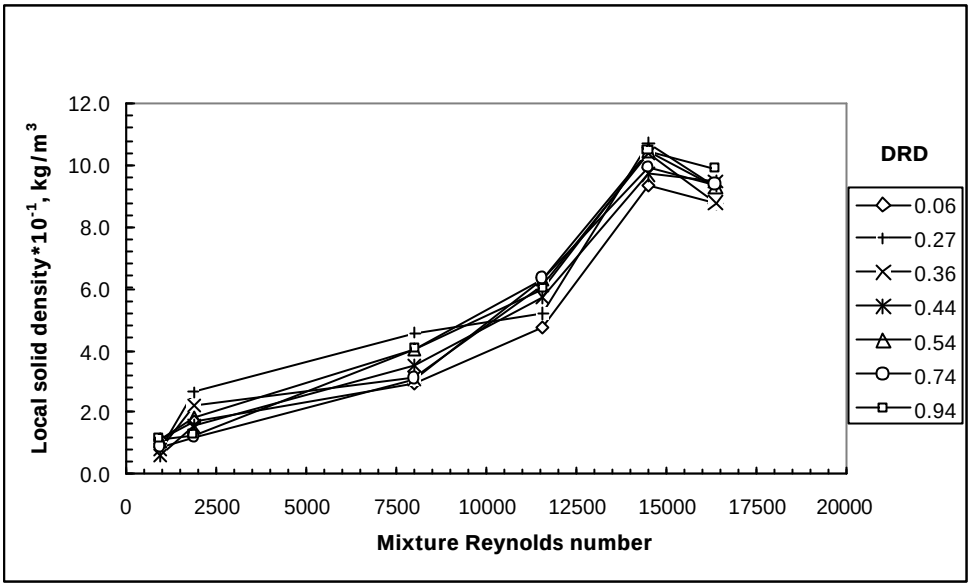

Figure 4.11.b. Local solid density ($\rho_s * 10^{-1}$) vs. mixture Reynolds number when dimensionless radial distance is fixed, for d_p=138 μm and C_f= 2% (v/v) at nonisokinetic conditions

In Figures 4.12.a and 4.12.b, when the particle size was 138 μm and feed solid concentration was 2% v/v (at isokinetic condition), local solid densities increased with the increasing mixture Reynolds number if radial position was fixed. Radial solid density profiles showed minima at dimensionless radial distance of λ=0.45.

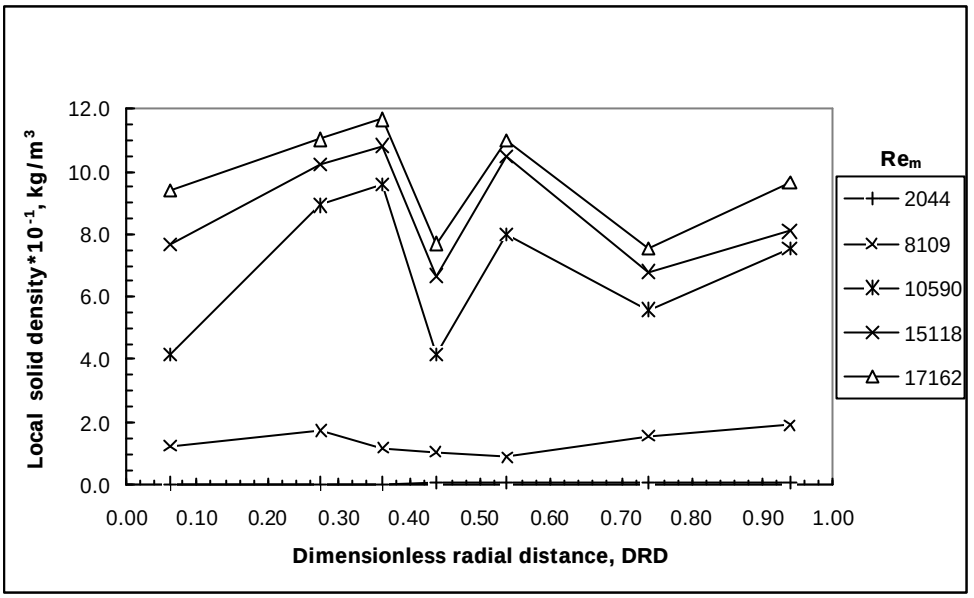

Figure 4.12.a. Local solid density ($\rho_s * 10^{-1}$) vs. dimensionless radial distance when mixture velocity is fixed, for d_p=138 μm and C_f= 2% (v/v) at isokinetic conditions

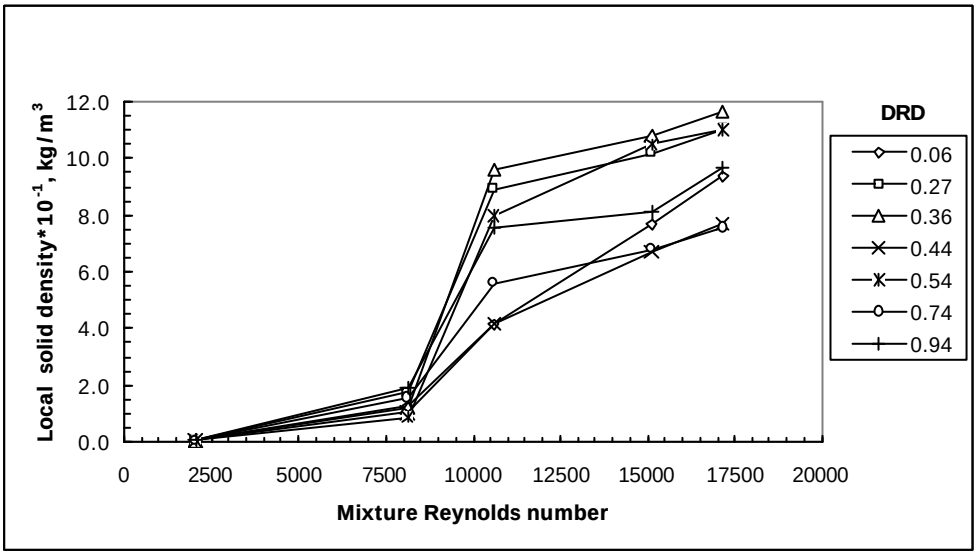

Figure 4.12.b. Local solid density ($\rho_s * 10^{-1}$) vs. mixture Reynolds number when dimensionless radial distance is fixed, for d_p=138 μm and C_f= 2% (v/v) at isokinetic conditions

Two-phase axial frictional pressure gradients and two-phase axial frictional pressure gradients including static head graphs were drawn against the mixture velocity and they are shown in Figures 4.13.a to 4.13.b. They showed similar trends. For this particle size (dp=138 μm), two-phase frictional pressure gradients are larger than those of the smaller particle size (dp=72 μm) at the same feed solid concentration.

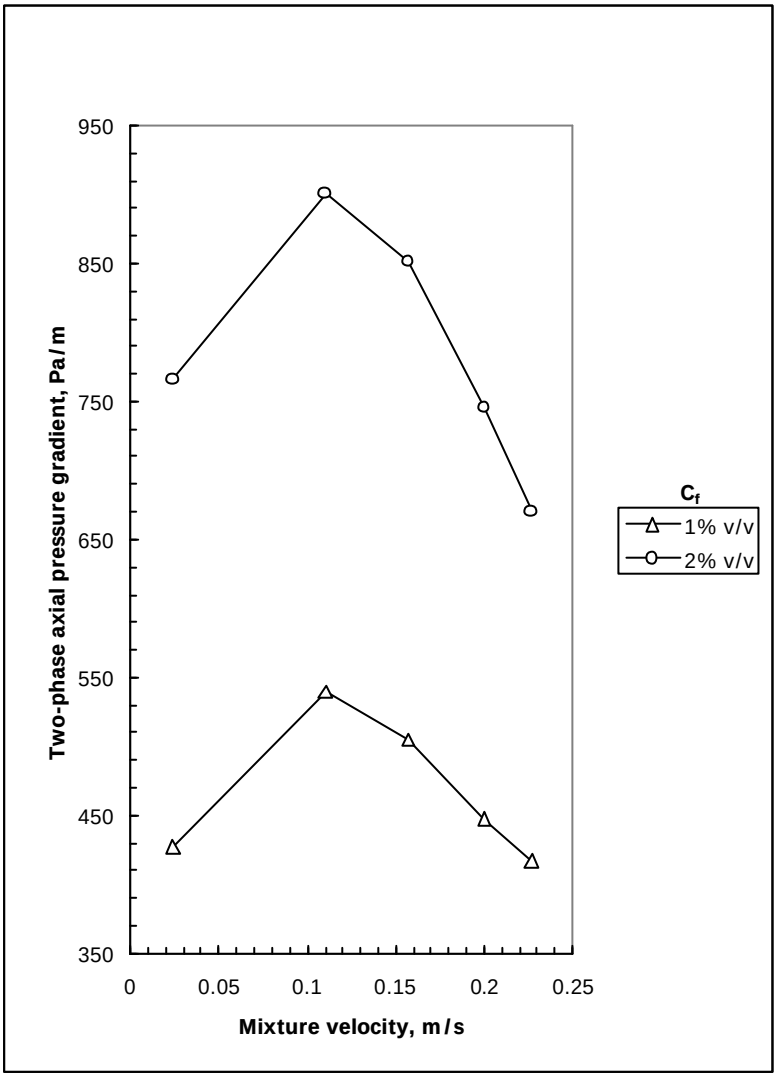

Figure 4.13.a. Two-phase axial pressure gradient vs. mixture velocity for different feed solid concentrations of particle size d_p=138 μm at isokinetic condition

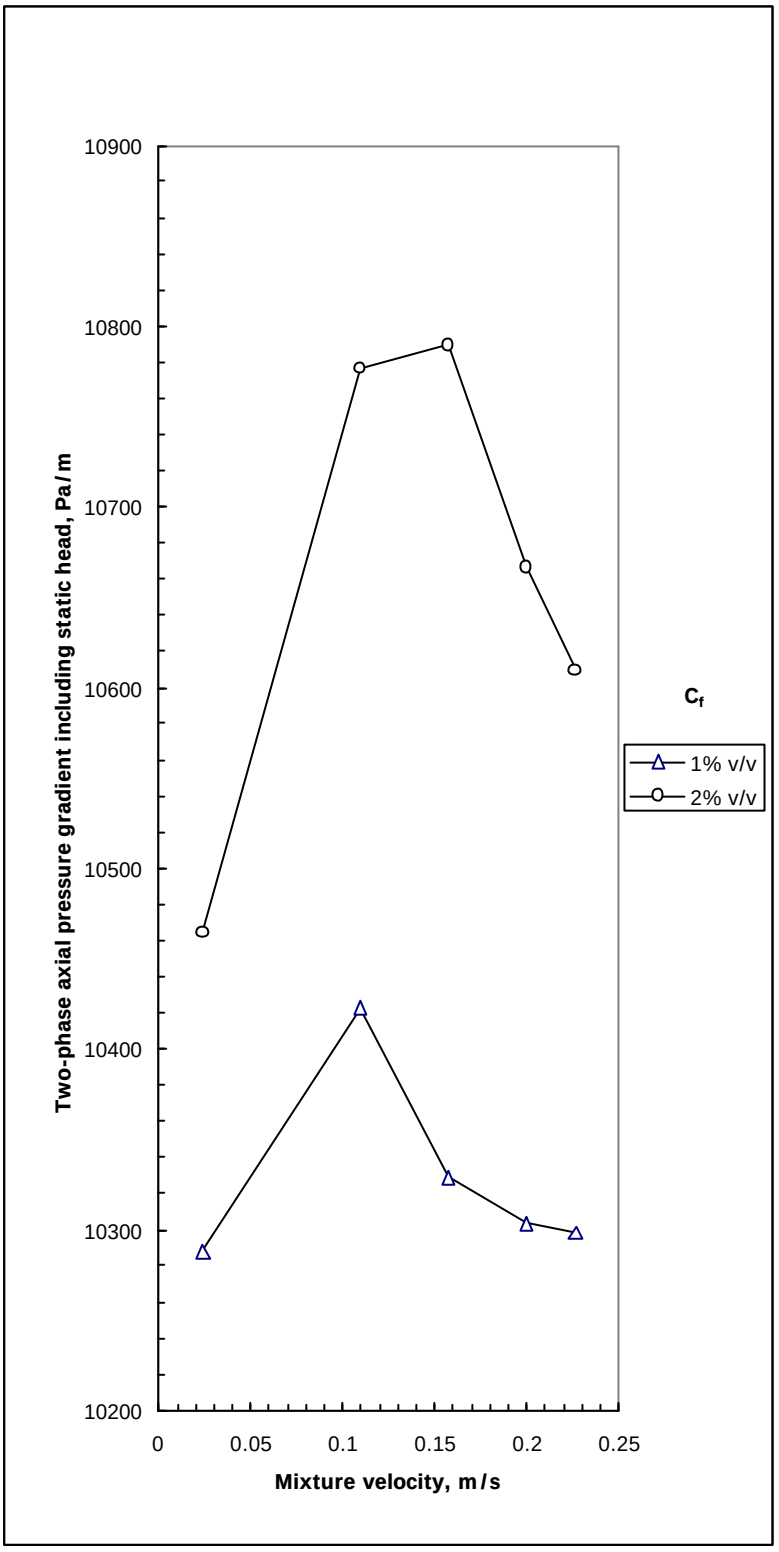

Figure 4.13.b. Two-phase axial pressure gradient (including static head) vs. mixture velocity for different feed solid concentrations of particle size dp=138 μm at isokinetic condition

Two-phase experimental friction factor versus mixture velocity graphs are presented in Figure 4.14. There was a decreasing trend in two-phase experimental friction factors as the mixture velocity increased for both feed solid concentrations of 1% and 2% v/v, as expected.

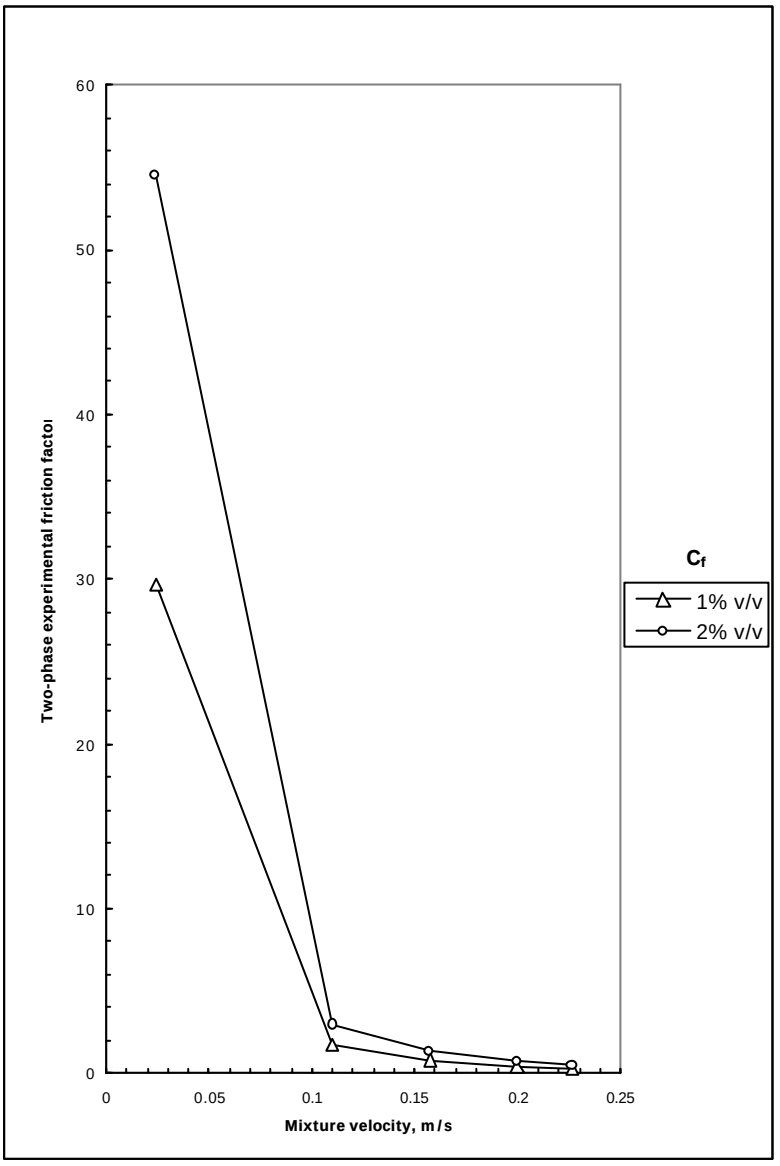

Figure 4.14. Two-phase experimental friction factor vs. mixture velocity when feed solid concentration is fixed, for d_p=138 μm at isokinetic condition

Generally it was found that the local solid densities around the outer wall of the annulus were higher than those near the inner wall, which was previously reported [21].

During the experiments, errors occurred from different sources: voltage fluctuations in the main power supply might have caused changes in the operation of the pump; thus the flow velocity in the annulus would show fluctuations; some manometer readings might not be very accurate due to the escape of solid particles to the manometer arms; some of the gravimetric measurement results might be erroneous due to the moisture absorbed by the dried solid samples; and there might be unnoticeable gas leakage from the isokinetic sampling unit, as the back-up pressure applied by N_2 gas to provide the same pressure in the flask (5) and sampling box (3), did not remain constant as needed.

Using the obtained data, the average transport solid-phase densities were calculated with the Simpson's rule [107] according to the formula

$$\overline{\rho}_s = \frac{\int_0^{2\pi}\int_{R_1}^{R_2} \rho_s(r)\, r\, d\theta\, dr}{\int_0^{2\pi}\int_{R_1}^{R_2} r\, d\theta\, dr} = \frac{\int_{R_1}^{R_2} \rho_s(r)\, r\, dr}{\frac{R_2^2}{2} - \frac{R_1^2}{2}} \quad \text{..... Eqn. (4.7)}$$

The results showed that $\overline{?}_s$ values were quite close to the measured average transport solid densities in the annulus and the average solid density in the feed tank during the operation. Actually 1% v/v or 25 v/v feed solid concentration did not mean too much. These were just the approximate values in the preparation of the feed slurry in the head tank; because, it was not possible to know the exact volume of the closed-loop system. When the solid density in the feed tank and the solid density in a sample taken from a point in the annulus above the test cross-section were determined, it was observed that they were in agreement with the $\overline{?}_s$ value obtained from the radial solid density profile by using the Simpson's rule. The error between the two is about maximum 15%, and it is much smaller for isokinetic

measurements than that of the nonisokinetic results. This proves the higher accuracy of the isokinetic results against the nonisokinetic measurements. The standard deviations in the determinations of pitot tube coefficient, local slurry velocities and local density measurements were calculated and these are given in Appendix B.

Pressure gradient measurements were repeated several times to get reproducibility and maximum error was obtained as 7.5%, under the same operating conditions.

Local solid densities measured in laminar flow regime at $Re_m = 2007$ yielded very small values indicating settling of solids in the bottom part of the closed-loop system.

RECOMMENDATIONS

1. In this study, the pressure differential between stagnation and static pressures of the pitot tube was measured by an inclined manometer. However, more sensitive devices are needed for very small pressure differentials. For instance, micro pressure transducers might give more accurate results.

2. A digital pressure gauge that displays three or preferably four decimal digits would make the radial local velocity and density measurements more accurate due to the higher accuracy required in the adjustment of the back-up pressure.

3. Methods other than isokinetic sampling could be used for more accurate measurement of radial solid density distributions, such as ultrasound, microwave techniques, photo sensor methodology, video recording technique [9] etc.

CHAPTER 5

CONCLUSIONS

Radial local solid densities in upward flowing water-feldspar mixtures were investigated in a vertical concentric annulus. 1% and 2% (v/v) feed solid concentrations (FSCs) were used. Experiments were conducted in the fully developed flow region. Local solid densities (LSDs), local slurry velocities, and axial pressure drops were determined experimentally. At the end of this study following results were obtained:

1. Radial dispersed solid densities were more uniform at low feed solid concentration of 1% v/v than those of 2% v/v. Increasing feed solid concentration and particle size caused different shapes of concentration profiles. The characteristics of the studied system probably affect this situation.

2. Radial dispersed solid densities changed with particle sizes, mixture velocities, and the relative velocity between the solid and liquid phases. Because, these relative velocities varied along the solid density profiles.

3. Radial local solid densities were obtained generally as higher near the outer wall than the inner wall of the annulus.

4. Two-phase axial frictional pressure drops along the test section of the annulus, increased with increasing feed solid concentration when the particle size was kept constant.

5. Two-phase axial frictional pressure drops along the test section of the annulus, increased with increasing particle size when mixture velocity and feed solid concentration were kept constant.

6. Two-phase axial frictional pressure drops along the test section of the experimental set-up, increased with increasing feed solid concentration when the mixture velocity was fixed.

7. Isokinetic sampling results showed more consistent increase in the local radial solid densities with the increasing mixture velocity at a constant value of radial distance.

8. The average transport solid phase densities calculated from the radial solid density profiles were in agreement with the transport solid density obtained by sampling from a line 130 cm above the test cross-section of the annulus. The % error between the two was about 15%. This error was found to be much higher for nonisokinetic local solid density data.

REFERENCES

[1] Soo, S.L., 1967, 'Fluid Dynamics of Multiphase Systems', Blaisdell Publication Company, Urbana.

[2] Lumley, J.L., 1978, 'Two-Phase and Non-Newtonian Flows', Applied Physics, Vol.12, pp. 289-324.

[3] Cox, R.G. & Mason, S.G., 1971, 'Suspended Particles in Fluid Flow through Tubes', A.Rev. Fluid Mech., Vol. 3, pp. 291-316.

[4] Yianneskis, M. & Whitelaw, J.H., 1984, 'Velocity Characteristics of Pipe and Jet Flows with High Particle Concentrations', ASME Fluids Engineering Conf.

[5] Roco, M.C. & Balakrishnam, N., 1985, 'Multi-Dimensional Flow Analysis of Solid-Liquid Mixtures', Journal of Rheology, Vol. 29 (4), pp. 431-456.

[6] Ribas, R., Lourenço, L. & Riethmuller, M.L., 1980, 'A Kinetic Model for a Gas-Particle Flow', Pneumotransport 5, Vth International Conference on the Pneumatic Transport of Solids in Pipes.

[7] Fadarani, S., Tüzün, U., Smith, D.L.O. & Thorpe, R.B., 1997, 'Discharge and Transport of Nearly Buoyant Granular Solids in Liquids, Part I. Tomographic Study of the Interstitial Voidage Effects Governing Flow Regimes', Chemical Engineering Science, Vol. 53, No. 3, pp. 553-574.

[8] Alajbegovic, A., Assad, A., Bonetto, F. & Lahey Jr., R.J., 1994, 'Phase Distribution and Turbulence Structure for Solid/Fluid Upflow in a Pipe', International Journal of Multiphase Flow, Vol. 20, No.3, pp.

453-479.

[9] Lareo, C., Nedderman, R.M. & Fryer, P.J., 1997, 'Particle Velocity Profiles For Solid-Liquid Food Flows In Vertical Pipes, Part II. Multiple Particles', Powder Technology, Vol. 93, pp. 35-45.

[10] Mankad, S. & Fryer, P.J., 1997, 'A Heterogeneous Flow Model for the Effect of Slip and Flow Velocities on Food Steriliser Design', Chemical Engineering Science, Vol. 52, No. 12, pp. 1835-1843.

[11] Soliman, R.H. & Collier, P.B., 1990, 'Pressure Drop in Slurry Lines', Hydrocarbon Processing, pp. 60-63.

[12] Roco, M.C. & Shook, C.A., Aug. 1983, 'Modelling of Slurry Flow: The Effect of Particle Size', The Canadian Journal of Chemical Engineering, Vol. 61, pp. 494-503.

[13] Nasr-El-Din, H., Shook, C.A. & Colwell, J., 1987, 'A Conductivity Probe for Measuring Local Concentrations in Slurry Systems', International Journal of Multiphase Flow, Vol. 13, No.3, pp. 365-378.

[14] Chen, R.C. & Kadambi, J.R., 1995, 'Discrimination Between Solid and Liquid Velocities in Slurry Flow Using Laser Doppler Velocimeter', Powder Technology, Vol. 85, pp. 127-134.

[15] Brauner, N., 1991, 'Two Phase Liquid-Liquid Annular Flow', International Journal of Multiphase Flow, Vol. 17, No. 1, pp. 59-76.

[16] Ayukawa, K., Kataoka, H. & Hirano, M., 1980, 'Concentration Profile, Velocity Profile and Pressure Drop in Upward Solid-Liquid Flow Through a Vertical Pipe', BHRA Fluid Engineering, Hydrotransport 7, Paper E2, pp. 195-202.

[17] Loli, A. M. & Joshi, J. B., 1989, 'Pressure Drop in Solid-Liquid Fluidized Beds', Powder Technology, Vol. 59, pp. 129-140.

[18] Sellgren, A., 1982, 'The Choice of Operating Velocity in Vertical

Solid-Water Pipeline Systems', BHRA Fluid Engineering, Hydrotransport 8, Paper D3, pp. 211-226.

[19] Noda, K., Takahashi, H. & Kawashima, T., Oct. 1984, 'Relation Between Behavior of Particles and Pressure Loss in Horizontal Pipes', BHRA Fluid Engineering, Hydrotransport 9, Paper D4, pp. 191-199.

[20] Vocadlo, J.J. & Charles, M.E., 1972, 'Prediction of Pressure Gradient for the Horizontal Turbulent Flow in Slurries', BHRA Fluid Engineering, Hydrotransport 2, Paper C1, pp. C1-1-C1-12.

[21] Özbelge, T.A., Beyaz, A., 2001, 'Dilute Solid-Liquid Upward Flows through a Vertical Annulus in a Closed Loop System', International Journal of Multiphase Flow, Vol. 27, pp. 737-752.

[22] Karabelas, A.J., July 1977, 'Vertical Distribution of Dilute Suspensions in Turbulent Pipe Flow', A. I. Ch. E. Journal, Vol. 23, No. 4, pp. 426-434.

[23] Michaelides, E.E. & Farmer, L.K., 1984, 'A Model for Slurry Flows Based on The Equations of Turbulence', Journal of Pipelines, Vol. 4, pp. 185-191.

[24] Soo, S.L., Ihrig, H.K.Jr & El Kouh, A.F., Sep. 1960, 'Experimental Determination of Statistical Properties of Two-Phase Turbulent Motion', Journal of Basic Engineering Transactions of The ASME, Vol., PP. 609-616.

[25] Rao, C.S. & Dukler, A.E., 1971, 'The Isokinetic-Momentum Probe. A New Technique for Measurement of Local Voids and Velocities in Flow of Dispersions', Industrial Engineering Chemistry Fundamentals, Vol. 10, No. 3, pp. 520-526.

[26] Eraslan, A.N. & Özbelge, T.A., 2003, 'Assesment of Flow and Heat Transfer Characteristics For Proposed Solid Density Distribution in Dilute Laminar Slurry Upflows through a Concentric Annulus', Chemical Engineering Science, Vol. 58, pp. 4055-4069.

[27] Kada, H. & Hanratty, T.J., 1960, 'Effect of Solids on Turbulence on a Fluid', A. I. Ch. E. Journal, Vol. 6, No. 4, pp. 624-630.

[28] Ohashi, H., Sugawara, T., Kikuchi, K.-I. & Ishé, M., 1980, 'Average Particle Velocity in Solid-Liquid Two-Phase Flow through Vertical and Horizontal Tubes', Vol. 13, No. 5, pp. 343-349.

[29] Mcdermott, W.F., 1970, 'Savage River Mines- The World's First Long-Distance Iron Ore Slurry Pipe-Line', The Canadian Mining and Metallurgical Journal, pp. 1378-1388.

[30] Lutjen, G.P., 1970, 'Marconaflo-The System and the Concept', Engineering and Mining Journal.

[31] Keska, J., 1978, 'Measurement of the Distribution and Overall Spatial Solid Body Content in the Process of Hydrotransport of Mixtures in Pipelines', BHRA Fluid Engineering, Hydrotransport 5, Paper G5, pp. 59-72.

[32] Mitchell, F. R. G. & De Alwis, A. A. P., 1989, 'Electrical Conductivity-meter for Food Samples', Journal of Physics-E: Scientific Instruments, Vol. 22, pp. 554-556.

[33] Scarlett, B. & Grimley, A., 1974, 'Particle Velocity and Concentration Profiles During Hydraulic Transport in a Circular Pipe', BHRA Fluid Engineering, Hydrotransport 3, Paper D3, pp. 23-37.

[34] Clarke, P.F. & Charles, M.E., August 1997, 'Experimental Test of a Model for Laminar Slurry Flow with Sedimentation', The Canadian Journal of Chemical Engineering, Vol. 75, pp. 692-703.

[35] Fregert, J., 1995, 'Velocity and Concentration Profiles of a Laminar Flow for a Fluid Containing Large Spheres in a Horizontal Pipe', Ph. D. Thesis, Lund University, Sweden.

[36] Özbelge, .T.A. & Somer, T.G., 1988, 'Hydrodynamic and Heat Transfer Characteristics of Liquid-Solid Suspensions Horizontal Turbulent Pipe Flow', Chemical Engineering Journal, Vol. 38, pp. 111-122.

[37] Stanley-Wood, N.G., Leewellyn, G.J. & Taylor, A., 1981, 'On-Stream Particle Size, Concentration and Velocity Measurements by Auto-Correlation of Scattered Laser Light', Powder Technology, Vol. 29, pp. 217-223.

[38] Voloudakis, K., Vrahliotis, P., Kastrinakis, E.G. & Nychas, S.G., 1999, 'The Behavior of a Conductivity Probe in Electrolytic Liquid/Solid Suspensions', Measurement Science and Technology, Vol. 10, pp. 100-105.

[39] Ncube, F., Kastrinakis, E.G., Nychas, S.C. & Lavdakis, K.E., 1991, 'Drifting Behavior of a Conductivity Probe', Journal of Hydraulic Research, Vol. 29, pp. 643-654.

[40] Nasr-El-Din, H.A., Mactaggart, R.S. & Masliyah, J.H., 1996, 'Local Solid Concentration Measurement in a Slurry Mixing Tank', Chemical Engineering Science, Vol. 51, No. 8, pp. 1209-1220.

[41] Özbelge, T., Lourenço, L.M. & Riethmuller, M.L., 1996, 'Particle Concentration Measurements in Turbulent Gas-Solid Flows through Horizontal Rectangular Ducts', Tr. J. Eng. and Environmental Sciences, Vol. 20, pp. 57-65.

[42] Hsu, F-L., Turian, R.M. & Ma, T-W. , March 1989, 'Flow of Noncolloidal Slurries in Pipelines', A. I. Ch. E. Journal, Vol. 35, No. 3, pp. 429-441.

[43] Nasr-El-Din, H., Shook, C.A. & Esmail, M.N., October 1985, 'Wall Sampling in Slurry Systems', The Canadian Journal of Chemical Engineering, Vol. 63, pp. 746-753.

[44] Furuta, T., Tsujimoto, S., Toshima, M., Okazaki, M. & Toei, R.,

October 1977, ‘Concentration Distribution of Particles in Solid-Liquid Two-Phase Flow Through Vertical Pipe’, pp. 605-615.

[45] Toda, M., Shimizu, T., Saito, S. & Maeda, S., 1972, Preprint for 37th Annual Meeting Society Chemical Engineering, Japan, pp. B-310.

[46] Koh, C.J., Hookham, P. & Leal, L.G., 1994, ‘An Experimental Investigation of Concentrated Suspension Flows in a Rectangular Channel’, Journal of Fluid Mechanics, Vol. 266, pp. 1-32.

[47] Engelmann, H.E., 1978, ‘Vertical Hydraulic Lifting of Large-Size Particles- A Contribution to Marine Mining’, Offshore Technology Conference, Houston, U.S.A.

[48] Sellgren, A., 1979, ‘Slurry Transportation of Ores and Industrial Minerals in a Vertical Pipe by Centrifugal Pumps-A Pilot Plant Investigation of Hydraulic Hoisting, Dissertation, Department of Hydraulics, Chalmers Univ. of Tech., Göteborg, Sweden.

[49] Özbelge, T.A.,1983, ‘Hydrodynamic and Heat Transfer Characteristics of Gas-Solid and Liquid-Solid Systems in Turbulent Flow’, Ph. D. Thesis, Middle East Technical University, Ankara.

[50] Ogawa, K., Yoshikawa, S., Suguro, A., Ikeda, J. & Ogawa, H., 1990, ‘Flow Characteristics and Circular Pipe Flow of Pulp-Suspension’, Journal of Chemical Engineering Of Japan, Vol. 23, No. 1, pp. 1-6.

[51] Brown, N.P. & Shook, C.A., August 1982, ‘A Probe for Particle Velocities: The Effect of Particle Size’, Hydrotransport 8, Paper G1, pp. 339-348.

[52] Doig, I.D. & Roper, G.H., May 1967, ‘Air Velocity Profiles in the Presence Of Cocurrently Transported Particles’, I & EC Fundamentals, Vol. 6, No. 2, pp. 247-255.

[53] Sun, S.F., Wu, Y.Y. & Zhao, R.Y., April 2001, ‘The Numerical

Calculation of Heat Transfer Performance for Annular Flow of Liquid Nitrogen in a Vertical Annular Channel', Cryogenics, Vol. 41(4), pp. 231-237.

[54] Dutta, B. & Sastry, S.K., 1990, 'Velocity Distributions of Food Particle Suspensions in Holding Tube Flow: Distribution Characteristics and Fastest Particle Velocities', Journal of Food Science, Vol. 55, No. 6, pp. 1703-1710.

[55] Sheen, S.H. & Raptis, A.C., Jan. 1985, 'BB5, Active Acoustic Cross Correlation Technique Applied to Flow Velocity Measurement in a Coal/Liquid Slurry', IEEE Transactions on Sonics and Ultrasonics, Vol. Su-32, No. 1, pp. 107.

[56] Darby, R., Mun, R. & Boger, D.V., Sep. 1992, 'Predict Friction Loss in Slurry Pipes', Chemical Engineering, pp. 116-119.

[57] Doron, P. & Barnea, D., 1992, 'Effect of the No-Slip Assumption on the Prediction of Solid-Liquid Flow Characteristics', International Journal of Multiphase Flow, Vol. 18, No. 3, pp. 617-622.

[58] Doron, P., Granica, D. & Barnea, D., 1987, 'Slurry Flow in Horizontal Pipes-Experimental and Modelling', International Journal of Multiphase Flow, Vol. 13, pp. 535-547.

[59] Prosperetti, A. & Jones, A. V., 1984, 'Pressure Forces in Disperse Two-Phase Flow', International Journal of Multiphase Flow, Vol. 10, No. 4, pp. 425-440.

[60] Ferre, A.L. & Shook, C.A., Apr-Jun 1998, 'Coarse Particle Wall Friction in Vertical Slurry Flows, Particulate Science and Technology', Vol.16(2),pp.125-133.

[61] Debreczeni, E., Meggyes, T. & Tarjan, I., 1978, 'Measurement Methods in an Experimental Rig for Hydraulic Transport', BHRA Fluid Engineering, Hydrotransport 5, Paper G1, pp. 1-20.

[62] Dukler, A.E., Wicks, M., Iii. & Cleveland, R.G., January 1964, 'Frictional Pressure Drop in Two-Phase Flow: A. A. Comparison of Existing Correlations for Pressure Loss and Holdup', A. I. Ch. E. Journal, Vol. 10, No. 1, pp. 38-43.

[63] Özbelge, T.A., 1997, 'A New Mixture Friction Factor Correlation for Vertical Upward Pneumatic Conveying of Solid Particles', Tr. J. of Engineering and Environmental Sciences, Vol. 21, pp. 253-255.

[64] Özbelge, T.A., 1984, 'Solids Friction Factor Correlation for Vertical Upward Pneumatic Conveyings', International Journal of Multiphase Flow, Vol. 10, pp. 459-465.

[65] Khan, A., Khan, A.A. & Varma, Y.B.G., Jan. 2002, 'Prediction of Two-Phase Frictional Pressure Drop for the Concurrent Gas & Newtonian Liquids Upflow Through Packed Beds', Chemical Engineering and Technology, Vol. 25 (1), pp. 51-55.

[66] Nouri, J.M., Umur, H. & Whitelaw, J.H., 1993, 'Flow of Newtonian and Non-Newtonian Fluids in Concentric and Eccentric Annuli', Journal of Fluid Mechanics, Vol. 253, pp. 617-641.

[67] Lawn, C.J. & Elliott, C.J., 1972, 'Fully Developed Turbulent Flow Through Concentric Annuli', Journal Mechanical Engineering Science, Vol. 14, No. 3, pp. 195-204.

[68] Wolf, A., Jayanti, S. & Hewitt, G.F., May 2001, 'Flow Development in Vertical Annular Flow', Chemical Engineering Science, Vol.56(10),pp.3221-3235.

[69] Fairhurst, P.G., Barigou, M., Fryer, P.J. & Pain, J.P., December, 1999, 'Particle Passage Time Distributions in Vertical Pipe Flow of Solid-Liquid Food Mixtures, Food and Bioproducts Processing', Vol. 77 (4), pp. 293-301.

[70] Quarmby, A., 1967, 'An Experimental Study of Turbulent Flow through Concentric Annuli', International Journal of Mech. Science,

Vol. 9, pp. 205-221.

[71] Sparrow, E.M. & Lin, S.H., December 1964, 'The Developing Laminar Flow and Pressure Drop in the Entrance Region of Annular Ducts', Journal of Basic Engineering, Transactions Of The ASME.

[72] Özbelge, T.A. & Köker, S.H., 1996, 'Heat Transfer Enhancement in Water-Feldspar Upflows through Vertical Annuli', International Journal Of Heat & Mass Transfer, Vol. 39, pp. 135-147.

[73] Cooke, R. & Lazarus, J.H., Oct. 1988, 'Isokinetic Sampling Probe for Slurry Flows', BHRA Fluid Engineering, Hydrotransport 11, Paper C1, pp. 117-130.

[74] Jones, O.C. Jr. & Leung, J.C.M., 1981, 'An Improvement in the Calculation of Turbulent Friction in Rectangular Ducts, ASME J. of Fluids Eng., Vol. 98, pp. 173-181.

[75] Masuda, H., Yoshida, H. & Iinoya, K., 1980, 'Theoretical Study of Electrostatic Effects on Isokinetic Dust Sampling', Journal of Chemical Engineering of Japan, Vol. 13, No. 6, pp. 467-472.

[76] Zhang, G.J. & Ishii, M., 1995, 'Isokinetic Sampling Probe and Image Processing System For Droplet Size Measurement in Two-Phase Flow', International Journal of Heat and Mass Transfer, Vol. 38, No. 11, pp. 2019-2027.

[77] Boothroyd, R.G. & Goldenberg, A.S., March 1970, 'Measurements in Flowing Gas-Solid Suspensions II', British Chemical Engineering, Vol. 15, No. 3, pp. 356-368.

[78] Boothroyd, R.G., 'Flowing Gas-Solid Suspensions', 1st Edition, Chapman and Hall LTD., 1971, London.

[79] Schraub, F.A., August 3-6, 1969, 'Isokinetic Probe and Other Two-Phase Sampling Devices: A Survey', 'Two-Phase Flow Instrumentation', 11thnational ASME/A. I. Ch. E. Heat Transfer

Conference, Minneapolis, Minnesota, Sponsored by ASME Heat Transfer Division, The American Society of Mechanical Engineers, New York, United Engineering Center, USA, pp. 47- 57.

[80] Brown, N.P. & Heywood, N.I., 1991, 'Slurry Handling Design of Solid-Liquid Systems', 1st Edition, Elsevier Applied Science, Great Britain.

[81] Kakka, R.S., Sc. B. & Phil. M., 1974, 'Review of Instruments for Measuring Flow Rate and Solids Concentration in Steel Works Slurry Pipeline', BHRA Fluid Engineering Hydrotransport 3, Paper F6, pp. 81-92.

[82] Ong, K.H. & Beck, M.S., 1975, 'Slurry Flow Velocity, Concentration and Particle Size Measurement Using Flow Noise and Correlation Techniques', Measurement Control, Vol. 8, pp. 453-463.

[83] Dyakowski, T., Jeanmeure, L.F.C. & Jaworski, A.J., 2000, 'Applications of Electrical Tomography for Gas-Solids and Liquid-Solids Flow', Powder Technology, Vol. 122, pp. 174-192.

[84] Weinstein, H., Shao, M., Schnitzlein, M. & Graff, R.A., in: K. Ostergaard, A. Sorensen (Eds.), 1986, Fluidization V, Engineering Foundation, New York, pp. 329.

[85] Zhang, H., Johnston, P.M., Zhu, J-X., Delasa, H.I. & Bergougnou, M.A., 1998, 'A Novel Calibration Procedure for a Fiber Optic Solids Concentration Probe', Powder Technology, Vol. 100, pp. 260-272.

[86] Chigier, N.A., Ungut, A. & Yule, A.J., 1979, 'Particle Size and Velocity Measurements in Planes By Laser Anemometer', Proc. 17th Symp. (Int.) on Combustion, pp. 315-324.

[87] Durst, F., 1982, 'Review-Combined Measurements of Particle Velocities, Size Distribution, and Concentration', Transactions of the ASME, Journal of Fluids Engineering, Vol. 104, pp. 284-296.

[88] Hess, C.F., 1984, 'Non-Intrusive Optical Single-Particle Counter for Measuring Size and Velocity 9of Droplets in a Spray', Applied Optics, Vol. 23, pp. 4375-4382.

[89] Allano, D., Gouesbet, G., Grehan, G. & Lisiecki, D., 1984, 'Droplet Sizing Using a Top-Hat Laser Beam Technique', Journal of Physics D: Applied Physics, Vol. 17, pp. 43-58.

[90] Maeda, M., Hishida, K., Sekine, M. & Watonabe, N., 1988, 'Measurements of Spray Jet Using LDV System with Particle Size Discrimination. Laser Anemometry in Fluid Mechanics-I' (Eds. R.J. Adrian Et Al.) Selected Papers From the 3rd Int. Symp. on Appl. of Laser Anemometry to Fluid Mechanics, pp. 375-386.

[91] Nasr-El-Din, H., Shook, C.A. & Colwell, J., Oct. 1986, 'Determination of Solids Concentration in Slurries', BHRA Fluid Engineering, Hydrotransport 10, Paper F1, pp. 191-198.

[92] Spitzer, D.W., Editor, 1991, 'Flow Measurement', Practical Guides for Measurement and Control, Instrument Society of America, 1st Edition, Research Triangle Park, USA.

[93] Gillespie, T. & Gunter, A.W., 1959, Trans. ASME. J. App. Mech., Vol.7, pp. 584.

[94] Gibson, H.G., Peskin, R.L., Dwyer, H.A. & Spencer, J.D., 1966, ASME-EIC Fluids Engineering Conf., pp. 66.

[95] Peskin, R.L. & Dwyer, H.A., Tech. Rpt. 101-ME-F, NYO 2930-1 Rutgers University, USA.

[96] Goldschmidt, V.W., 1965, Journal Of Coll. Science, Vol. 20, pp. 617.

[97] Richardson, J.F. & McLeman, M., 1960, Trans. Inst. Chem. Engrs., Vol. 38, pp. 25.

[98] Domnick, J., Durst, F., Raszillier, H. & Zeisel, H., 1987, 'A Method to Measure Mass and Volume Flow Rates of Two-Phase Flow', International Journal of Multiphase Flow, Vol. 13, No. 5, pp. 685-697.

[99] Durst, F. & Zare, M., 1975, 'Laser-Doppler Measurements in Two-Phase Flows', Proceedings of the LDA-Symposium, University of Denmark.

[100] Pryakhin, A.E. & Faibyshev, A.E., 1985, 'Signal Converter for Nuclear-Magnetic Flow-Meter', Instruments and Experimental Techniques, Vol. 28, Pt. 1, pp. 723-724.

[101] Beck, M.S., Drane, J., Plaskowski, A. & Wainwright, N., 1968, 'Particle Velocity and Mass Flow Measurement in Pneumatic Conveyors', Powder Technology, Vol. 2, pp. 269-277.

[102] Beck, M.S., Gough, J.R. & Mendis, P.J., 1970, 'Flow Velocity Measurement in a Hydraulic Conveyor', Proc. 1st Int. Conf. on Hydraulic Transport of Solids, BHRA Fluid Engineering, Cranfield, UK, Paper B3.

[103] Baker, R.C., 1989, 'An Introductory Guide to Flow Measurement', Mechanical Engineering Publications Limited, London, 1st Edition, Great Britain.

[104] Doolittle, J.S., 1957, 'Mechanical Engineering Laboratory Instrumentation and Its Application', McGraw-Hill Book Company, Inc., 1st Edition, USA.

[105] Cheremisinoff, N.P. & Cheremisinoff, P.N., 1987, 'Instrumentation for Process Flow Engineering', 1st Edition, Technomic Publishing Co., Inc., USA.

[106] McCabe, W.L., Smith, J.C. & Harriot, P., 1993, 'Unit Operations of Chemical Engineering', 5th Edition, McGraw-Hill International Editions, Singapore.

[107] Fogler, H.S., 1992, 'Elements of Chemical Reaction Engineering',

2nd Edition, Prentice-Hall, Inc., US.

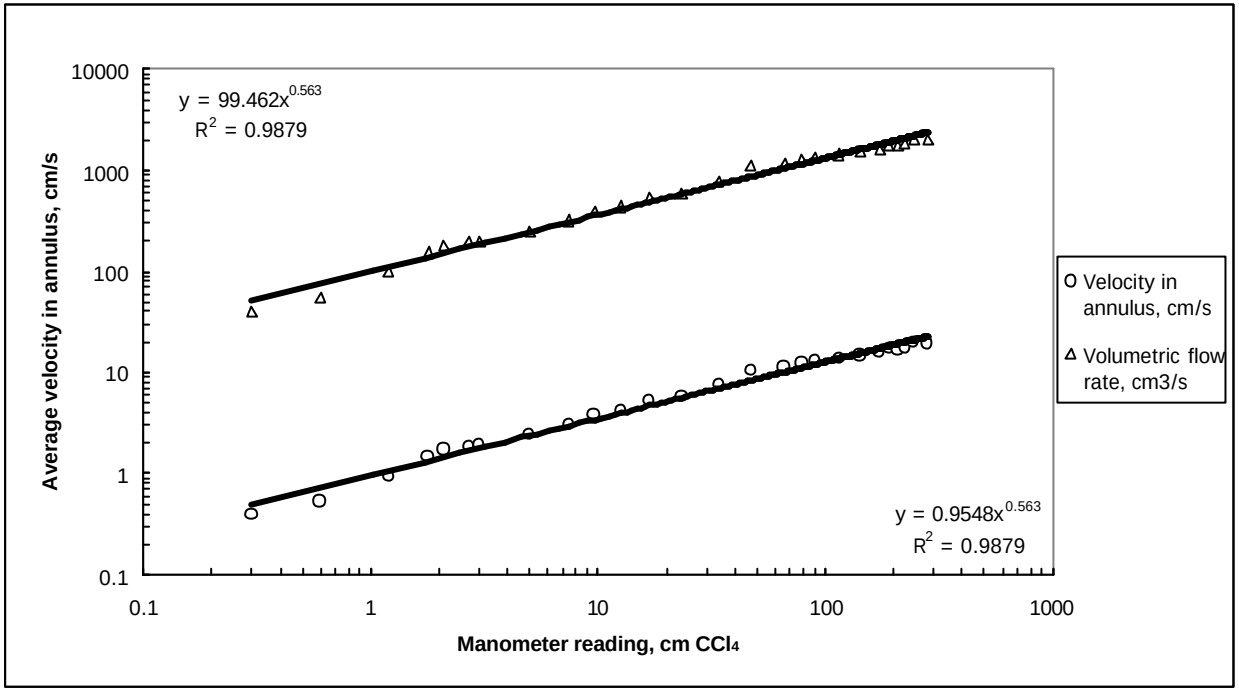

Figure A.1. Calibration curve of the orificemeter

$$U_{ann} = 0.9548(\Delta H_{CCl4})^{0.563}$$

$$Q = 99.462(\Delta H_{CCl4})^{0.563}$$

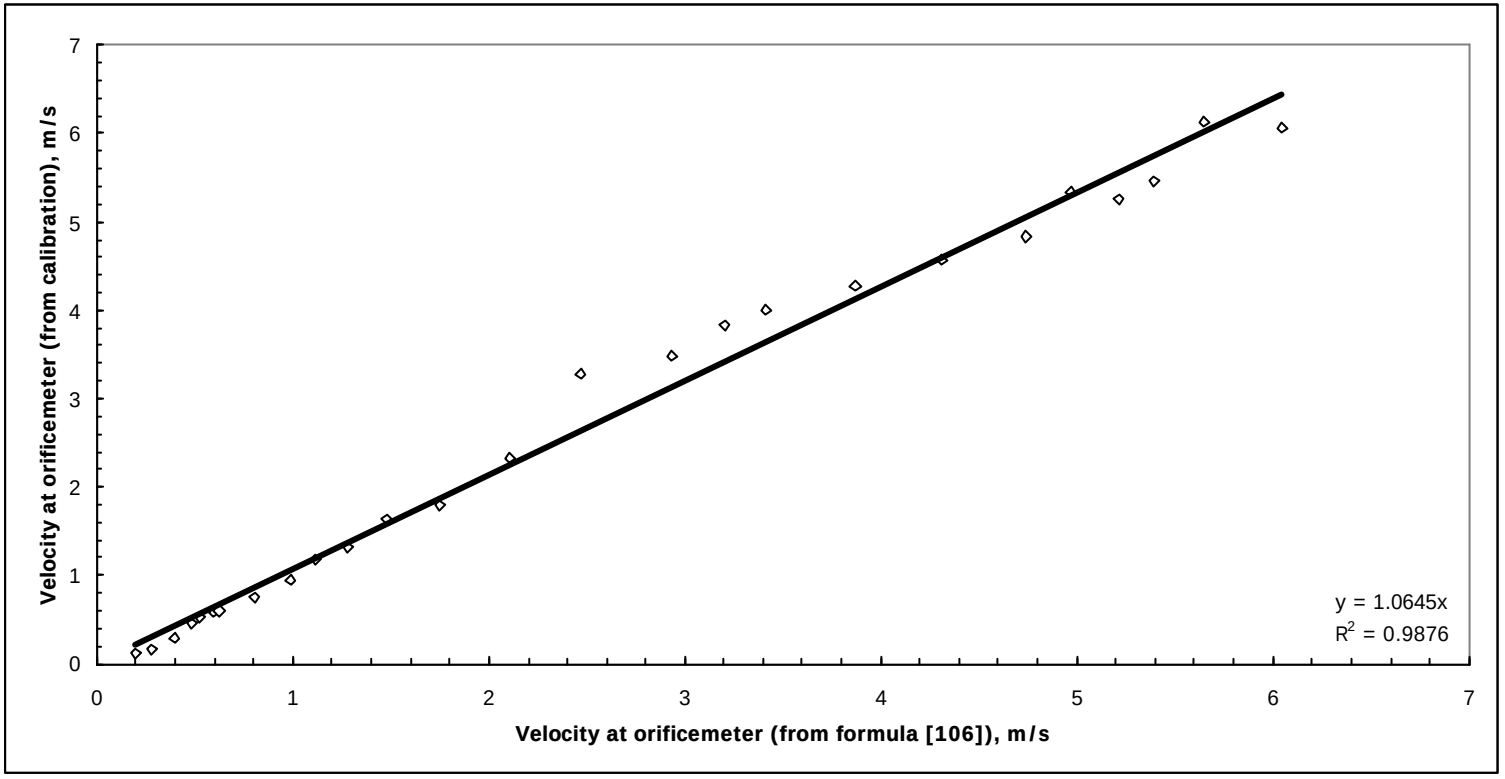

Figure A.2. Orificemeter coeffficient

Orificemeter coefficient= 1.0645

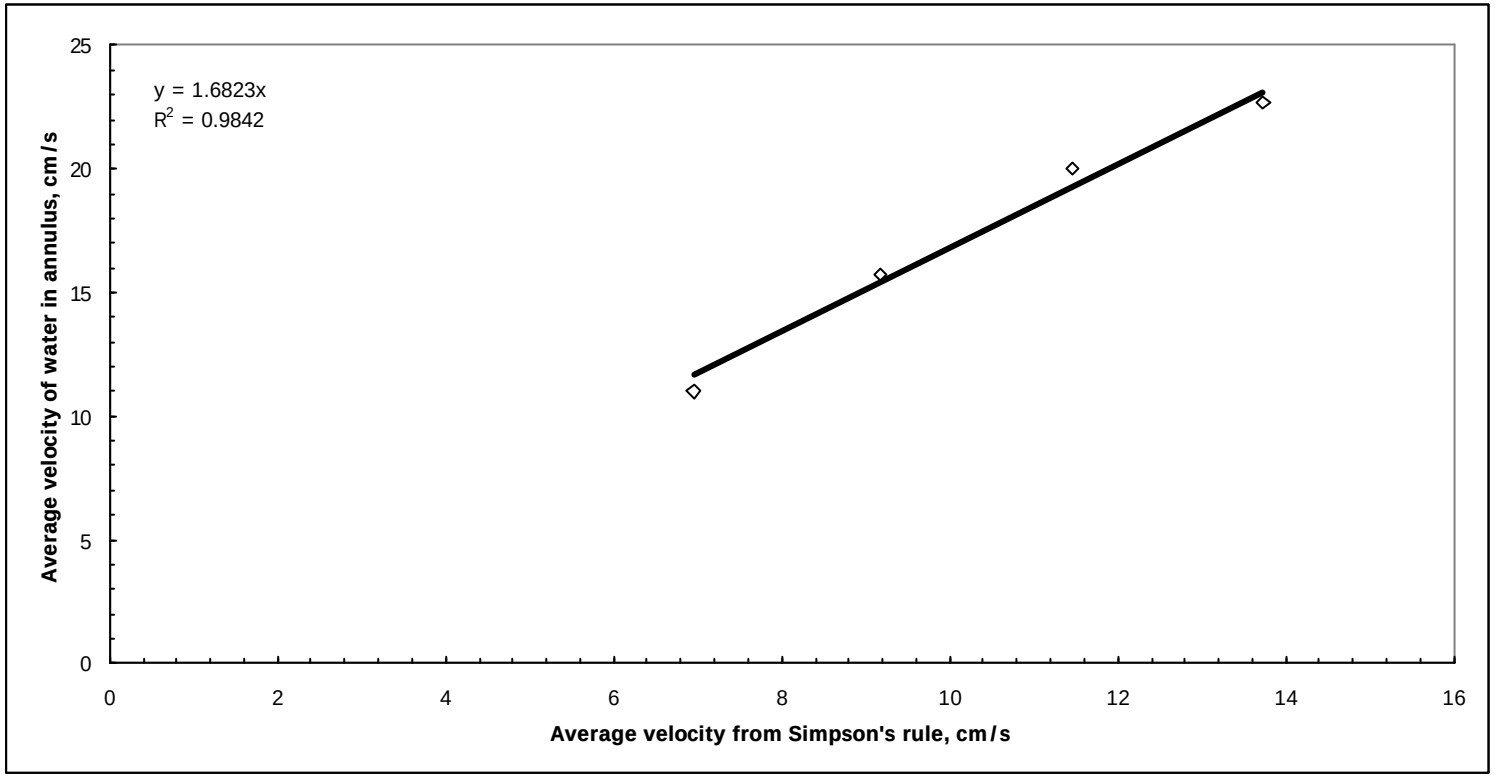

Figure A.3. Pitot tube coefficient

Pitot tube coefficient= 1.6823

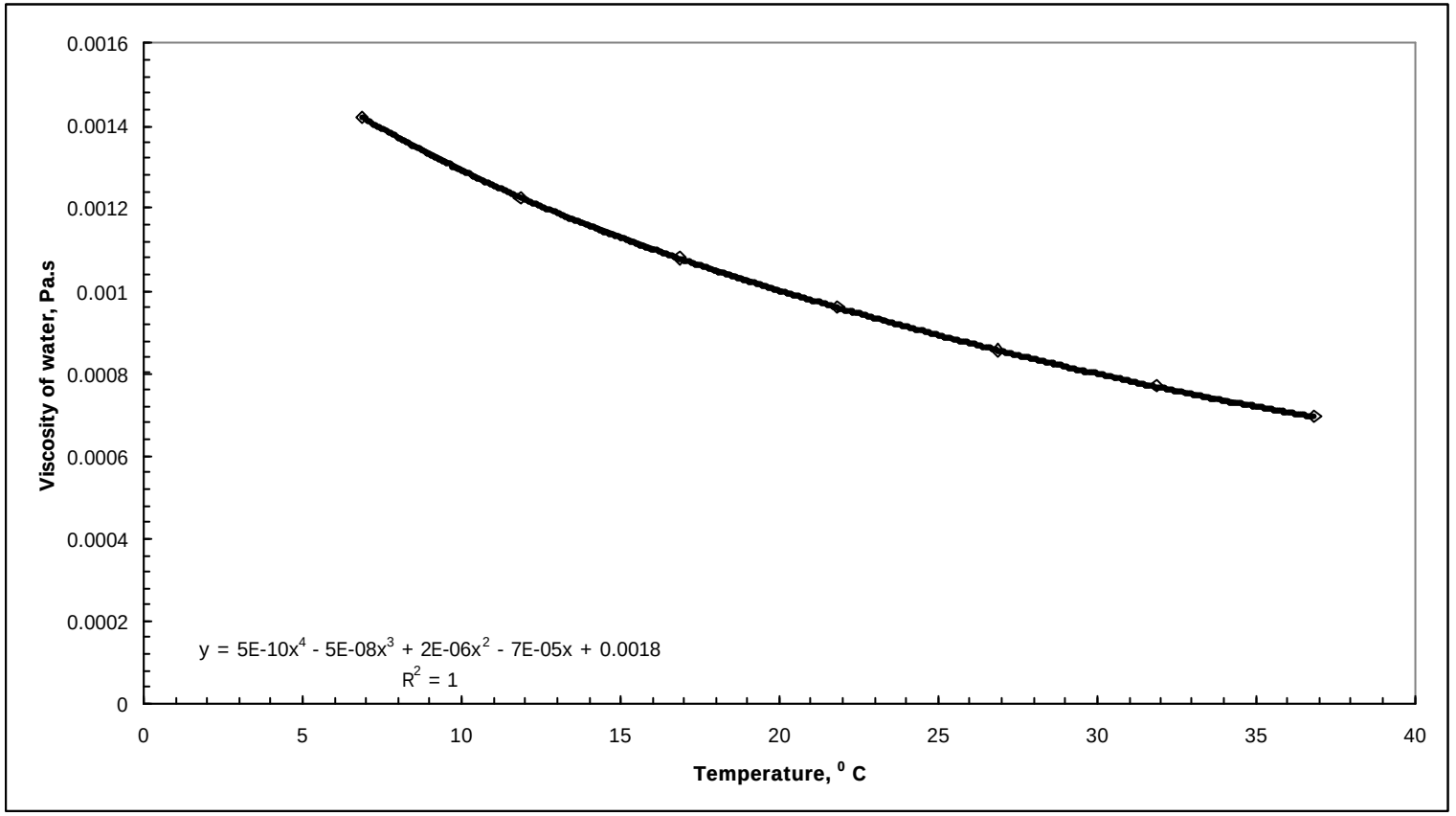

Figure A.4. Viscosity of water vs. temperature

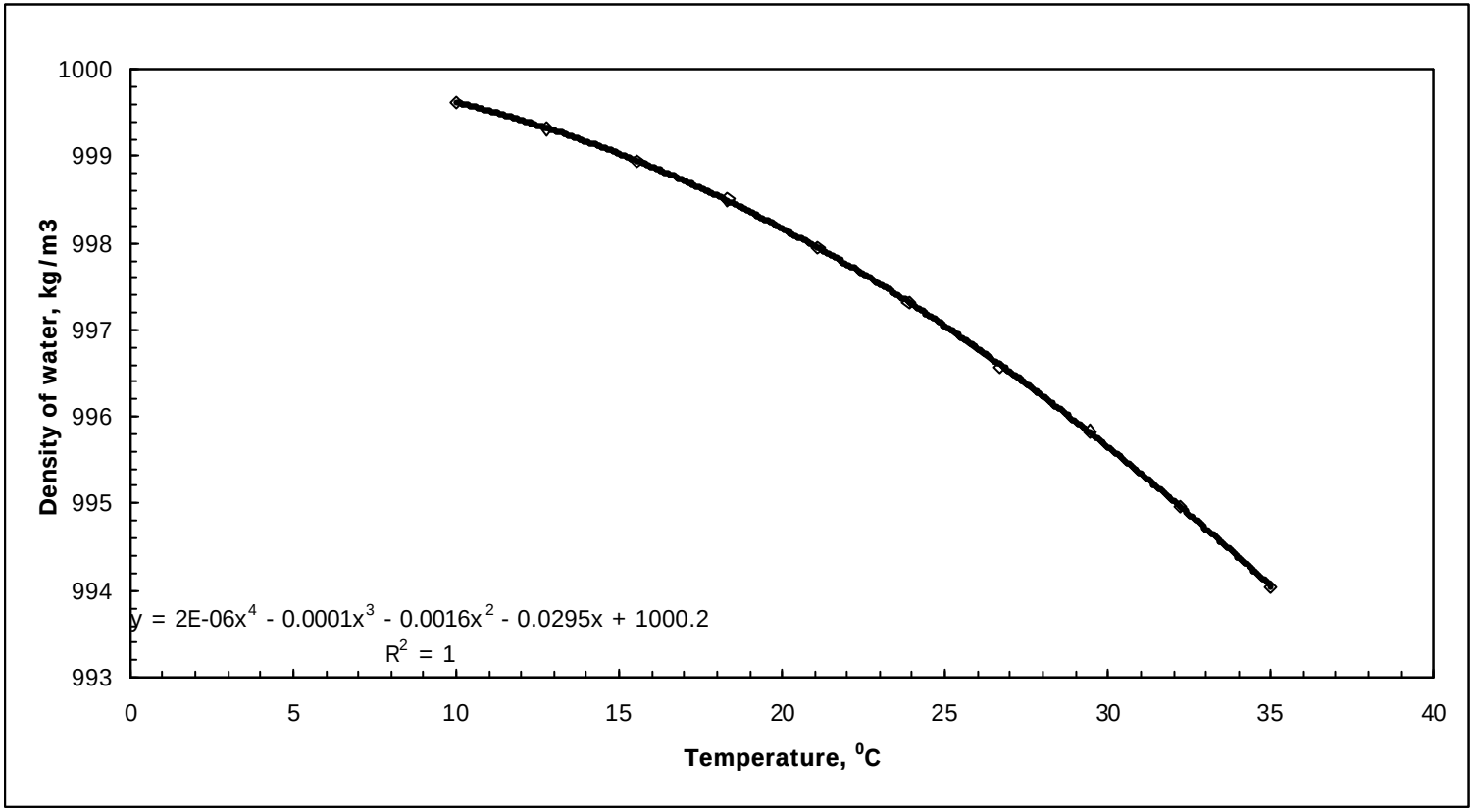

Figure A.5. Density of water vs. temperature

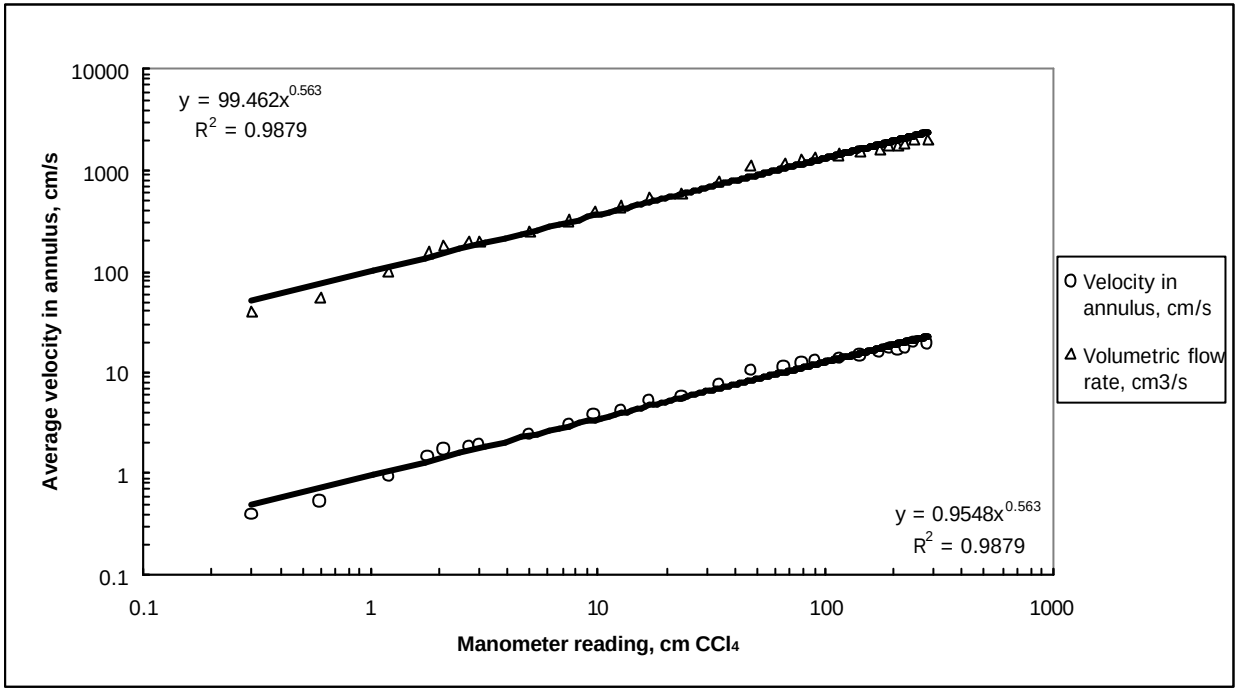

Figure A.1. Calibration curve of the orificemeter

$$U_{ann} = 0.9548(\Delta H_{CCl4})^{0.563}$$

$$Q = 99.462(\Delta H_{CCl4})^{0.563}$$

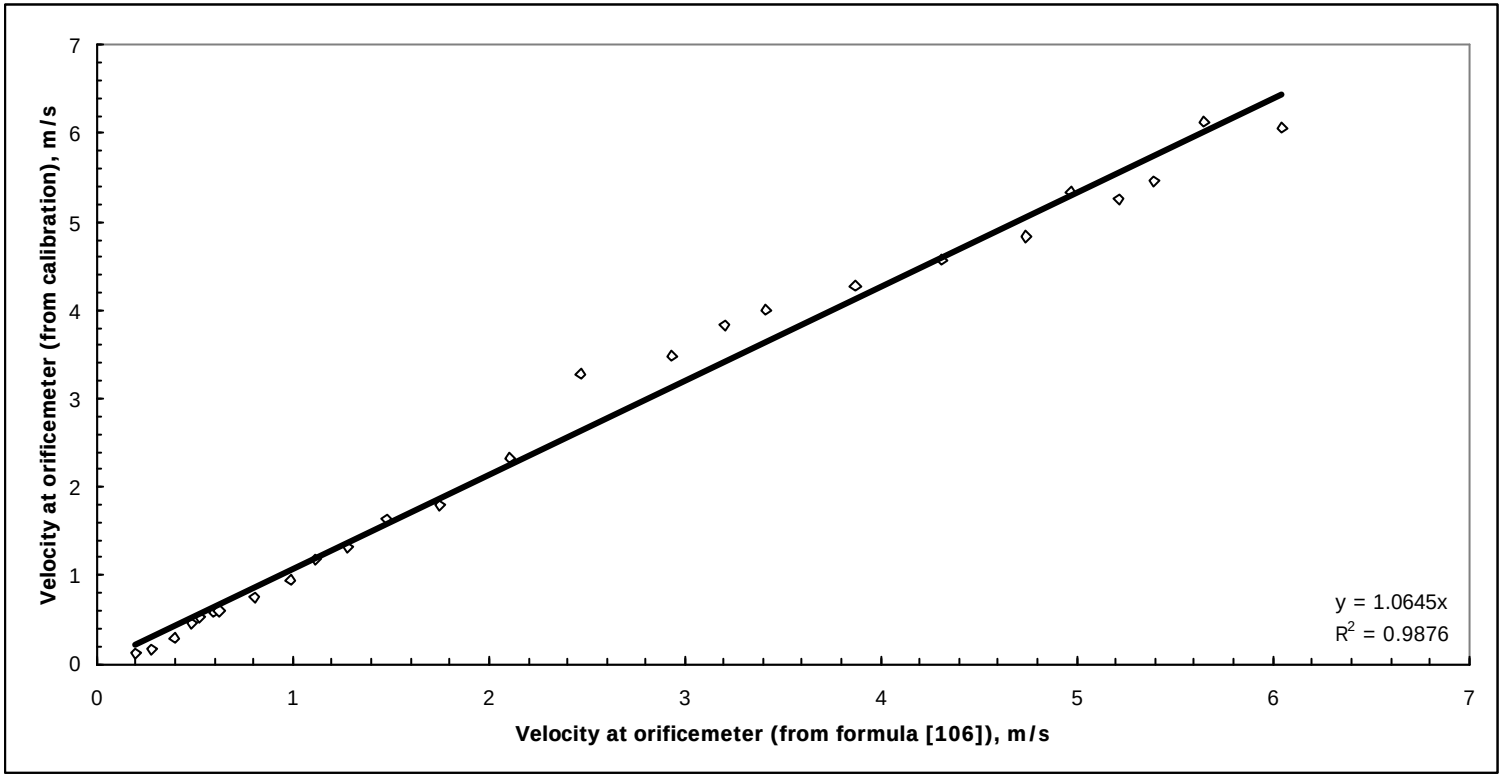

Figure A.2. Orificemeter coeffficient

Orificemeter coefficient= 1.0645

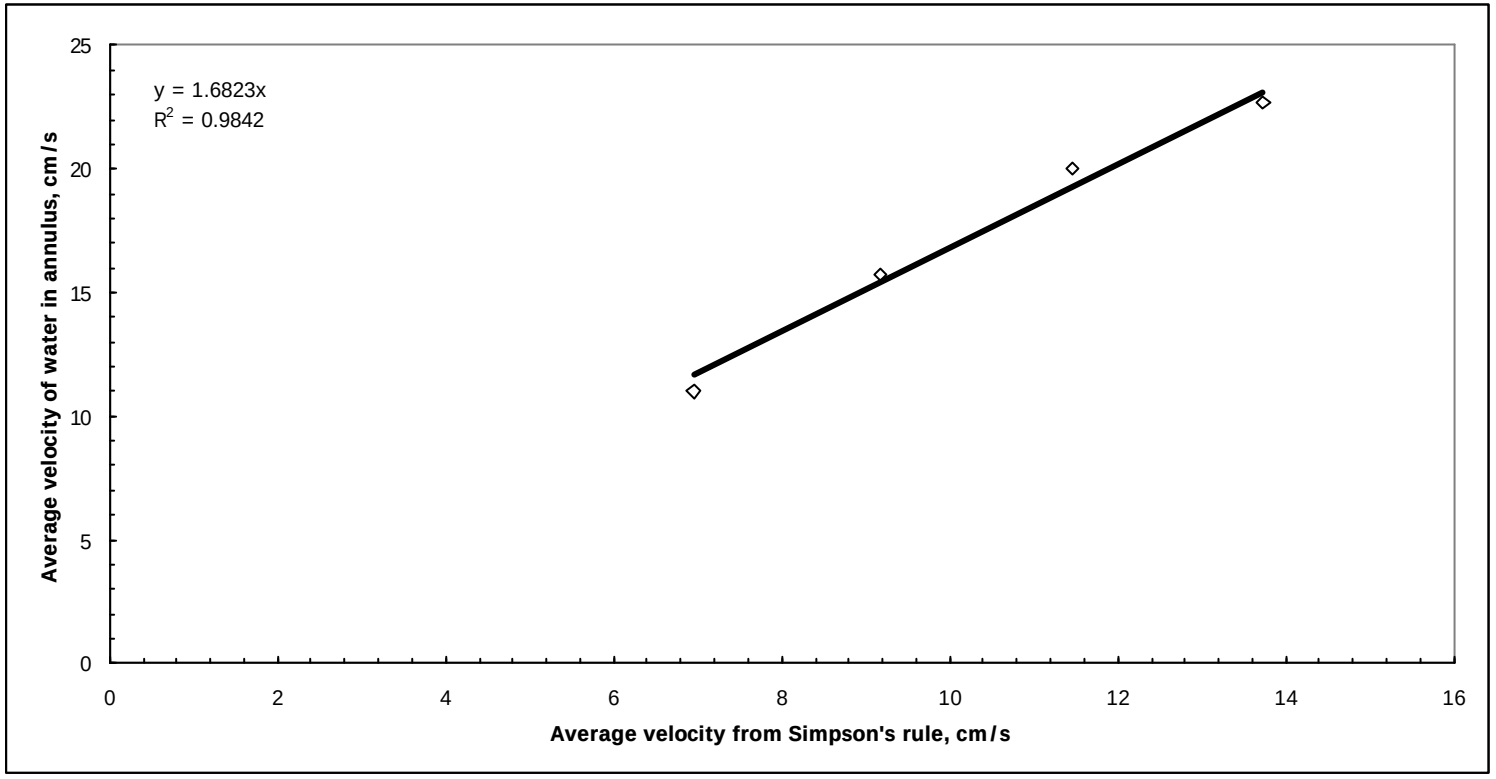

Figure A.3. Pitot tube coefficient

Pitot tube coefficient= 1.6823

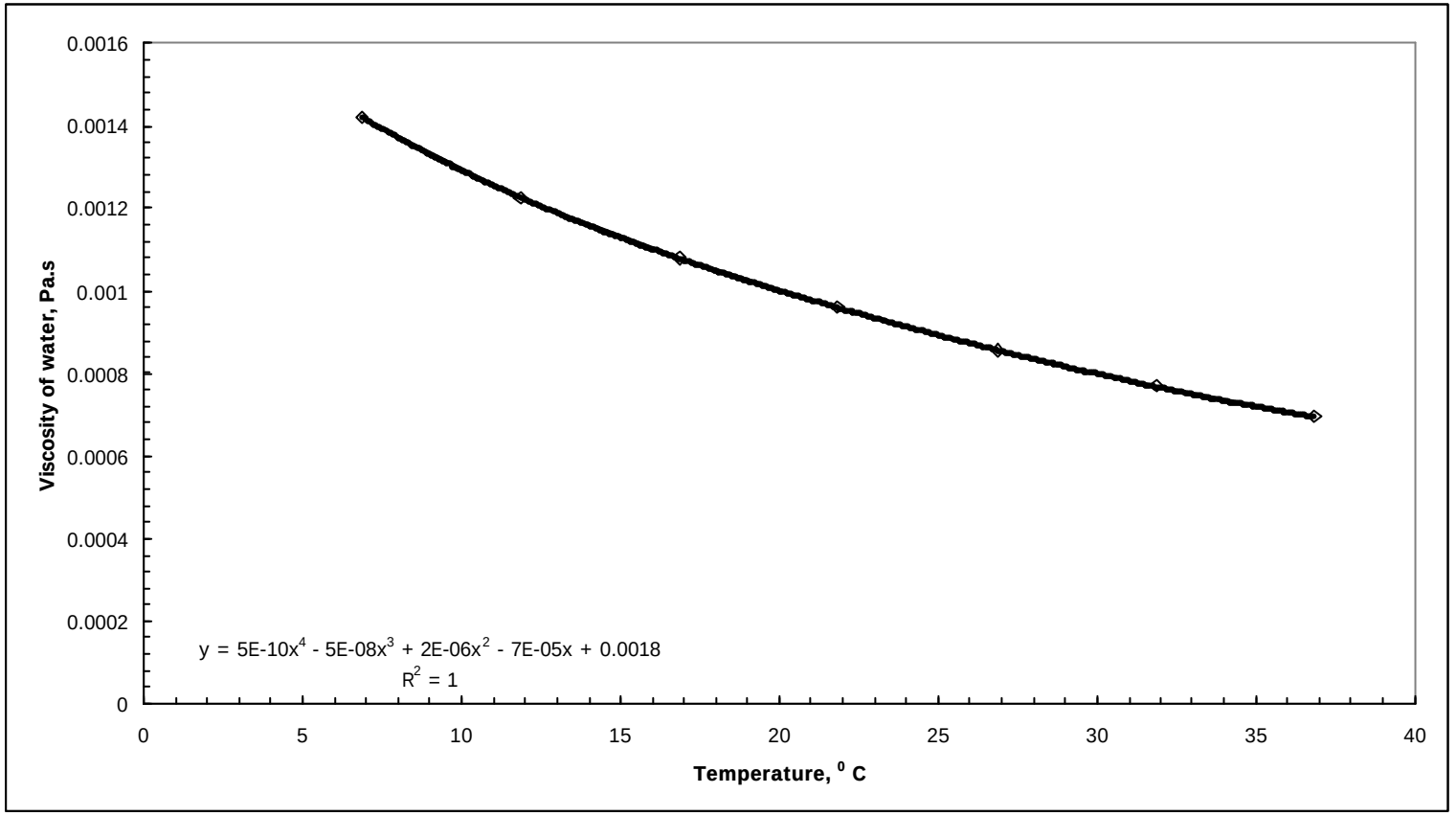

Figure A.4. Viscosity of water vs. temperature

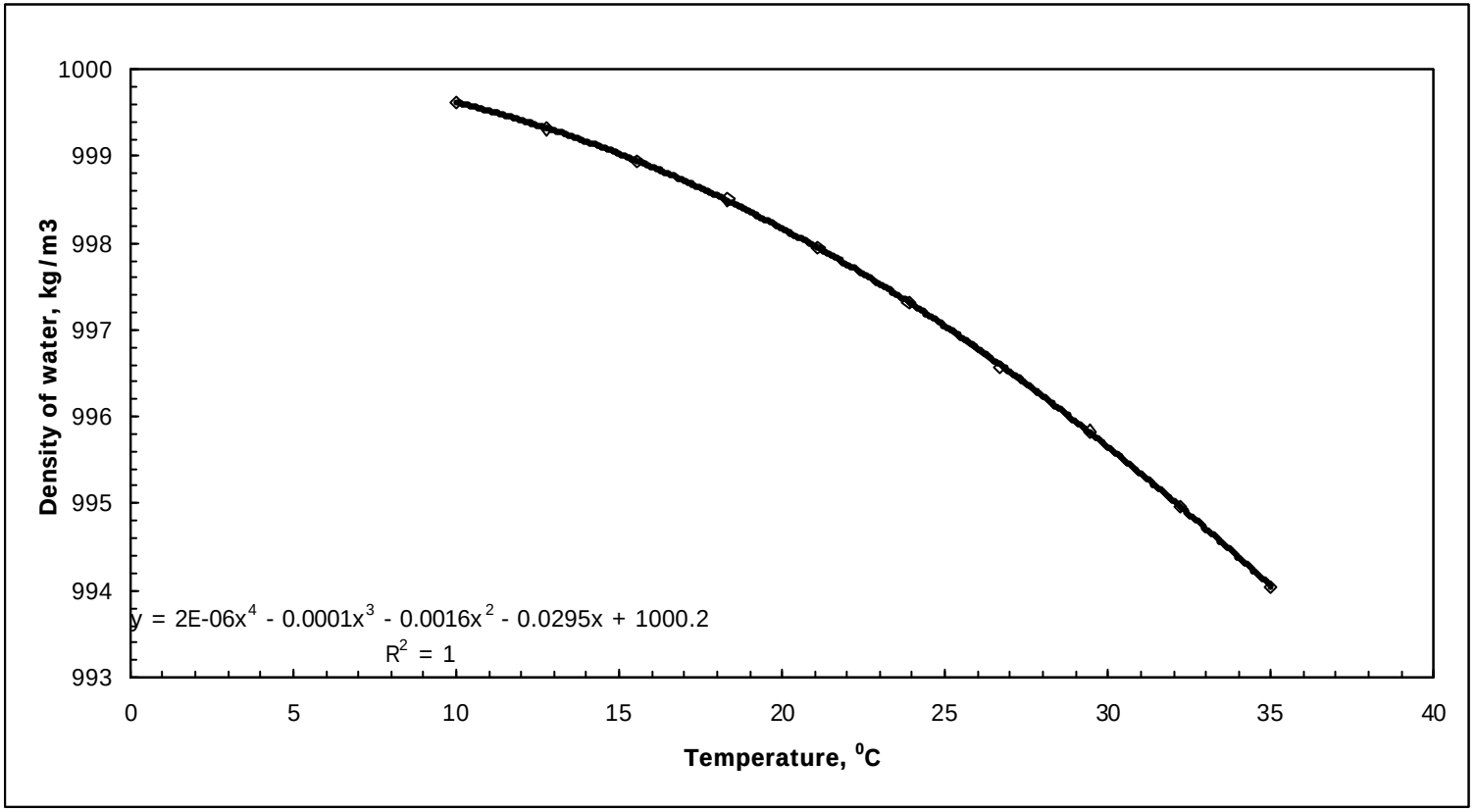

Figure A.5. Density of water vs. temperature

APPENDIX B

SAMPLE CALCULATION

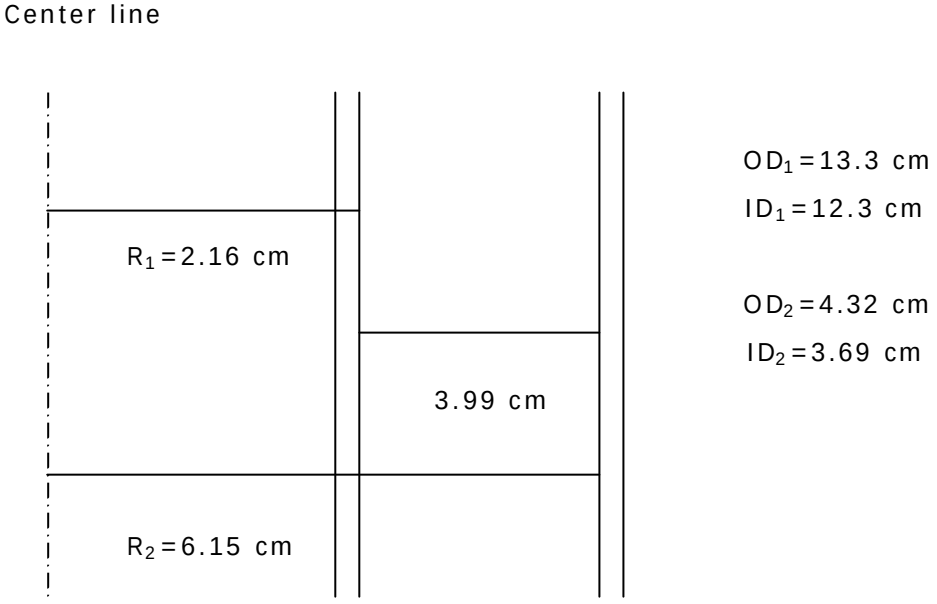

Figure B.1. Dimensions of the annulus

$D_e = ID_1 - OD_2 = 12.3 - 4.32 = 7.98\ cm = 0.0798\ m$

$$A_{ann} = \frac{p\left[ID_1^2 \quad OD_2^2\right]}{4} = \frac{p\left[0.123^2 \quad 0.0432^2\right]}{4} = 0.0104166\ m^2$$

$$\text{Aspect Ratio } K = \frac{4.32}{12.3} = 0.3512$$

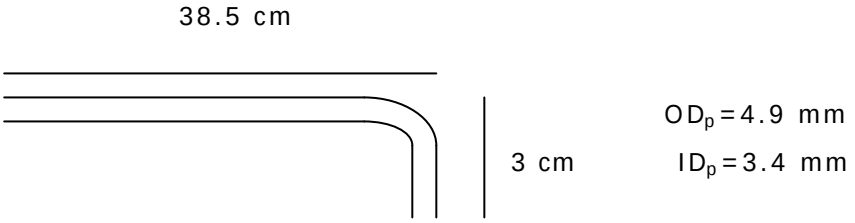

Figure B.2. Dimensions of the sampling probe

$$A_p = \frac{p(3.4E\ \ 3)^2}{4} = 9.0792E\ \ 6 m^2$$

To find the density and viscosity of water at different temperatures, some literature data was used [106]. Known density and viscosity versus temperature graphs were drawn and they were fitted to the following equations.

$$\rho_W = 2E - 0.6T^4 - 0.0001T^3 - 0.0016T^2 - 0.0295T + 1000.2 \quad \text{.....Equation (B.1)}$$

$$\mu_W = 5E - 10T^4 - 5E - 0.8T^3 + 2E - 0.6T^2 - 7E - 0.5T + 0.0018 \quad \text{..... Equation (B.2)}$$

$T = 19.4^0 C$ (for the data Table 4.1 and 4.2)

with Equations (B.1) and (B.2)

$\rho_W = 998.579\ kg/m^3$

$\mu_w = 0.000901\ Pa.s$

$\Delta H_{Hg} = 5.4$ cm

Calibration of the orificemeter was performed in terms of CCl_4 reading. Readings from Hg manometer was converted to CCl_4 reading by the following:

$$(?_{CCl_4} - ?_w)\, g \Delta H_{CCl_4} = (?_{Hg} - ?_w)\, g\, \Delta H_{Hg}$$

Velocity in annulus

$$U_{ann} = 0.9548 . ?H_{CCl_4}^{0.563} \quad \text{.....Equation (B.3)}$$

$$Re_w = \frac{\rho_w U_{ann} D_e}{\mu_w} = \frac{(998.579)(0.1382)(0.0798)}{0.000901} = 12232$$

Laminar Region:

$$f_w = \frac{16}{Re} \cdot \phi_a \quad \text{.....Equation (B.4)}$$

where $\phi_a = 1.48$ for K = 0.35

$$?P_w = \frac{32 . \mu_w . L . U_{ann}}{D_e^2} \quad \text{.....Equation (B.5)}$$

Turbulent Region:

$$f_w = \frac{0.0791}{Re^{0.25}} \quad \text{.....Equation (B.6)}$$

$$?P_w = \frac{2 . f_w . L . U_{ann}^2 . ?_w}{D_e} \quad \text{.....Equation (B.7)}$$

Using Eqn. (B.6) and (B.7)

$$f_w = \frac{0.0791}{(12232)^{0.25}} = 0.00752$$

$$\Delta P_w = \frac{2\,(0.00752)\,2\,(0.1382)^2\,(998.579)}{0.0798} = 7.19 \text{ Pa}$$

Calculation of the density of (Benzene+CCl_4) mixture:

1. Empty pycnometer was weighed: P grams
2. Pycnometer was filled with distilled water and weighed again: R grams
3. Pycnometer was filled with (CCl_4+benzene) mixture and weighed once more: S grams

R-P= T grams

S-P= Y grams

Density of (CCl_4 + benzene) mixture= Y/T (g/cm^3)

P= 9.6232 grams

R= 19.6409 grams

S= 21.8300 grams

ρ_{tf}= (S-P)/(R-P)=(21.8300-9.6232)/(19.6409-9.6232)

ρ_{tf}= 1.2185 g/cm^3

Calculation for inclined manometer:

$$V_L = K\sqrt{\frac{2\Delta P_{im}}{\rho_w}} \qquad \text{(for the data in Table C.3.b)}$$

$$\Delta P_{im} = (\rho_{tf} - \rho_w)\, g\, \Delta H_{im} \sin 0.94^0$$

$$= (1218.513 - 997.902)\, 9.80665\, (0.211)(0.0164) = 7.487 \text{ Pa}$$

$$V_L = \sqrt{\frac{2(7.487)}{997.902}} = 0.123 \text{ m/s}$$

Calculation for Simpson's rule:

$$\int_{x_0}^{x_N} f(x)dx = \frac{3}{8}h\left[\begin{matrix} f(x_0) + 3f(x_1) + 3f(x_2) + 2f(x_3) + 3f(x_4) + \\ 3f(x_5) + 2f(x_6) + 3f(x_7) + 3f(x_8) + f(x_9) \end{matrix}\right] \qquad [107]$$

$$N = 9 \qquad h = \frac{x_9 - x_0}{9} = \frac{3.99 - 0}{9} = 0.44333$$

$$U_{avg} = \frac{\int_0^{2\pi}\int_{R_1}^{R_2} V(r)\, r\, d\theta\, dr}{\int_0^{2\pi}\int_{R_1}^{R_2} r\, d\theta\, dr} = \frac{\int_{R_1}^{R_2} V(r)\, r\, dr}{\frac{R_2^2}{2} - \frac{R_1^2}{2}}$$

Nh=0.44333 for N=1

Nh=0.88666 for N=2

Nh=1.32999 for N=3

Nh=1.77332 for N=4

Nh=2.21665 for N=5

Nh=2.65998 for N=6

Nh=3.10331 for N=7

Nh=3.54664 for N=8

at N=0 and N=9 V(r)=0

R_1+Nh=2.16+0.44333=2.60333

R_1+Nh=2.16+0.88666 =3.0466

R_1+Nh=2.16+1.32999 =3.48999

R_1+Nh=2.16+1.77332 =3.93332

R_1+Nh=2.16+2.21665 =4.37665

R_1+Nh=2.16+2.65998 =4.81998

R_1+Nh=2.16+3.10331 =5.26331

R_1+Nh=2.16+3.54664 =5.70664

$$\int_{x0}^{x9} f(x)\,dx = \frac{3}{8}(0.44333)\begin{bmatrix} 3(2.60333)(13.3)+3(3.04666)(14.6)+2(3.48999)(16.3)+ \\ 3(3.93332)+3(4.37665)(16.3)+2(4.81998)(15.5)+ \\ 3(5.26331)(14.5)+3(5.70664)(13.5) \end{bmatrix}$$

=227.644

$$U_{avg} = \frac{\int_{R1}^{R2} V(r)\,r\,dr}{\frac{R_2^2}{2}-\frac{R_1^2}{2}} = \frac{227.644}{16.57845} = 13.73\ cm/s$$

Calculation of local solid density:

(for the data in Table C.8.b)

W_t= 40.6314 g

W_{t+w+s}= 49.2651 g

W_{t+s}= 40.8692 g

W_p=0.2378 g

W_w=8.3959 g

$$\rho_s = \frac{W_p}{\left[\frac{W_w}{\rho_w} + \frac{W_p}{\rho_p}\right]} = \frac{0.2378}{\left[\frac{8.3959}{0.9987078} + \frac{0.2378}{2.4}\right]} = 0.027957 \ \ g/cm^3$$

Radial local solid concentrations were found following the same procedure for other six points along the radial direction and average radial local solid density was calculated by using Simpson's rule.

$$\bar{\rho}_s = \frac{\int_0^{2\pi}\int_{R_1}^{R_2} \rho_s(r)\, r\, d\theta\, dr}{\int_0^{2\pi}\int_{R_1}^{R_2} r\, d\theta\, dr} = \frac{\int_{R_1}^{R_2} \rho_s(r)\, r\, dr}{\frac{R_2^2}{2} - \frac{R_1^2}{2}}$$

$$\int_{x_0}^{xN} f(x)dx = \frac{h}{8}\left[\begin{matrix} f(x_0) + 4f(x_1) + 2f(x_2) + 4f(x_3) + 2f(x_4) \\ + 4f(x_5) + 2f(x_6) + 4f(x_7) + f(x_8) \end{matrix}\right] \qquad [107]$$

$$N=8 \qquad h = \frac{x_8 - x_0}{8} = \frac{6.15 - 2.16}{8} = 0.49875$$

Nh=0.49875 for N=1

Nh=0.9975 for N=2

Nh=1.49625 for N=3

Nh=1.995 for N=4

Nh=2.49375 for N=5

Nh=2.9925 for N=6

Nh=3.49125 for N=7

at N=0 and N=8 $\rho_s(r)=0$

R_1+Nh=2.16+0.49875 = 2.65875

$R_1 + Nh = 2.16 + 0.9975 = 3.1575$

$R_1 + Nh = 2.16 + 1.49625 = 3.65625$

$R_1 + Nh = 2.16 + 1.995 = 4.155$

$R_1 + Nh = 2.16 + 2.49375 = 4.65375$

$R_1 + Nh = 2.16 + 2.9925 = 5.1525$

$R_1 + Nh = 2.16 + 3.49125 = 5.65125$

$$\int_{x0}^{x9} f(x)\,dx = \frac{0.49875}{3}\begin{bmatrix} 4\,(2.65875)(0.0319) + 2\,(3.1575)(0.034) + 4\,(3.65625)(0.032) + \\ 2\,(4.155)(0.0315) + 4\,(4.65375)(0.03385) + 2\,(5.1525)(0.034) + \\ 4\,(5.65125)(0.0344) \end{bmatrix}$$

$$= 0.505709$$

$$\overline{\rho}_s = \frac{\int_{R1}^{R2} \rho_s\,(r)\,r\,dr}{\frac{R_2^2}{2} - \frac{R_1^2}{2}} = \frac{0.505709}{16.57845} = 0.030504\ g/cm^3$$

$$\overline{\rho}_m = \overline{\rho}_s + (1 - \overline{\phi}_s)\,\rho_w = \rho_p\,\overline{\phi}_s + \rho_w\,(1 - \overline{\phi}_s)$$

$$\overline{\phi}_s = \frac{\overline{\rho}_s}{\rho_p} = \frac{0.0305049}{2.4} = 0.01271$$

$\overline{?}_m = 0.030504 + 0.998692(1 - 0.01271) = 1.016502\ g/cm^3$

$$\overline{\mu}_m = \mu_w\,(1 + 2.5\,\overline{\phi}_s) = 0.000928\ (1 + 2.5\ (0.01271)) = 0.000957\ Pa.s$$

$$Re_m = \frac{D_e\,\overline{\rho}_m\,U_{ann}}{\overline{\mu}_m} = \frac{(0.0798)(1.016502)(0.2267)}{0.000957} = 19216$$

$$f_m = \frac{0.0791}{Re_m^{0.25}} = \frac{0.0791}{(19216)^{0.25}} = 0.006718$$

$$?P_{tp} = (?_{CCl_4} - \overline{?}_m) \cdot g \cdot h$$

where $\bar{\rho}_m$ is the average mixture concentration, and h is the manometer reading.

$?P_{tp} = (1590 - 1016.502) \cdot 9.80665 \cdot (0.09) = 506.1684\,Pa$

$$f_{mexp} = \frac{De \cdot ?P_{tp}}{2U_{ann}^2 L \bar{\rho}_m} = \frac{0.0798\,(506.1684)}{2\,(0.2267)^2\,(2)\,(1016.502)} = 0.193298$$

<u>Standard deviation for different data obtained at different phases of experimentation</u>

Standard deviation for pitot tube coefficient:

Pitot tube coefficient

K= 1.65

K= 1.743

K= 1.715

K= 1.583

$\bar{K}$ = 1.673 where $\bar{K}$ is the average of the pitot tube coefficients

K= 1.6823 (from the slope of the line in Figure A.3)

$s = \sqrt{\frac{\Sigma\,(K - \bar{K})^2}{n-1}} = \sqrt{\frac{0.01529}{4-1}}$ where s is the standard deviation for pitot tube

s=0.0714

$K = \bar{K} \pm s$

K=1.6823 ± 0.0714

Standard deviation for local velocity data with pitot tube:

U_L= 0.1225 m/s

U_L= 0.1256 m/s

U_L= 0.1289 m/s

$U_L = 0.1315$ m/s

$U_L = 0.1325$ m/s

$U_L = 0.1341$ m/s

$\overline{U_L} = 0.1292$ m/s where $\overline{U_L}$ is the average local velocity

$$s_v = \sqrt{\frac{(U_L - \overline{U_L})^2}{n - 1}} = \sqrt{\frac{0.00009813}{5}}$$ where s_v is the standard deviation for local velocity

$s_v = 0.0044$

$U_L = \overline{U_L} \pm s_v$

$U_L = 0.1292 \pm 0.0044$

Standard deviation for local solid density:

$\rho_s = 0.03464$ g/cm^3

$\rho_s = 0.036909$ g/cm^3

$\rho_s = 0.0291$ g/cm^3

$\rho_s = 0.027957$ g/cm^3

$\overline{?_s} = 0.032152$ g/cm^3

$$s_D = \sqrt{\frac{S(?_s - \overline{?_s})^2}{n-1}} = \sqrt{\frac{0.00005573}{3}}$$

$s_D = 0.00431$

$?_s = \overline{?_s} \pm s_D$

$\rho_s = 0.032152 \pm 0.00431$

APPENDIX C

Table C.1. Calibration data for the orificemeter

m_w, kg	t, sec	T, ^{0}C	$\mu_w x10^4$, Pa.s	ρ_w, kg/m^3
1.625	40.47	20.2	8.7	998.5
1.933	35.21	20.1	8.8	998.5
2.973	30.45	20.1	8.8	998.5
3.948	25.69	20.0	8.8	998.5
3.638	20.47	19.8	8.9	998.5
3.892	20.12	19.8	8.9	998.5
3.703	18.41	19.7	8.9	998.5
3.456	13.74	19.6	8.9	998.6
4.798	15.11	19.4	9.0	998.6
5.919	14.97	19.5	9.0	998.6
6.423	14.56	19.3	9.0	998.6
7.978	14.57	19.1	9.1	998.6
8.503	14.18	18.8	9.2	998.7
10.864	13.97	18.5	9.3	998.7
12.517	11.43	18.3	9.4	998.7
11.91	10.24	18.4	9.4	998.7
12.509	9.76	18.2	9.4	998.8
12.235	9.13	18.0	9.5	998.8
12.666	8.86	17.7	9.6	998.8
12.434	8.14	17.8	9.6	998.8
12.042	7.45	17.9	9.5	998.8
13.15	7.36	17.7	9.6	998.8
12.545	7.14	17.5	9.7	998.9
12.668	6.94	17.4	9.7	998.9
13.846	6.75	17.2	9.8	998.9
12.671	6.25	17.5	9.7	998.9

Table C.1. Calibration data for the orificemeter (Cont'd)

T, ^{0}C	$\dot{m}$ x10^2, kg/s	$\dot{Q}$ x10^6, m^3/s	U_ox10^3, m/s	U_{ann} x10^3, m/s	Re_w
20.2	4.0	40.2	120.1	3.9	352
20.1	5.5	55.0	164.2	5.3	480
20.1	9.8	97.8	292.0	9.4	853
20	15.4	153.9	459.6	14.8	1338
19.8	17.8	178.0	531.5	17.1	1535
19.8	19.3	193.7	578.4	18.6	1671
9.7	20.1	201.4	601.5	19.3	1731
19.6	25.2	251.9	752.1	24.2	2156
19.4	31.8	318.0	949.5	30.5	2702
19.5	39.5	396.0	1182.3	38.0	3377
19.3	44.1	441.8	1319.0	42.4	3739
19.1	54.8	548.3	1637.2	52.6	4606
18.8	60.0	600.5	1793.0	57.6	4987
18.5	77.8	778.7	2325.0	74.8	6396
18.3	109.5	1096.5	3274.0	105.3	8940
18.4	116.3	1164.6	3477.2	111.8	9530
18.2	128.2	1283.3	3831.7	123.2	10424
18	134.0	1341.7	4006.2	128.9	10819
17.7	143.0	1431.3	4273.6	137.4	11415
17.8	152.8	15293.5	4566.4	146.8	12242
17.9	161.6	1618.3	4832.1	155.4	13002
17.7	178.7	1788.8	5341.1	171.7	14267
17.5	175.7	1759.0	5252.2	168.9	13928
17.4	182.5	1827.5	5456.5	175.4	14417
17.2	205.1	2053.6	6131.6	197.1	16084
17.5	202.7	2029.7	6060.4	194.9	16071

Table C.2. Orificemeter coefficient data

U_o (from formula [106])x10^3, m/s	U_o (from calibration)x10^3, m/s
197.7	120.1
279.6	164.2
395.4	292.0
484.3	460.0
523.1	531.4
593.1	578.4
625.2	601.5
807.1	752.1
985.2	949.5
1117.2	1182.3
1279.2	1319.0
1480.2	1637.2
1746.5	1792.9
2106.4	2325.0
2469.9	3274.0
2931.9	3477.3
3203.1	3831.7
3412.6	4006.2
3869.4	4273.6
4310.1	4566.4
4739.1	4832.1
4967.5	5341.1
5212.6	5252.2
5395.5	5456.5
5646.5	6131.6
6049.6	6060.4

Table C.3.a. Raw data for approximate (K=1) local velocities (Rew= 24067)

$rx10^4$, m	$\Delta H_{im} x10^2$, m TF					
24.5	21.1	22.2	23.4	24.3	24.7	25.3
75.5	25.6	26.8	27.8	28.5	31.3	32.2
109.5	32.1	33.7	34.3	35.1	35.4	36.2
144.5	35.1	36.6	37.5	38.1	38.8	39.4
175.5	35.3	36.8	37.9	38.3	39.1	39.6
214.5	34.7	35.8	36.7	37.6	37.9	38.5
254.5	32.1	33.2	34.2	35.6	36.1	36.4
294.5	30.3	30.8	31.3	31.8	32.2	32.6
334.5	25.5	25.9	26.5	26.9	27.6	28.4
374.5	22.5	23.0	23.7	24.6	25.0	25.8

Table C.3.b. Approximate (K=1) local velocity data for Re_w =24067

$rx10^4$, m	$V_L x10^3$, m/s						$s_v x10^3$, m/s
*** 24.5	122.5	125.6	128.9	131.5	132.5	134.1	4.4
75.5	135.0	138.1	140.6	142.4	149.3	151.4	6.4
109.5	151.1	154.9	156.3	158.1	158.8	160.6	3.3
144.5	158.0	161.4	163.4	164.6	166.1	167.4	3.4
175.5	158.5	161.8	164.2	165.1	166.8	167.9	3.4
214.5	157.1	159.7	161.6	163.6	164.2	165.5	3.2
254.5	151.2	153.7	156.0	159.2	160.4	160.9	3.9
294.5	146.9	148.1	149.2	150.4	151.4	152.3	2.0
334.5	134.7	135.7	137.3	138.3	140.1	142.2	2.8
374.5	126.5	127.9	129.8	132.2	133.3	135.4	3.4

*** Sample calculation is given for this run.

Table C.3.c. Raw data for approximate (K=1) local velocities (Re_w = 20167)

$rx10^4$, m	$\Delta H_{im} x10^2$, m TF					
24.5	15.9	16.5	17.0	17.6	18.7	20.0
75.5	19.8	21.2	22.3	23.4	24.6	25.8
109.5	22.8	23.4	24.6	25.5	26.5	27.6
144.5	25.2	26.1	26.9	27.3	28.5	29.4
175.5	24.9	25.9	26.7	27.0	28.3	29.2
214.5	23.1	23.8	24.4	25.3	25.9	26.2
254.5	22.0	22.5	22.9	23.4	23.9	24.4
294.5	19.3	19.8	20.4	20.9	21.7	22.1
334.5	17.5	18.1	18.5	19.2	19.9	20.8
374.5	16.2	16.9	17.5	18.1	18.6	19.5

Table C.3.d. Approximate (K=1) local velocity data for Re_w =20167

$rx10^4$, m	$V_L x10^3$, m/s						$s_v x10^3$, m/s
24.5	106.3	108.3	109.9	111.8	115.3	119.2	4.8
75.5	118.6	122.8	125.9	129.0	132.2	135.5	6.2
109.5	127.3	129.0	132.2	134.6	137.2	140.0	4.8
144.5	133.9	136.3	138.3	139.4	142.3	144.6	3.9
175.5	133.0	135.8	137.7	138.5	141.9	144.1	4.0
214.5	128.2	130.1	131.7	134.1	135.7	136.5	3.3
254.5	125.0	126.4	127.6	128.9	130.3	131.7	2.5
294.5	117.1	118.6	120.3	121.9	124.1	125.3	3.2
334.5	111.5	113.4	114.6	116.8	118.9	121.6	3.7
374.5	107.2	109.6	111.5	113.4	115.0	117.7	3.8

Table C.3.e. Raw data for approximate (K=1) local velocities (Rew = 15115)

$rx10^4$, m	$\Delta H_{im} x10^2$, m TF					
24.5	10.5	10.9	11.3	11.8	12.5	13.2
75.5	12.3	13.0	13.7	14.3	14.9	15.8
109.5	15.9	16.6	17.0	17.4	18.1	18.8
144.5	17.0	17.5	18.1	18.7	19.3	19.8
175.5	16.5	16.8	17.2	17.7	17.9	18.2
214.5	14.9	15.5	15.9	16.3	16.7	17.3
254.5	12.7	13.2	13.8	14.3	14.8	15.2
294.5	11.9	12.4	12.8	13.1	13.7	14.1
334.5	10.8	11.2	11.5	12.0	12.4	12.9
374.5	10.4	11.0	11.6	11.9	12.1	12.6

Table C.3.f. Approximate (K=1) local velocity data for Re_w =15115

$rx10^4$, m	$V_L x10^3$, m/s						$s_v x10^3$, m/s
24.5	86.4	88.0	89.7	91.6	94.3	96.9	4.0
75.5	93.6	96.2	98.7	100.9	103.0	106.1	4.5
109.5	106.2	108.5	109.8	111.1	113.3	115.5	3.4
144.5	109.8	111.4	113.3	115.2	117.0	118.5	3.3
175.5	108.2	109.2	110.5	112.1	112.7	113.6	2.1
214.5	102.9	105.0	106.3	107.7	109.0	110.9	2.9
254.5	94.9	96.8	98.9	100.7	102.4	103.8	3.4
294.5	91.9	93.8	95.3	96.4	98.6	100.0	3.0
334.5	87.5	89.2	90.3	92.2	93.8	95.6	3.0
374.5	85.9	88.3	90.7	91.9	92.7	94.6	3.1

Table C.3.g. Raw data for approximate (K=1) local velocities (Rew = 10116)

$rx10^4$, m	$\Delta H_{im} x10^2$, m TF					
24.5	6.4	7.0	7.4	7.7	8.0	8.5
75.5	7.8	8.2	8.5	8.8	9.2	9.7
109.5	8.5	8.8	9.2	9.5	10.0	10.4
144.5	9.0	9.2	9.5	9.9	10.1	10.5
175.5	8.1	8.4	8.8	9.2	9.5	11.2
214.5	7.5	7.9	8.2	8.5	8.7	9.0
254.5	6.9	7.2	7.6	7.9	8.3	8.9
294.5	6.6	6.9	7.3	7.7	8.2	8.6
334.5	6.5	6.8	7.2	7.6	8.1	8.5
374.5	6.3	6.7	7.1	7.5	8.0	8.7

Table C.3.h. Approximate (K=1) local velocity data for Re_w =10116

$rx10^4$, m	$V_L x10^3$, m/s						$s_v x10^3$, m/s
24.5	67.3	70.4	72.4	73.9	75.3	77.6	3.6
75.5	74.4	76.3	77.7	79.0	80.8	82.9	3.1
109.5	77.6	79.0	80.8	82.1	84.3	85.9	3.1
144.5	79.9	80.8	82.1	83.9	84.7	86.3	2.4
175.5	75.8	77.2	79.0	80.8	82.1	89.2	4.8
214.5	73.0	74.9	76.3	77.6	78.5	79.9	2.5
254.5	69.9	71.5	73.4	74.8	76.7	79.4	3.5
294.5	68.4	69.9	72.0	73.9	76.3	78.1	3.7
334.5	67.9	69.4	71.4	73.4	75.8	77.6	3.7
374.5	66.9	68.9	71.0	72.9	75.3	78.6	4.3

Table C.4. a. Approximate (K=1) and true (K=1.6823) local velocities at different radial positions for Rew = 24067

$rx10^4$, m	V_Lx10^3, m/s	V_Tx10^3, m/s
0	0	0
“ 24.5	129.3	217.4
75.5	142.9	240.4
109.5	156.7	263.7
144.5	163.6	275.1
175.5	164.0	275.9
214.5	162.0	272.6
254.5	157.0	264.1
294.5	149.7	251.9
334.5	138.1	232.3
374.5	130.9	220.8
399	0	0

“ Sample calculation is given for this run in Appendix B

Table C.4.b. Approximate (K=1) and true (K=1.6823) local velocities at different radial positions for Rew = 20167

$rx10^4$, m	V_Lx10^3, m/s	V_Tx10^3, m/s
0	0	0
24.5	111.8	188.1
75.5	122.2	205.5
109.5	133.6	224.7
144.5	139.1	234.0
175.5	138.6	233.1
214.5	132.8	223.4
254.5	128.4	216.0
294.5	121.2	204.0
334.5	116.2	195.5
374.5	112.5	189.2
399	0	0

Table C.4.c. Approximate (K=1) and true (K=1.6823) local velocities at different radial positions for Re_w =15115

$rx10^4$, m	$V_L x10^3$, m/s	$V_T x10^3$, m/s
0	0	0
24.5	91.2	153.5
75.5	99.8	167.9
109.5	110.8	186.3
144.5	114.3	192.2
175.5	111.1	186.9
214.5	107.0	180.0
254.5	99.6	167.6
294.5	96.0	161.5
334.5	91.5	153.9
374.5	90.7	152.6
399	0	0

Table C.4.d. Approximate (K=1) and true (K=1.6823) local velocities at different radial positions for Rew = 10116

$rx10^4$, m	$V_L x10^3$, m/s	$V_T x10^3$, m/s
0	0	0
24.5	72.9	122.7
75.5	78.6	132.2
109.5	81.7	137.4
144.5	83.0	139.6
175.5	80.8	135.9
214.5	76.7	129.1
254.5	74.4	125.1
294.5	72.9	122.7
334.5	72.7	122.3
374.5	72.5	121.9
399	0	0

Table C.5. Average velocities obtained from orificemeter measuement and Simpson's rule applied to approximate (K=1) local velociy data

Re_w	U_{ann} x10^3, m/s	U_sx10^3, m/s
24067	226.7	137.3
20167	199.9	114.7
15115	157.4	91.8
10116	110.0	69.5

Velocity distribution in Laminar flow regime was found from Equation (C.1) (Eraslan & Özbelge, 2003).

U(r)= A+Br2+C lnr .....Equation C.1

Table C.6. Coefficients of the velocity distributions in the laminar flow regime

Re_w	A	B	C
1004	0.33	-26.03	0.08
2007	0.67	-52.67	0.17

Calculation procedure of the coefficients A, B, and C is given in [26].

Table C.7. Calculated results for radial true (K=1.6823) local velocities in the laminar flow regime

	Re_w =1004	Re_w =2007
rx10^4, m	U_Tx10^3, m/s	U_Tx10^3, m/s
24.5	6.3	12.7
109.5	18.8	38.1
144.5	21.1	42.6
175.5	21.8	44.2
214.5	21.4	43.3
294.5	15.9	32.2
374.5	5.1	10.3

Table C.8.a. Raw data for local solid density calculations dp=72 μm and C_f=1% (v/v) at nonisokinetic conditions

Wt= A	Wt+w+s= B	Ww+s= B-A	Wt+s =C	Ws=C-A	Ww=B-C	$\rho_{s*}10^{-1}$, kg/m^3
0.0120 m/s						
46.5576	86.7424	40.1848	47.0604	0.5028	39.682	1.26
50.447	99.6938	49.2468	51.1256	0.6786	48.5682	1.39
40.4488	71.681	31.2322	40.8742	0.4254	30.8068	1.37
44.5765	76.1885	31.612	45.0052	0.4287	31.1833	1.37
51.0689	88.0826	37.0137	51.5316	0.4627	36.551	1.26
41.2127	73.2776	32.0649	41.5811	0.3684	31.6965	1.16
36.9881	72.9574	35.9693	37.455	0.4669	35.5024	1.31
0.0239 m/s						
46.5521	88.3269	41.7748	47.1116	0.5595	41.2153	1.35
50.4504	87.5587	37.1083	50.9932	0.5428	36.5655	1.47
40.4488	79.6528	39.204	41.0313	0.5825	38.6215	1.50
44.5753	82.6594	38.0841	45.1715	0.5962	37.4879	1.58
51.0663	77.6952	26.6289	51.4591	0.3928	26.2361	1.49
41.2099	73.6971	32.4872	41.694	0.4841	32.0031	1.50
36.9882	78.5876	41.5994	37.5967	0.6085	40.9909	1.47
0.1100 m/s						
46.548	80.418	33.87	47.5308	0.9828	32.8872	2.95
50.4442	85.704	35.2598	51.5056	1.0614	34.1984	3.06
40.4511	68.8278	28.3767	41.3521	0.901	27.4757	3.23
44.5744	80.9952	36.4208	45.7188	1.1444	35.2764	3.20
51.069	75.002	23.933	51.7993	0.7303	23.2027	3.10
41.2122	82.7642	41.552	42.4868	1.2746	40.2774	3.12
36.993	69.628	32.635	37.9704	0.9774	31.6576	3.04
0.1574 m/s						
46.5415	77.6087	31.0672	47.5436	1.0021	30.0651	3.28
50.4474	89.7657	39.3183	51.7202	1.2728	38.0455	3.30
40.4499	74.4985	34.0486	41.5797	1.1298	32.9188	3.38
44.5745	79.1676	34.5931	45.7012	1.1267	33.4664	3.32
51.0681	90.8715	39.8034	52.3259	1.2578	38.5456	3.22

41.2114	73.1435	31.9321	42.2232	1.0118	30.9203	3.22
36.9901	70.9957	34.0056	38.1047	1.1146	32.891	3.34
0.1999 m/s						
46.5497	89.7667	43.217	47.761	1.2113	42.0057	2.85
50.4513	90.0674	39.6161	51.575	1.1237	38.4924	2.88
40.4509	84.2417	43.7908	41.7285	1.2776	42.5132	2.96
44.5778	85.0695	40.4917	45.6948	1.117	39.3747	2.80
51.0686	92.2361	41.1675	52.2015	1.1329	40.0346	2.79
41.2073	80.2322	39.0249	42.3067	1.0994	37.9255	2.86
36.9933	79.7948	42.8015	38.1237	1.1304	41.6711	2.68
0.2267 m/s						
46.5459	91.357	44.8111	48.0134	1.4675	43.3436	3.33
50.4419	92.4037	41.9618	51.8995	1.4576	40.5042	3.54
40.4464	87.1613	46.7149	42.0854	1.639	45.0759	3.58
44.5708	88.0385	43.4677	46.0991	1.5283	41.9394	3.58
51.0657	94.6922	43.6265	52.6032	1.5375	42.089	3.59
41.2073	83.7704	42.5631	42.6404	1.4331	41.13	3.43
36.9859	81.7354	44.7495	38.5247	1.5388	43.2107	3.50

Table C.8.b. Raw data for local solid density calculations d_p=72 μm and C_f=1% (v/v) at isokinetic conditions

Wt= A	Wt+w+s= B	Ww+s= B-A	Wt+s =C	Ws=C-A	Ww=B-C	$\rho_{s*}10^{-1}$, kg/m^3
0.0239 m/s						
38.0668	41.0684	3.0016	38.0826	0.0158	2.9858	0.53
39.3495	41.3061	1.9566	39.3563	0.0068	1.9498	0.35
40.146	44.3934	4.2474	40.1539	0.0079	4.2395	0.19
36.9841	39.4756	2.4915	36.9973	0.0132	2.4783	0.53
40.9431	43.8704	2.9273	40.96	0.0169	2.9104	0.58
40.2175	42.291	2.0735	40.2254	0.0079	2.0656	0.38
43.9607	46.2515	2.2908	43.976	0.0153	2.2755	0.67
0.1100 m/s						
51.4125	75.5679	24.1554	51.5692	0.1567	23.9987	0.65
39.0438	67.8063	28.7625	39.2544	0.2106	28.5519	0.73
48.9643	72.6913	23.727	49.0987	0.1344	23.5926	0.57

36.4815	66.8927	30.4112	36.6712	0.1897	30.2215	0.63
42.9709	70.3339	27.363	43.1434	0.1725	27.1905	0.63
50.2639	80.4805	30.2166	50.4621	0.1982	30.0184	0.66
49.3034	77.2519	27.9485	49.5594	0.256	27.6925	0.92
0.1574 m/s						
51.4114	83.1501	31.7387	51.7795	0.3681	31.3706	1.17
39.0712	78.3716	39.3004	39.4258	0.3546	38.9458	0.91
48.9656	81.7396	32.774	49.215	0.2494	32.5246	0.76
36.4832	69.0892	32.606	36.7653	0.2821	32.3239	0.87
42.9746	76.8796	33.905	43.3345	0.3599	33.5451	1.07
50.2665	80.7723	30.5058	50.6142	0.3477	30.1581	1.15
49.3043	90.382	41.0777	49.8315	0.5272	40.5505	1.29
0.1999 m/s						
37.5418	49.0015	11.4597	37.7006	0.1588	11.3009	1.40
41.3231	54.1081	12.785	41.6057	0.2826	12.5024	2.24
40.148	51.2082	11.0602	40.3897	0.2417	10.8185	2.21
40.079	51.5892	11.5102	40.295	0.216	11.2942	1.90
39.3712	53.4857	14.1145	39.6542	0.283	13.8315	2.03
40.2162	50.8249	10.6087	40.4251	0.2089	10.3998	1.99
43.8659	52.1912	8.3253	43.9981	0.1322	8.1931	1.60
0.2267 m/s						
40.6314	49.2651	8.6337	40.8692	0.2378	8.3959	2.80
39.3471	46.9084	7.5613	39.6012	0.2541	7.3072	3.42
44.4751	53.0407	8.5656	44.7504	0.2753	8.2903	3.27
45.0176	52.8014	7.7838	45.2391	0.2215	7.5623	2.89
40.9422	48.3348	7.3926	41.1801	0.2379	7.1547	3.28
39.6764	46.298	6.6216	39.8969	0.2205	6.4011	3.39
^40.609	48.9494	8.3404	40.8661	0.2571	8.0833	3.13

^ Sample calculation is given for this run in Appendix B

Table C.9.a. Raw data for local solid density calculations dp=72 μm and Cf =2% (v/v) at nonisokinetic conditions

Wt= A	Wt+w+s= B	Ww+s= B-A	Wt+s =C	Ws=C-A	Ww=B-C	$\rho_{s*}10^{-1}$, kg/m^3
0.0120 m/s						
40.666	84.7776	44.1116	42.3276	1.6616	42.45	3.85
41.8524	81.5142	39.6618	43.5139	1.6615	38.0003	4.29
43.2251	86.3817	43.1566	44.9438	1.7187	41.4379	4.07
43.3732	82.5878	39.2146	45.1837	1.8105	37.4041	4.74
41.6892	79.8665	38.1773	43.4972	1.808	36.3693	4.86
42.4007	82.6572	40.2565	44.2779	1.8772	38.3793	4.79
41.9613	78.1366	36.1753	43.7575	1.7962	34.3791	5.11
0.0239 m/s						
38.1862	78.8599	40.6737	40.0651	1.8789	38.7948	4.74
40.3865	78.7058	38.3193	42.3807	1.9942	36.3251	5.36
41.2223	81.0502	39.8279	43.2045	1.9822	37.8457	5.12
43.4373	83.8638	40.4265	45.6124	2.1751	38.2514	5.55
40.3591	85.057	44.6979	42.7916	2.4325	42.2654	5.62
40.2129	81.6386	41.4257	42.4407	2.2278	39.1979	5.55
45.3393	84.3842	39.0449	47.2672	1.9279	37.117	5.08
0.1100 m/s						
38.0709	68.5224	30.4515	39.8672	1.7963	28.6552	6.10
40.957	71.9444	30.9874	43.3174	2.3604	28.627	7.96
41.6092	73.024	31.4148	43.9918	2.3826	29.0322	7.93
41.6282	72.9132	31.285	44.0164	2.3882	28.8968	7.98
40.4913	74.783	34.2917	43.1796	2.6883	31.6034	8.21
41.6873	68.5449	26.8576	43.5622	1.8749	24.9827	7.27
39.1162	72.8785	33.7623	41.6153	2.4991	31.2632	7.73
0.1574 m/s						
53.6515	86.6922	33.0407	55.7559	2.1044	30.9363	6.61
46.275	83.2499	36.9749	49.4368	3.1618	33.8131	8.99
45.3773	83.6118	38.2345	48.5834	3.2061	35.0284	8.81
44.9489	78.5463	33.5974	47.6034	2.6545	30.9429	8.27
46.9386	84.7634	37.8248	50.1384	3.1998	34.625	8.89
45.3217	82.513	37.1913	48.4381	3.1164	34.0749	8.80

46.3273	87.8113	41.484	49.5895	3.2622	38.2218	8.23
0.1999 m/s						
38.8366	66.4242	27.5876	40.466	1.6294	25.9582	6.11
40.1695	65.4115	25.242	41.8524	1.6829	23.5591	6.93
41.4675	67.7817	26.3142	43.2251	1.7576	24.5566	6.94
41.235	72.7291	31.4941	43.3732	2.1382	29.3559	7.06
39.8891	67.3523	27.4632	41.6892	1.8001	25.6631	6.81
40.5177	68.8773	28.3596	42.4007	1.883	26.4766	6.90
39.9569	69.8814	29.9245	41.9613	2.0044	27.9201	6.96
0.2267 m/s						
37.683	72.0628	34.3798	40.3719	2.6889	31.6909	8.19
40.827	79.1126	38.2856	44.1873	3.3603	34.9253	9.24
42.1703	79.8278	37.6575	45.4857	3.3154	34.3421	9.27
41.4704	75.9417	34.4713	44.5549	3.0845	31.3868	9.43
41.5331	74.4829	32.9498	44.3716	2.8385	30.1113	9.063
43.5669	79.3779	35.811	46.5979	3.031	32.78	8.89
39.4607	73.282	33.8213	42.4889	3.0282	30.7931	9.44

Table C.9.b. Raw data for local solid density calculations dp=72 μm and Cf=2% (v/v) at isokinetic conditions

Wt= A	Wt+w+s= B	Ww+s= B-A	Wt+s =C	Ws=C-A	Ww=B-C	$\rho_{s*}10^{-1}$, kg/m^3
0.0239 m/s						
40.5824	41.9181	1.3357	40.5834	0.001	1.3347	0.07
41.1858	45.6894	4.5036	41.1886	0.0028	4.5008	0.06
39.6594	43.3519	3.6925	39.6628	0.0034	3.6891	0.09
45.3122	49.2808	3.9686	45.315	0.0028	3.9658	0.07
41.7005	45.9088	4.2083	41.7037	0.0032	4.2051	0.08
45.2679	48.0163	2.7484	45.2699	0.002	2.7464	0.07
44.3607	46.2153	1.8546	44.3623	0.0016	1.853	0.09
0.1100 m/s						
51.4089	84.3849	32.976	51.5528	0.1439	32.8321	0.44
39.041	53.695	14.654	39.1959	0.1549	14.4991	1.06
48.9617	70.5108	21.5491	49.1705	0.2088	21.3403	0.97
36.4795	59.5825	23.103	36.7899	0.3104	22.7926	1.35

42.9692	63.3722	20.403	43.2216	0.2524	20.1506	1.24
50.2624	67.0718	16.8094	50.3703	0.1079	16.7015	0.64
49.3007	72.2334	22.9327	49.6027	0.302	22.6307	1.33
0.1574 m/s						
47.0092	67.0573	20.0481	47.4374	0.4282	19.6199	2.16
50.9384	68.8228	17.8844	51.3817	0.4433	17.4411	2.51
40.6931	63.6997	23.0066	41.0806	0.3875	22.6191	1.70
45.1138	71.5806	26.4668	45.8256	0.7118	25.755	2.73
51.3912	75.9946	24.6034	52.1661	0.7749	23.8285	3.20
41.5242	66.6471	25.1229	42.1574	0.6332	24.4897	2.56
37.4727	67.0837	29.611	38.2301	0.7574	28.8536	2.59
0.1999 m/s						
41.1694	50.31	9.1406	41.837	0.6676	8.473	7.62
41.1602	48.8455	7.6853	41.6966	0.5364	7.1489	7.27
45.9972	58.4839	12.4867	46.9038	0.9066	11.5801	7.57
37.14	48.2516	11.1116	37.9282	0.7882	10.3234	7.39
38.4315	47.8036	9.3721	39.1225	0.691	8.6811	7.69
41.3993	48.2804	6.8811	41.8469	0.4476	6.4335	6.75
40.763	48.3106	7.5476	41.372	0.609	6.9386	8.46
0.2267 m/s						
46.923	56.8094	9.8864	47.7477	0.8247	9.0617	8.76
40.5701	46.7714	6.2013	41.1522	0.5821	5.6192	9.92
43.3847	51.349	7.9643	44.1178	0.7331	7.2312	9.72
45.103	51.8412	6.7382	45.626	0.523	6.2152	8.12
40.7388	49.3589	8.6201	41.5017	0.7629	7.8572	9.32
41.548	50.8071	9.2591	42.3312	0.7832	8.4759	8.89
43.4427	50.7303	7.2876	44.1143	0.6716	6.616	9.73

Table C.10.a. Raw data for local solid density calculations dp=138 μm and Cf=1% (v/v) at nonisokinetic conditions

Wt= A	Wt+w+s= B	Ww+s= B-A	Wt+s =C	Ws=C-A	Ww=B-C	$\rho_{s*}10^{-1}$, kg/m^3
0.0120 m/s						
46.5515	87.4877	40.9362	46.6678	0.1163	40.8199	0.28
50.4478	88.3966	37.9488	50.5351	0.0873	37.8615	0.23
40.4481	73.7575	33.3094	40.6004	0.1523	33.1571	0.46

44.5737	82.3958	37.8221	44.7541	0.1804	37.6417	0.48
51.0671	91.0167	39.9496	51.2251	0.158	39.7916	0.40
41.2086	77.93	36.7214	41.3434	0.1348	36.5866	0.37
36.988	73.299	36.311	37.0992	0.1112	36.1998	0.31
0.0239 m/s						
46.5466	86.7424	40.1958	46.7505	0.2039	39.9919	0.51
50.4453	99.6938	49.2485	50.7309	0.2856	48.9629	0.58
40.447	71.681	31.234	40.672	0.225	31.009	0.72
44.5741	76.1885	31.6144	44.7875	0.2134	31.401	0.68
51.0669	88.0826	37.0157	51.3057	0.2388	36.7769	0.65
41.2086	73.2776	32.069	41.3941	0.1855	31.8835	0.58
36.9863	72.9574	35.9711	37.2047	0.2184	35.7527	0.61
0.1100 m/s						
46.5476	84.7626	38.215	47.2059	0.6583	37.5567	1.74
50.4445	86.571	36.1265	51.1485	0.704	35.4225	1.97
40.4479	73.349	32.9011	41.0396	0.5917	32.3094	1.82
44.5741	79.2439	34.6698	45.1827	0.6086	34.0612	1.77
51.0633	83.5723	32.509	51.6283	0.565	31.944	1.75
41.2103	72.5117	31.3014	41.7479	0.5376	30.7638	1.73
36.9877	71.5529	34.5652	37.651	0.6633	33.9019	1.94
0.1574 m/s						
46.5511	82.6589	36.1078	47.2997	0.7486	35.3592	2.10
50.4473	80.5792	30.1319	51.1171	0.6698	29.4621	2.25
40.4447	68.7431	28.2984	41.1142	0.6695	27.6289	2.40
44.5776	77.8455	33.2679	45.3245	0.7469	32.521	2.27
51.0682	78.6912	27.623	51.6712	0.603	27.02	2.21
41.2095	76.3374	35.1279	41.9044	0.6949	34.433	2.00
36.9826	69.5784	32.5958	37.6853	0.7027	31.8931	2.18
0.1999 m/s						
46.5471	77.3782	30.8311	47.2679	0.7208	30.1103	2.37
50.4457	79.066	28.6203	51.1014	0.6557	27.9646	2.32
40.4494	71.8257	31.3763	41.2535	0.8041	30.5722	2.60
44.5712	78.1794	33.6082	45.4284	0.8572	32.751	2.59
51.0681	87.0625	35.9944	51.9592	0.8911	35.1033	2.51
41.2093	75.8396	34.6303	42.0214	0.8121	33.8182	2.37
36.9875	75.7056	38.7181	37.9065	0.919	37.7991	2.40

0.2267 m/s						
46.5547	85.0928	38.5381	47.5873	1.0326	37.5055	2.72
50.4486	84.807	34.3584	51.414	0.9654	33.393	2.85
40.4497	70.0689	29.6192	41.3064	0.8567	28.7625	2.94
44.5763	79.5123	34.936	45.6137	1.0374	33.8986	3.02
51.0684	80.9075	29.8391	51.9195	0.8511	28.988	2.90
41.2123	78.0563	36.844	42.3079	1.0956	35.7484	3.02
36.9836	68.9182	31.9346	37.9313	0.9477	30.9869	3.02

Table C.10.b. Raw data for local solid density calculations dp=138 μm and Cf=1% (v/v) at isokinetic conditions

Wt= A	Wt+w+s= B	Ww+s= B-A	Wt+s =C	Ws=C-A	Ww=B-C	$\rho_{s*}10^{-1}$, kg/m^3
0.0239 m/s						
41.9527	46.0186	4.0659	41.9551	0.0024	4.0635	0.06
46.2246	54.0012	7.7766	46.2286	0.004	7.7726	0.05
45.0342	50.0581	5.0239	45.0379	0.0037	5.0202	0.07
45.0999	47.3541	2.2542	45.1013	0.0014	2.2528	0.06
40.4381	42.981	2.5429	40.4397	0.0016	2.5413	0.06
41.5461	43.9944	2.4483	41.5476	0.0015	2.4468	0.06
43.4362	45.7126	2.2764	43.4382	0.002	2.2744	0.09
0.1100 m/s						
40.9228	52.1941	11.2713	41.0286	0.1058	11.1655	0.94
43.7131	50.4758	6.7627	43.8887	0.1756	6.5871	2.63
40.2346	45.1556	4.921	40.3399	0.1053	4.8157	2.16
39.6496	47.6813	8.0317	39.8542	0.2046	7.8271	2.58
40.6606	43.7935	3.1329	40.7346	0.074	3.0589	2.39
41.5456	46.2973	4.7517	41.6155	0.0699	4.6818	1.48
43.4407	48.3194	4.8787	43.6304	0.1897	4.689	3.97
0.1574 m/s						
50.4462	74.3584	23.9122	50.5915	0.1453	23.7669	0.61
44.5734	73.4551	28.8817	44.8174	0.244	28.6377	0.85
41.2086	76.3202	35.1116	41.3555	0.1469	34.9647	0.42
51.4103	65.213	13.8027	51.4907	0.0804	13.7223	0.58
48.9674	70.5571	21.5897	49.1307	0.1633	21.4264	0.76
42.9745	70.9633	27.9888	43.1064	0.1319	27.8569	0.47
49.303	72.144	22.841	49.4341	0.1311	22.7099	0.58

0.1999 m/s						
50.4511	81.5596	31.1085	50.6942	0.2431	30.8654	0.78
44.5747	71.3733	26.7986	44.9916	0.4169	26.3817	1.57
41.2094	86.5759	45.3665	41.4783	0.2689	45.0976	0.59
51.4116	85.277	33.8654	51.8237	0.4121	33.4533	1.22
48.9653	78.9259	29.9606	49.464	0.4987	29.4619	1.68
42.9722	76.5098	33.5376	43.3721	0.3999	33.1377	1.20
49.3032	84.142	34.8388	49.6736	0.3704	34.4684	1.07
0.2267 m/s						
40.6321	48.6988	8.0667	41.0865	0.4544	7.6123	5.82
40.674	54.3338	13.6598	41.5806	0.9066	12.7532	6.90
40.1461	52.7683	12.6222	40.6445	0.4984	12.1238	4.04
45.0169	57.0402	12.0233	46.1775	1.1606	10.8627	10.22
40.9429	51.7909	10.848	41.3443	0.4014	10.4466	3.78
39.677	51.6326	11.9556	40.3945	0.7175	11.2381	6.21
40.6089	53.5562	12.9473	41.3383	0.7294	12.2179	5.82

Table C.11.a. Raw data for local solid density calculations dp=138 μm and Cf=2% (v/v) at nonisokinetic conditions

Wt= A	Wt+w+s= B	Ww+s= B-A	Wt+s =C	Ws=C-A	Ww=B-C	$\rho_{s*}10^{-1}$, kg/m^3
0.0120 m/s						
44.1554	77.6832	33.5278	44.5142	0.3588	33.169	1.08
44.1924	73.542	29.3496	44.4197	0.2273	29.1223	0.78
43.0794	69.5445	26.4651	43.2867	0.2073	26.2578	0.79
40.9184	76.7107	35.7923	41.1363	0.2179	35.5744	0.61
40.0977	82.1388	42.0411	40.5458	0.4481	41.593	1.07
40.939	80.1098	39.1708	41.2784	0.3394	38.8314	0.87
44.5338	79.2256	34.6918	44.9183	0.3845	34.3073	1.11
0.0239 m/s						
38.0045	79.1059	41.1014	38.7032	0.6987	40.4027	1.72
41.4367	75.5218	34.0851	42.3316	0.8949	33.1902	2.66
41.1601	69.9287	28.7686	41.784	0.6239	28.1447	2.19
40.346	77.9656	37.6196	40.9179	0.5719	37.0477	1.53
41.2578	83.255	41.9972	42.0225	0.7647	41.2325	1.84
43.3891	81.3742	37.9851	43.8473	0.4582	37.5269	1.21

39.4261	80.4132	40.9871	39.9371	0.511	40.4761	1.25
0.1100 m/s						
43.9274	69.0099	25.0825	44.6519	0.7245	24.358	2.94
44.176	71.2752	27.0992	45.3857	1.2097	25.8895	4.58
43.646	72.6615	29.0155	44.5293	0.8833	28.1322	3.10
40.3238	69.4084	29.0846	41.3246	1.0008	28.0838	3.51
45.206	72.9799	27.7739	46.2989	1.0929	26.681	4.02
40.2995	72.6422	32.3427	41.2789	0.9794	31.3633	3.08
43.9968	75.6913	31.6945	45.2457	1.2489	30.4456	4.03
0.1574 m/s						
37.6858	67.8016	30.1158	39.0772	1.3914	28.7244	4.74
40.8298	68.4963	27.6665	42.2244	1.3946	26.2719	5.19
42.1776	70.5725	28.3949	43.8591	1.6815	26.7134	6.13
41.479	69.147	27.668	43.0183	1.5393	26.1287	5.75
41.5374	68.7143	27.1769	43.1919	1.6545	25.5224	6.31
43.5693	75.8159	32.2466	45.5387	1.9694	30.2772	6.33
39.4673	70.794	31.3267	41.2832	1.8159	29.5108	5.99
0.1999 m/s						
50.0995	79.9424	29.8429	52.7515	2.652	27.1909	9.36
43.9159	73.3621	29.4462	46.8851	2.9692	26.477	10.70
43.1461	78.5521	35.406	46.6187	3.4726	31.9334	10.39
42.7452	73.5417	30.7965	45.5789	2.8337	27.9628	9.72
44.82	72.4012	27.5812	47.5476	2.7276	24.8536	10.49
43.1568	73.4512	30.2944	46.003	2.8462	27.4482	9.93
44.2286	75.2186	30.99	47.292	3.0634	27.9266	10.48
0.2267 m/s						
38.1974	69.9385	31.7411	40.8521	2.6547	29.0864	8.79
40.3991	76.5245	36.1254	43.5895	3.1904	32.935	9.30
41.2429	75.0434	33.8005	44.0752	2.8323	30.9682	8.80
43.4445	76.7101	33.2656	46.4337	2.9892	30.2764	9.48
40.3716	73.9057	33.5341	43.3227	2.9511	30.583	9.27
40.2272	74.5588	34.3316	43.2851	3.0579	31.2737	9.39
45.3656	78.2382	32.8726	48.4432	3.0776	29.795	9.90

Table C.11.b. Raw data for local solid density calculations dp=138 μm and Cf=2% (v/v) at isokinetic conditions

Wt= A	Wt+w+s= B	Ww+s= B-A	Wt+s =C	Ws=C-A	Ww=B-C	$\rho_{s*}10^{-1}$, kg/m^3
0.0239 m/s						
41.9538	43.6523	1.6985	41.9546	0.0008	1.6977	0.05
44.3043	47.3062	3.0019	44.3057	0.0014	3.0005	0.05
45.037	48.0163	2.9793	45.0385	0.0015	2.9778	0.05
45.1006	48.2181	3.1175	45.1022	0.0016	3.1159	0.05
40.6616	43.5791	2.9175	40.6632	0.0016	2.9159	0.06
41.5491	44.3925	2.8434	41.5506	0.0015	2.8419	0.05
43.4422	45.9413	2.4991	43.4436	0.0014	2.4977	0.06
0.1574 m/s						
43.457	47.6249	4.1679	43.6258	0.1688	3.9991	4.15
40.5685	48.3272	7.7587	41.2276	0.6591	7.0996	8.93
44.4783	53.1885	8.7102	45.2698	0.7915	7.9187	9.59
44.2077	52.7035	8.4958	44.5534	0.3457	8.1501	4.17
40.7623	47.578	6.8157	41.2833	0.521	6.2947	8.00
41.2242	49.5745	8.3503	41.6781	0.4539	7.8964	5.61
43.9602	52.2221	8.2619	44.5585	0.5983	7.6636	7.56
0.1999 m/s						
40.7699	57.671	16.9011	42.015	1.2451	15.656	7.69
40.575	55.5183	14.9433	42.0176	1.4426	13.5007	10.22
43.3857	53.7144	10.3287	44.4392	1.0535	9.2752	10.83
37.7421	46.9961	9.254	38.3389	0.5968	8.6572	6.69
40.7399	48.1135	7.3736	41.4699	0.73	6.6436	10.50
48.2622	56.4143	8.1521	48.797	0.5348	7.6173	6.81
43.4409	52.2221	8.7812	44.1204	0.6795	8.1017	8.10
0.2267 m/s						
41.2141	55.5973	14.3832	42.4981	1.284	13.0992	9.41
40.6755	55.0407	14.3652	42.1671	1.4916	12.8736	11.04
40.147	50.7723	10.6253	41.3101	1.1631	9.4622	11.68
40.0785	50.454	10.3755	40.8445	0.766	9.6095	7.71
39.373	52.2135	12.8405	40.7039	1.3309	11.5096	11.02
41.224	55.2915	14.0675	42.2425	1.0185	13.049	7.55
40.609	53.3046	12.6956	41.7715	1.1625	11.5331	9.66

Table C.12.a. Data for local solid density ($\rho_s * 10^{-1}$) (kg/m^3) vs. dimensionless radial distance (DRD) when mixture velocity is fixed for $d_p = 72$ μm and $C_f = 1\%$ (v/v) at nonisokinetic conditions

DRD	U_{ann}, m/s (and corrseponding mixture Reynolds number)					
	0.0120 $Re_m = 1051$	0.0239 $Re_m = 2016$	0.1100 $Re_m = 9297$	0.1574 $Re_m = 13535$	0.1999 $Re_m = 17534$	0.2267 $Re_m = 20000$
0.06	1.26	1.35	2.95	3.28	2.85	3.33
0.27	1.39	1.47	3.06	3.30	2.88	3.54
0.36	1.37	1.50	3.23	3.38	2.96	3.58
0.44	1.37	1.58	3.20	3.32	2.80	3.58
0.54	1.26	1.49	3.10	3.22	2.79	3.59
0.74	1.16	1.50	3.12	3.22	2.86	3.43
0.94	1.31	1.47	3.04	3.34	2.68	3.50

Table C.12.b. Data for radial local solid density ($\rho_s * 10^{-1}$) (kg/m^3) vs. mixture velocity when dimensionless radial distance (DRD) is fixed for $d_p = 72$ μm and $C_f = 1\%$ (v/v) at nonisokinetic conditions

U_{ann}, m/s	DRD						
	0.06	0.27	0.36	0.44	0.54	0.74	0.94
0.0120 $Re_m = 1051$	1.26	1.39	1.37	1.37	1.26	1.16	1.31
0.0239 $Re_m = 2016$	1.35	1.47	1.50	1.58	1.49	1.50	1.47
0.1100 $Re_m = 9297$	2.95	3.06	3.23	3.20	3.10	3.12	3.04
0.1574 $Re_m = 13535$	3.28	3.30	3.38	3.32	3.22	3.22	3.34
0.1999 $Re_m = 17534$	2.85	2.88	2.96	2.80	2.79	2.86	2.68
0.2267 $Re_m = 20000$	3.33	3.54	3.58	3.58	3.59	3.43	3.50

Table C.13.a. Data for local solid density ($\rho_s * 10^{-1}$) (kg/m^3) vs. dimensionless radial distance (DRD) when mixture velocity is fixed for $d_p = 72$ μm and $C_f = 1\%$ (v/v) at isokinetic conditions

DRD	U_{ann}, m/s				
	0.0239 $Re_m = 1800$	0.1100 $Re_m = 9399$	0.1574 $Re_m = 13699$	0.1999 $Re_m = 16532$	0.2267 $Re_m = 19216$
0.06	0.53	0.65	1.17	1.40	2.80
0.27	0.35	0.73	0.91	2.24	3.42
0.36	0.19	0.57	0.76	2.21	3.27
0.44	0.53	0.63	0.87	1.90	2.89
0.54	0.58	0.63	1.07	2.03	3.28
0.74	0.38	0.66	1.15	1.99	3.39
0.94	0.67	0.92	1.29	1.60	3.13

Table C.13.b. Data for radial local solid density ($\rho_s * 10^{-1}$) (kg/m^3) vs. mixture velocity when dimensionless radial distance (DRD) is fixed for $d_p = 72$ μm and $C_f = 1\%$ (v/v) at isokinetic conditions

U_{ann}, m/s	DRD						
	0.06	0.27	0.36	0.44	0.54	0.74	0.94
0.0239 $Re_m = 1800$	0.53	0.35	0.19	0.53	0.58	0.38	0.67
0.1100 $Re_m = 9399$	0.65	0.73	0.57	0.63	0.63	0.66	0.92
0.1574 $Re_m = 13699$	1.17	0.91	0.76	0.87	1.07	1.15	1.29
0.1999 $Re_m = 16532$	1.40	2.24	2.21	1.90	2.03	1.99	1.60
0.2267 $Re_m = 19216$	2.80	3.42	3.27	2.89	3.28	3.39	3.13

Table C.14.a. Data for local solid density ($\rho_s * 10^{-1}$) (kg/m^3) vs. dimensionless radial distance (DRD) when mixture velocity is fixed for $d_p = 72$ μm and $C_f = 2\%$ (v/v) at nonisokinetic conditions

DRD	U_{ann}, m/s					
	0.0120 $Re_m = 991$	0.0239 $Re_m = 1831$	0.1100 $Re_m = 8699$	0.1574 $Re_m = 12616$	0.1999 $Re_m = 15999$	0.2267 $Re_m = 17703$
0.06	3.85	4.74	6.10	6.61	6.11	8.19
0.27	4.29	5.36	7.96	8.99	6.93	9.24
0.36	4.07	5.12	7.93	8.81	6.94	9.27
0.44	4.74	5.55	7.98	8.27	7.06	9.43
0.54	4.86	5.62	8.21	8.89	6.81	9.06
0.74	4.79	5.55	7.27	8.80	6.90	8.89
0.94	5.11	5.08	7.73	8.23	6.96	9.44

Table C.14.b Data for radial local solid density ($\rho_s * 10^{-1}$) (kg/m^3) vs. mixture velocity when dimensionless radial distance (DRD) is fixed for $d_p = 72$ μm and $C_f = 2\%$ (v/v) at nonisokinetic conditions

U_{ann}, m/s	DRD						
	0.06	0.27	0.36	0.44	0.54	0.74	0.94
0.0120 $Re_m = 991$	3.85	4.29	4.07	4.74	4.86	4.79	5.11
0.0239 $Re_m = 1831$	4.74	5.36	5.12	5.55	5.62	5.55	5.08
0.1100 $Re_m = 8699$	6.10	7.96	7.93	7.98	8.21	7.27	7.73
0.1574 $Re_m = 12616$	6.61	8.99	8.81	8.27	8.89	8.80	8.23
0.1999 $Re_m = 15999$	6.11	6.93	6.94	7.06	6.81	6.90	6.96
0.2267 $Re_m = 17703$	8.19	9.24	9.27	9.43	9.06	8.89	9.44

Table C.15.a. Data for local solid density ($\rho_s * 10^{-1}$) (kg/m^3) vs. dimensionless radial distance (DRD) when mixture velocity is fixed for $d_p = 72$ μm and $C_f = 2\%$ (v/v) at isokinetic conditions

DRD	U_{ann}, m/s				
	0.0239 $Re_m = 1902$	0.1100 $Re_m = 8952$	0.1574 $Re_m = 12938$	0.1999 $Re_m = 16201$	0.2267 $Re_m = 17626$
0.06	0.07	0.44	2.16	7.62	8.76
0.27	0.06	1.06	2.51	7.27	9.92
0.36	0.09	0.97	1.70	7.57	9.72
0.44	0.07	1.35	2.73	7.39	8.12
0.54	0.08	1.24	3.20	7.69	9.32
0.74	0.07	0.64	2.56	6.75	8.89
0.94	0.09	1.33	2.59	8.46	9.73

Table C.15.b. Data for radial local solid density ($\rho_s * 10^{-1}$) (kg/m^3) vs. mixture velocity when dimensionless radial distance (DRD) is fixed for $d_p = 72$ μm and $C_f = 2\%$ (v/v) at isokinetic conditions

U_{ann}, m/s	DRD						
	0.06	0.27	0.36	0.44	0.54	0.74	0.94
0.0239 $Re_m = 1902$	0.07	0.06	0.09	0.07	0.08	0.07	0.09
0.1100 $Re_m = 8952$	0.44	1.06	0.97	1.35	1.24	0.64	1.33
0.1574 $Re_m = 12938$	2.16	2.51	1.70	2.73	3.20	2.56	2.59
0.1999 $Re_m = 16201$	7.62	7.27	7.57	7.39	7.69	6.75	8.46
0.2267 $Re_m = 17626$	8.76	9.92	9.72	8.12	9.32	8.89	9.73

Table C.16.a. Two-phase axial pressure gradient vs. mixture velocity for different feed solid concentrations of particle size d_p=72 μm

U_{ann}, m/s	C_f	
	1% v/v	2% v/v
0.0239	377.93	607.85
0.1100	403.29	761.33
0.1574	327.10	679.31
0.1999	276.14	644.15
0.2267	253.08	587.62

Table C.16.b. Two-phase axial pressure gradient (including static head) vs. mixture velocity for different feed solid concentrations of size d_p=72 μm

U_{ann}, m/s	C_F	
	1% v/v	2% v/v
0.0239	10200.64	10466.02
0.1100	10234.45	10608.01
0.1574	10181.15	10610.96
0.1999	10175.17	10561.41
0.2267	10221.56	10530.03

Table C.16.c. Two-phase experimental friction factor vs. mixture velocity when feed solid concentration is fixed for d_p=72 μm

U_{ann}, m/s	C_f	
	1% v/v	2% v/v
0.0239	26.36	42.24
0.1100	1.33	2.50
0.1574	0.52	1.08
0.1999	0.27	0.64
0.2267	0.19	0.45

Table C.17.a. Data for local solid density ($\rho_s * 10^{-1}$) (kg/m^3) vs. dimensionless radial distance (DRD) when mixture velocity is fixed for d_p=138 μm and C_f= 1% (v/v) at nonisokinetic conditions

DRD	U_{ann}, m/s					
	0.0120 Re_m=1060	0.0239 Re_m=2038	0.1100 Re_m=9395	0.1574 Re_m=13815	0.1999 Re_m=17431	0.2267 Re_m=20116
0.06	0.28	0.51	1.74	2.10	2.37	2.72
0.27	0.23	0.58	1.97	2.25	2.32	2.85
0.36	0.46	0.72	1.82	2.40	2.60	2.94
0.44	0.48	0.68	1.77	2.27	2.59	3.02
0.54	0.40	0.65	1.75	2.21	2.51	2.90
0.74	0.37	0.58	1.73	2.00	2.37	3.02
0.94	0.31	0.61	1.94	2.18	2.40	3.02

Table C.17.b. Data for radial local solid density ($\rho_s * 10^{-1}$) (kg/m^3) vs. mixture velocity when dimensionless radial distance (DRD) is fixed for d_p=138 μm and C_f= 1% (v/v) at nonisokinetic conditions

U_{ann}, m/s	DRD						
	0.06	0.27	0.36	0.44	0.54	0.74	0.94
0.0120 Re_m=1060	0.28	0.23	0.46	0.48	0.40	0.37	0.31
0.0239 Re_m=2038	0.51	0.58	0.72	0.68	0.65	0.58	0.61
0.1100 Re_m=9395	1.74	1.97	1.82	1.77	1.75	1.73	1.94
0.1574 Re_m=13535	2.10	2.25	2.40	2.27	2.21	2.00	2.18
0.1999 Re_m=17431	2.37	2.32	2.60	2.59	2.51	2.37	2.40
0.2267 Re_m=20116	2.72	2.85	2.94	3.02	2.90	3.02	3.02

Table C.18.a. Data for local solid density ($\rho_s * 10^{-1}$) (kg/m^3) vs. dimensionless radial distance (DRD) when mixture velocity is fixed for d_p=138 μm and C_f= 1% (v/v) at isokinetic conditions

DRD	U_{ann}, m/s				
	0.0239 Re_m=1768	0.1100 Re_m=8555	0.1574 Re_m=13197	0.1999 Re_m=17535	0.2267 Re_m=18862
0.06	0.06	0.94	0.61	0.78	5.82
0.27	0.05	2.63	0.85	1.57	6.90
0.36	0.07	2.16	0.42	0.59	4.04
0.44	0.06	2.58	0.58	1.22	10.22
0.54	0.06	2.39	0.76	1.68	3.78
0.74	0.06	1.48	0.47	1.20	6.21
0.94	0.09	3.97	0.58	1.07	5.82

Table C.18.b. Data for radial local solid density ($\rho_s * 10^{-1}$) (kg/m^3) vs. mixture velocity when dimensionless radial distance (DRD) is fixed for d_p=138 μm and C_f= 1% (v/v) at isokinetic conditions

U_{ann}, m/s	DRD						
	0.06	0.27	0.36	0.44	0.54	0.74	0.94
0.0239 Re_m=1768	0.06	0.05	0.07	0.06	0.06	0.06	0.09
0.1100 Re_m=8555	0.94	2.63	2.16	2.58	2.39	1.48	3.97
0.1574 Re_m=13197	0.61	0.85	0.42	0.58	0.76	0.47	0.58
0.1999 Re_m=17535	0.78	1.57	0.59	1.22	1.68	1.20	1.07
0.2267 Re_m=18862	5.82	6.90	4.04	10.22	3.78	6.21	5.82

Table C.19.a. Data for local solid density ($\rho_s * 10^{-1}$) (kg/m^3) vs. dimensionless radial distance (DRD) when mixture velocity is fixed for d_p=138 μm and C_f= 2% (v/v) at nonisokinetic conditions

DRD	U_{ann}, m/s					
	0.0120 Re_m=934	0.0239 Re_m=1860	0.1100 Re_m=8000	0.1574 Re_m=11571	0.1999 Re_m=14572	0.2267 Re_m=16364
0.06	1.08	1.72	2.94	4.74	9.36	8.79
0.27	0.78	2.66	4.58	5.19	10.70	9.30
0.36	0.79	2.19	3.10	6.13	10.39	8.80
0.44	0.61	1.53	3.51	5.75	9.72	9.48
0.54	1.07	1.84	4.02	6.31	10.49	9.27
0.74	0.87	1.21	3.08	6.33	9.93	9.39
0.94	1.11	1.25	4.03	5.99	10.48	9.90

Table C.19.b. Data for radial local solid density ($\rho_s * 10^{-1}$) (kg/m^3) vs. mixture velocity when dimensionless radial distance (DRD) is fixed for d_p=138 μm and C_f= 2% (v/v) at nonisokinetic conditions

U_{ann}, m/s	DRD						
	0.06	0.27	0.36	0.44	0.54	0.74	0.94
0.0120 Re_m=934	1.08	0.78	0.79	0.61	1.07	0.87	1.11
0.0239 Re_m=1860	1.72	2.66	2.19	1.53	1.84	1.21	1.25
0.1100 Re_m=8000	2.94	4.58	3.10	3.51	4.02	3.08	4.03
0.1574 Re_m=11571	4.74	5.19	6.13	5.75	6.31	6.33	5.99
0.1999 Re_m=14572	9.36	10.70	10.39	9.72	10.49	9.93	10.48
0.2267 Re_m=16364	8.79	9.30	8.80	9.48	9.27	9.39	9.90

Table C.20.a. Data for local solid density ($\rho_s * 10^{-1}$) (kg/m^3) vs. dimensionless radial distance (DRD) when mixture velocity is fixed for d_p=138 μm and C_f= 2% (v/v) at isokinetic conditions

DRD	U_{ann}, m/s				
	0.0239 Re_m=2044	0.1100 Re_m=8109	0.1574 Re_m=10590	0.1999 Re_m=15118	0.2267 Re_m=17162
0.06	0.05	1.25	4.15	7.69	9.41
0.27	0.05	1.74	8.93	10.22	11.04
0.36	0.05	1.19	9.59	10.83	11.68
0.44	0.05	1.05	4.17	6.69	7.71
0.54	0.05	0.88	8.00	10.50	11.02
0.74	0.05	1.57	5.61	6.81	7.55
0.94	0.06	1.91	7.56	8.10	9.66

Table C.20.b. Data for radial local solid density ($\rho_s * 10^{-1}$) (kg/m^3) vs. mixture velocity when dimensionless radial distance (DRD) is fixed for d_p=138 μm and C_f= 2% (v/v) at isokinetic conditions

U_{ann}, m/s	DRD						
	0.06	0.27	0.36	0.44	0.54	0.74	0.94
0.0239 Re_m=2044	0.05	0.05	0.05	0.05	0.05	0.05	0.06
0.1100 Re_m=8109	1.25	1.74	1.19	1.05	0.88	1.57	1.91
0.1574 Re_m=10590	4.15	8.93	9.59	4.17	8.00	5.61	7.56
0.1999 Re_m=15118	7.69	10.22	10.83	6.69	10.50	6.81	8.10
0.2267 Re_m=17162	9.41	11.04	11.68	7.71	11.02	7.55	9.66

Table C.21.a. Two-phase axial pressure gradient vs. mixture velocity for different feed solid concentrations of size d_p=138 μm

U_{ann}, m/s	C_f	
	1% v/v	2% v/v
0.0239	427.00	766.25
0.1100	539.54	900.38
0.1574	504.74	850.93
0.1999	447.46	745.87
0.2267	416.93	669.89

Table C.21.b. Two-phase axial pressure gradient (including static head) vs. mixture velocity for different feed solid concentrations of size d_p=138 μm

U_{ann}, m/s	C_f	
	1% v/v	2% v/v
0.0239	10287.99	10464.58
0.1100	10422.66	10776.25
0.1574	10328.88	10789.48
0.1999	10303.36	10666.44
0.2267	10298.13	10609.36

Table C.21.c. Two-phase experimental friction factor vs. mixture velocity when feed solid concentration is fixed for d_p=138 μm

U_{ann}, m/s	C_f	
	1% v/v	2% v/v
0.0239	29.66	54.48
0.1100	1.77	2.95
0.1574	0.81	1.35
0.1999	0.44	0.74
0.2267	0.32	0.51